MOLECULAR SCATTERING
FROM
SUPERTHERMAL BEAMS

by

Brian Swanson Duchart.

Thesis presented for the degree of

Doctor of Philosophy

University of Edinburgh.

March, 1971

To the Memory of my Parents

CONTENTS

ACKNOWLEDGEMENTS

I wish to thank Dr. M. A. D. Fluendy and Dr. K. P. Lawley for their advice and encouragement.

I would also like to thank the other members of the Edinburgh Molecular Beam Group, in particular I am indebted to Mr. W. Stevenson for his miracles in metal.

I am indebted to the University of Edinburgh for the provision of laboratory, library and computing facilities and also to the Science Research Council for support during the period of this work.

SUMMARY

Differential cross-sections in the superthermal energy range have been measured for the scattering of potassium from mercury and molecular iodine. Such interactions are of importance in such fields as high temperature chemistry, plasma physics and astrophysics.

A major part of the work was the design and construction of a suitable apparatus I.E. one capable of measuring small angle differential cross-sections with high resolution.

The main features of the apparatus are outlined. The beam sources, their construction and performance, the detector and associated data collection system are described in some detail.

The main beam source was of the ionisation/neutralisation type and was capable of producing superthermal beams of potassium, rubidium and caesium. The cross-beam source was of the simple thermal type.

The detector consisted of a surface ioniser, a mass spectrometer and electron multiplier. Particle counting techniques were used. In order to increase the signal to noise ratio the cross beam was modulated. Data were punched on paper tape and subsequently analysed by computer.

Facilities were developed to allow measurement

of energy loss spectra by time of flight.

An expression relating the apparatus resolution to the beam and detector dimensions was derived and the effects of resolution on the measured scattered intensity calculated numerically.

The potassium/mercury data were interpreted as arising from a single elastic potential. The scattering pattern for a Lennard-Jones (8,6) potential with $\epsilon = 0.087 \times 10^{-12}$ ergs and $r_m = 4.8$ Å was calculated by the method of partial waves. The scattering pattern, corrected for apparatus resolution, was a reasonable fit to the data, however it was found that a better fit could be obtained with a "harder" (18,6) potential and the same values of ϵ and r_m.

The spectator stripping model of potassium/iodine, which has proved so useful at thermal energies, was extended to super-thermal energies by integrating the classical equations of motion. It was found that above about 2.5 e.v. the possibility of reaction could be ignored. An attempt was made therefore to interpret the data as arising from either the diabatic covalent potential or the adiabatic covalent/ionic potential. Neither completely described the data. It was proposed that the scattering could be described in terms of contributions from both diabatic and adiabatic potentials.

Although the data allowed tentative conclusions only, they did justify the belief that such experiments were capable of yielding information on previously unexplored regions of molecular interactions.

CHAPTER 1.

INTRODUCTION.

INTRODUCTION

This work is an account of the design and construction of a molecular-beam apparatus capable of measuring differential scattering cross-sections in the super-thermal energy range. Results are reported for the two systems K/Hg, K/I_2.

Many phenomena of everyday experience of the world around us arise as a result of the interaction, collision, of countless numbers of unseen atomic particles. Such observations as gas pressure and diffusion, the conduction of heat, the properties of the liquid and solid states and the chemical reactivity of certain substances are obvious examples. Clearly an understanding of these phenomena requires a knowledge of the forces acting between the discrete atomic particles and the relationships between these forces and the macroscopically observable effects.

The relations between microscopic and macroscopic properties are dealt with by the theories of statistical mechanics, see for example Hirschfelder, Curtiss and Bird's book "Molecular Theory of Gases and Liquids." The best known example of such a treatment is to be found in the kinetic theory of gases. Starting with the model of a gas as a collection of small "billiard balls" the equation of state of an ideal gas may be derived.

It is the first problem, that of determining the forces acting between atomic particles which was the concern of this work.

Intermolecular Forces

The characterisation and determination of intermolecular forces has been a subject of great activity in recent years and several excellent reviews of the subject exist, in particular see Advances in Chemical Physics volume 12, the book by Margenau and Kestner (MAR 69) and the article by Pauly and Toennies (PAU 65). In consequence only a very brief resume will be attempted here.

In principle intermolecular forces may be calculated using the Schrodinger equation, this has been achieved for a few simple systems H_2^+, HeH^{2+} but for any more complex system the sheer size of the computation renders it impossible and various approximations must be resorted to. It is normal to classify intermolecular forces as long range, intermediate range or short range; this classification arises mainly from the different approximations required in the different regions. At long range there is little electronic overlap, at intermediate ranges the electron clouds perturb each other slightly while at short ranges considerable perturbation occurs. Needless to say it is the theory of long-range forces which has been most extensively developed.

The most easily understood long-range forces are those arising from permanent multipole moments, using measured dipole, quadrapole moments etc., these may be described quite accurately. A second order interaction may arise as a result of the induction of a multipole moment in

one molecule by the permanent multipole moment of another molecule, again this may be described in terms of the measured multipole moments and polarizabilities of the free molecules. Probably the most important of the long-range forces are the dispersion forces, these may be thought of as arising from fluctuations in the electronic charge clouds. An instantaneous multipole in one molecule may induce a multipole in another molecule and interact with it.

It can be shown that the dispersion energy is given by

$$\phi(r) = -C/r^6 - C'/r^8 - C''/r^{10}$$

The first term, the induced dipole/induced dipole term, is normally the only one considered. Various approximations exist for estimating the coefficient C from known molecular quantities (MAS 67), (MAR 69), the absolute values obtained must, however, be treated with caution. The approximations are useful, none the less, in that they predict relationships between the C coefficients of related systems.

Although the physical origins of short range forces are clear there exists no good theoretical information. The forces may be accounted for in terms of the Pauli exclusion principle and the Hellmann-Feynman theorem. When two atoms having zero net spin approach the electron clouds tend to avoid each other, the resulting decrease in the screening of the nuclei leads to repulsion. Clearly

there is a similarity between this situation and chemical bonding in which an increase in nuclear shielding arises from a build up of electrons in the inter-nuclear region.

If the potentials for some of the molecular states of a system are known then it may be possible to estimate the potential for another molecular state by use of the Heitler-London valence bond theory or the perfect-pairing approximation (COU 52). In the absence of such information the best that can be done is a prediction of the form of the potential. In the intermediate range the situation is even more bleak, a procedure has been developed by Dalgarno and Lynn (DAL 56) but because of algebraic complexity has not been extended beyond the case of two helium atoms. The situation at present is that one simply adds long and short range forces together and hopes for the best.

Although little quantitative information is forthcoming from theory it is most important, none the less, that theory suggest the qualitative form of the potential in a particular case. Without such a guideline experimental results can not, in general, be unambiguously interpreted.

Experimental determination of intermolecular forces.

Experimental information is obtained from three major sources; spectroscopic observations, the bulk properties of matter and beam scattering experiments.

A wealth of information is available from

spectroscopy (GAY 68). Bound states may be found from the vibration-rotation bands, pre-dissociation yields the energies at which different levels cross and information about repulsive levels may be obtained from the intensity distributions in continua. Spectroscopic observations are, however, limited to stable diatomics and only those levels accessible from the ground state. In recent years the pressure broadening of spectral lines has been used, to obtain intermolecular forces.

It has been pointed out that many phenomena of everyday experience are a manifestation of the interaction of atomic particles; it seems natural, therefore, to turn to these phenomena for information on intermolecular forces. In principle any bulk property could be used to determine intermolecular forces, however in practice very few are used as several very restrictive criteria must be met. There must be a fully developed statistical theory connecting the macroscopic observable and the intermolecular forces, the forces must not be so buried in theory that the observable is almost insensitive to them. Properties which have proved most useful in this context are virial coefficients, transport properties of gases and heats of sublimation of crystals (HIR 54), (MAS 67). The general procedure is to assume some form for the potential guided by theory and intuition, and attempt to reproduce the experimental data. Unfortunately potentials obtained in this way are rarely unique, also the one potential often fails to describe both transport properties and virial coefficients. Despite

these difficulties bulk properties are still the main source of intermolecular potentials. In studies of bulk properties one is essentially measuring the effects of countless atomic collisions, each having different trajectories and energies. In beam experiments single collisions between particles of known energy and in known quantum states may be studied. In the last fifteen years molecular beam scattering has been used increasingly in the determination of intermolecular forces and in the study of the molecular dynamics of chemical reactions. A molecular beam is defined as a unidirectional stream of gas in which the density or random velocity is so low that collisions between beam molecules do not occur. In order to avoid scattering by other molecules the background pressure in the experimental chamber should be about 10^{-6} torr or less. As molecules in the beam suffer no collisions before the scattering region their energy and internal states may, in general, be well defined.

After interaction with other molecules in the scattering region the initial beam intensity I_0 is reduced to I given by

$$I = I_0 \exp(-n l Q(v))$$

where n is the particle density in the scattering region and l is the length of the scattering region. $Q(v)$ is the total cross-section and represents the number of particles scattered out of the main beam by elastic, inelastic and reactive processes. The angular distribution of material

scattered from the main beam is given by the differential cross-section $6(\theta, \phi, v)$.

Clearly

$$Q(v) = \int 6(\theta, \phi, v)\, d\Omega$$

In experiments designed to measure the total cross-section the main beam is usually passed through a chamber containing the scattering gas at a known pressure. The total cross-section may then be obtained from the main-beam attenuation. Variation of the total cross-section with velocity yields information about the intermolecular potential (MOT 65), (BER 66). In differential-cross section work the main beam is crossed with a secondary beam and the scattered intensity measured by rotating a suitable detector around the main beam.

Molecular beam scattering experiments may be divided into three classes depending on the beam energy. Thermal beams, those having energies less than 0.5 e.v. are produced by effusion of the beam material from a small orifice in a heated oven. The upper energy is limited by the material of the oven. The vast majority of work to date has been in the thermal energy region, elastic, inelastic and reactive collisions having been studied, there are now extensive reviews of the subject (BER 67), (PAU 65), (PAU 68), (HER 66), (GRE 66), (HER 65), (BER 64) and no more will be said here. High energy beams, those having energies greater than about 200 e.v. are formed by accelerating ions to the desired energy then neutralising the ions, usually by resonant

charge transfer. This method has normally been applied to the measurement of total elastic cross sections and yields information about the short range part of the potential (AMD 66) (MAS 62). The results obtained are very sensitive to apparatus averaging, a fact which was not fully recognised in much of the early work. For want of a better definition super-thermal beams may be defined as those having energies between thermal and high energy beams, I.E. 0.5 e.v. - 200 e.v. It is a sad fact that although this energy range is, in many ways, the most interesting and useful it is also the least experimentally accessible. It is only in the last decade that sources capable of working in this energy range have been developed and only recently have many results been obtained (PAU 70), (CRO 70), (LOS 70).

Super-thermal molecular beams cover an equivalent temperature range of 5×10^3 to 2×10^6 ^oK and hence provide a powerful tool for the study of many diverse phenomena.

Measurement of total and differential elastic cross sections is expected to shed light on short and intermediate range forces (CRO 70), this is of interest in the calculation of high temperature gaseous transport properties, which are not accessible to direct measurement, in the theory of flames and shocks (MAS 67), in theories of radiation damage (MON 57) and in calculation of steric hinderance in molecules. It would be extremely difficult to obtain such information by any other means.

It is, however, the possibility of studying inelastic and reactive processes which arouses most interest. The transfer of energy from translational to vibrational and rotational is the initial step in many chemical reactions, a knowledge of the energy transfer cross-section is therefore of fundamental importance to an understanding of chemical kinetics. Super-thermal beams linked with time of flight techniques provides a method of measuring the excitation efficiency of specific modes. Work on these lines has been done for the ion-molecule system Li^+/H_2 (SCH 68). Reactive systems studied to date with thermal beams have been restricted to those having essentially zero activation energy, this has been a serious limitation. The advent of higher energy beams means that systems having large activation energies may be studied. The activation energy itself may be determined absolutely from the reaction threshold.

It is clear that molecular-beam scattering studies in the energy range 0.5-200 e.v. will yield information of importance in many fields.

CHAPTER II.

THEORY

Elastic Scattering Theory

Classical Mechanics.

Although the predictions of classical mechanics are generally not applicable to collisions between atoms, the concepts which arise in classical mechanics are useful in the description of any scattering system (GOL 50).

Consider two particles of masses M1 and M2 and velocities V1 and V2 which interact along a potential $V(r)$, where r is the internuclear separation. By removing the motion of the centre of mass the system may be reduced to a one body problem; that in which a particle of mass

$$\mu = \frac{M_1 . M_2}{M_1 + M_2}$$

moves in the field of a fixed centre of force with a velocity $\underline{Vr} = \underline{V1} + \underline{V2}$.

Using the principles of conservation of energy and angular momentum the angle of deflection may be obtained as a function of the impact parameter b, the distance of closest approach in the absence of the interaction V(r).

$$\Theta(b) = \pi - 2b \int_{r_c}^{\infty} dr / r^2 \left(1 - \frac{b^2}{r^2} - \frac{V(r)}{E}\right)^{1/2}$$

where $E = \frac{1}{2}\mu Vr^2$ is the collision energy and r_c is the distance of closest approach given by

$$\left(1 - \frac{b^2}{r_c^2} - \frac{V(r_c)}{E}\right) = 0$$

The deflection function for a typical interatomic potential (Fig. 2,1a) is shown in Fig. (2, 1b). It will be seen that for small values of b the potential is repulsive and $\Theta(b)$ is positive, as b increases so the potential becomes

attractive, $\Theta(b)$ falls to a minimum and then goes to zero as b is further increased. It will be seen that more than one value of b may contribute to a given Θ , in classical theory the different contributions are simply added. The scattered intensity as a function of Θ may be found as follows: Particles having impact parameters between b and $b + \Delta b$ will be scattered through an angle Θ

$$\therefore \quad 2\pi b \Delta b = -2\pi \, 6(\Theta) \sin(\Theta) \Delta\Theta$$

where $6(\Theta)$ is the differential cross-section

$$\therefore \quad 6(\Theta) = \frac{-b}{\sin(\Theta)} \frac{db}{d\Theta}$$

The predicted scattered intensity as a function of Θ is shown in Fig. (2,1c). There are several points of interest. It will be seen that $\Theta(b) = 0$ at $b = b_g$ this is known as a glory singularity. Another singularity occurs at $b = b_r$ where $db/d\Theta$ is infinite, $\Theta(b_r)$ is known as the rainbow angle. Measurement of such features as the rainbow may be used to obtain information about the interaction potential V(r) (BER 64). However such singularities are unphysical and are a failure of classical mechanics, other failures include the inability to explain observed oscillatory structure and the angular dependence of small angle scattering.

Quantum Mechanics

The quantum mechanical treatment may be found in detail in the books by Mott and Massey (MOT 65) Wu and Ohmura(WU 62) etc., a recent review by Bernstein deals

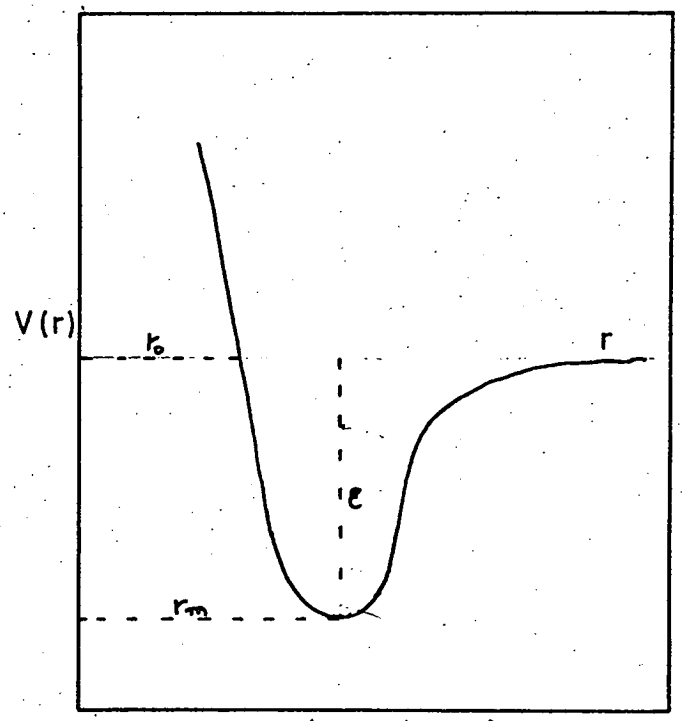

Fig.(2,1a) r

Typical intermolecular potential

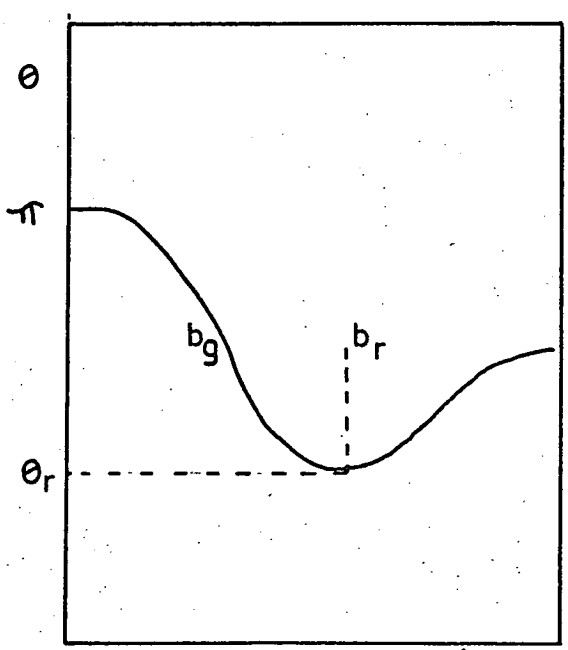

Fig. (2,1b) b

Deflection function

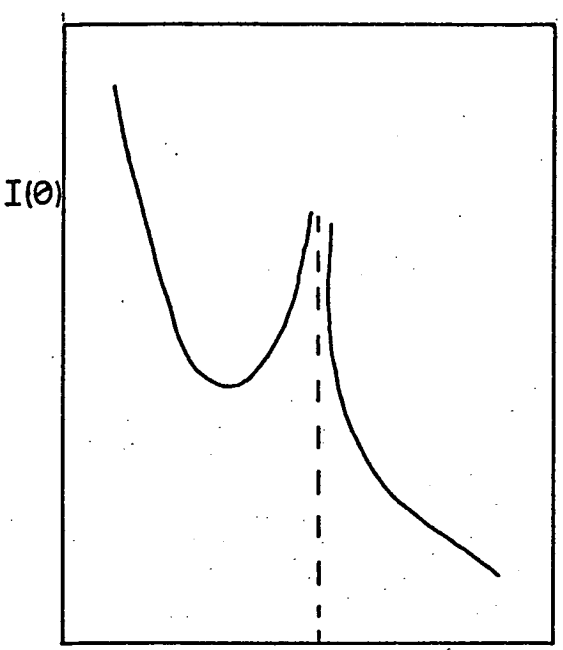

Fig. (2,1c)

Scattered intensity

with the salient features (BER 66). A very brief resume will be given here.

The method used is that of partial wave analysis, originally applied in the nineteenth century by Rayleigh to the scattering of sound waves and adapted in 1927 by Faxen and Holtsmark to the scattering of atomic particles.

Consider the scattering of a particle of mass μ and energy E. Associated with the particle is a wave function ψ which must contain information about the particle before and after scattering. The picture is that of a plane wave incident on the potential and a spherical wave scattered outwards from it. The wave function may be written as

$$\psi = e^{ikz} + f(\theta)\frac{1}{r}e^{ikr}$$

where

$$k = \mu v/\hbar$$

It can be shown that the differential cross-section is given by

$$\sigma(\theta) = f(\theta) \times f^{*}(\theta)$$

The wave function ψ is then expressed as the sum of partial waves

$$\psi(r,\theta) = \sum_{l=0}^{\infty} b_l R_l(kr) P_l(\cos\theta)$$

associated with the l the partial wave is an angular momentum $\sqrt{l(l+1)}$ hence l may be identified with the classical impact parameter b by the relation

$$b = \sqrt{l(l+1)}/k$$

On substituting the expression for $\psi(r,\theta)$ in the Schroedinger equation and after some manipulation it is possible to show that

$$f(\theta) = \frac{1}{k} \sum_{l=0}^{\infty} (2l+1) e^{i\eta_l} \sin\eta_l P_l(\cos\theta)$$

It may also be shown that the total cross-section Q is given by

$$Q = \int \sigma(\theta)\, d\tau$$

$$= \frac{4\pi}{k^2} \sum_{l=0}^{\infty} (2l+1) \sin^2\eta_l$$

The quantity η_l , known as the phase shift, is the phase difference between the outgoing scattered wave and the outgoing wave in the absence of a potential. The phase shift contains all the scattering information. The great power of this method lies in the fact that the expression for $f(\theta)$ is fairly rapidly convergent, especially at thermal energies. The variation of η_l with l for a typical potential is shown in Fig. (2,2).

The main differences between the quantum and classical treatments are the removal of the classical singularities and the prediction of interference. It was stated above that contributions to a given θ from different b values were simply added in classical theory, in the quantum mechanical treatment, being essentially wave like, each contribution has associated with it a phase angle and hence interference may occur. Fig. (2,4) shows a typical calculated scattering pattern, such quantum oscillations

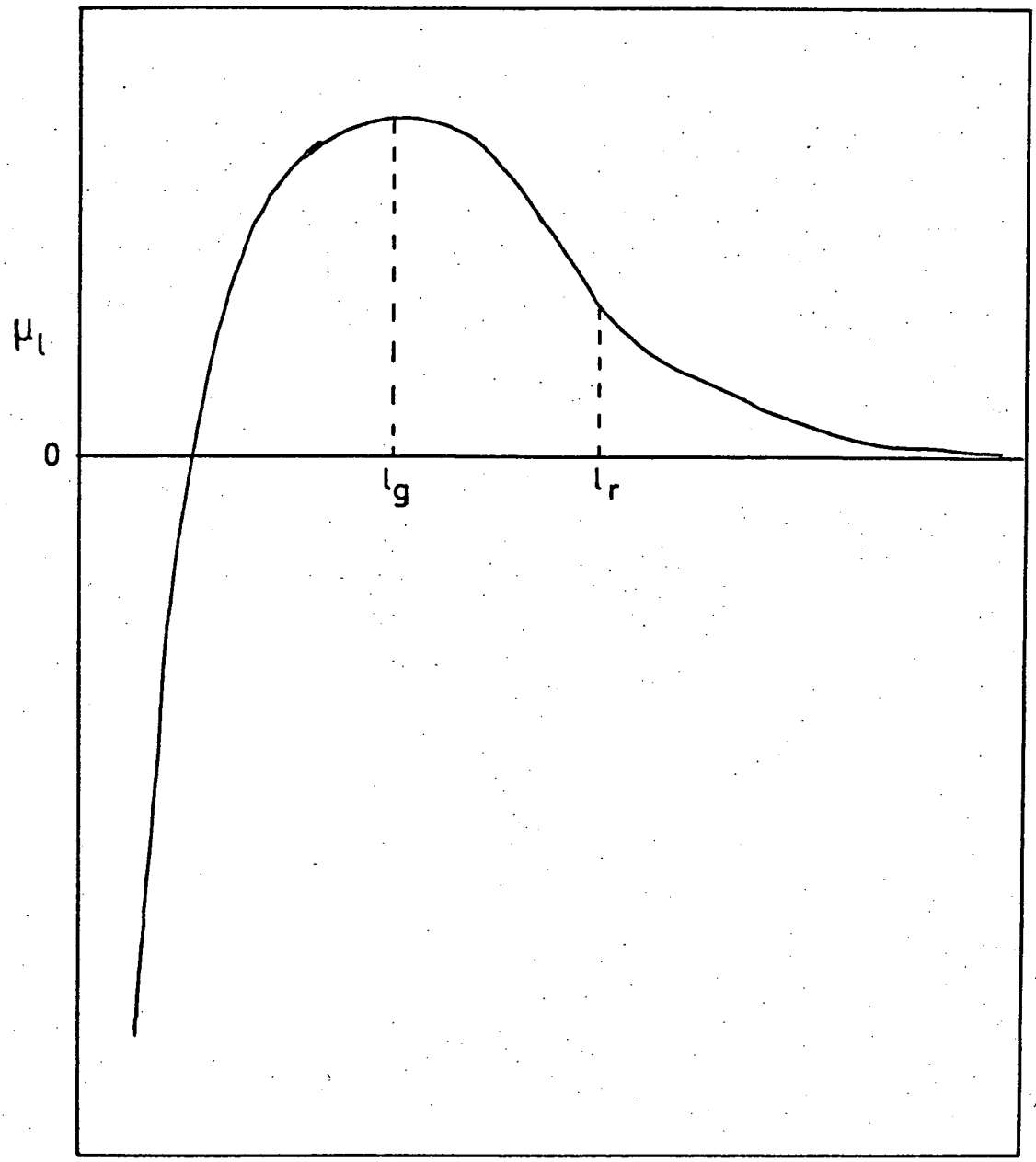

Fig. (2.2)

Typical phase shift curve.

have in fact been observed in the laboratory (BER 60), (COW 69a). These and other quantum effects in elastic scattering are discussed in detail by Bernstein (BER 66).

When there exists, concurrent with elastic scattering, inelastic and reactive scattering then the situation is greatly complicated. It is, however, possible to treat the elastic scattering using the optical model (BER 66), (GRE 66). In this model the interaction potential is assumed complex, the imaginary part representing reaction. A complex potential implies complex phase shifts which may be written as

$$\eta_\ell = \eta_\ell^\circ + i\,\varepsilon_\ell$$

It may then be shown that

$$\sigma(\theta) = \tfrac{1}{k^2}\Big[\Big(\sum_{\ell=0}^{\infty}(2\ell+1)\sin 2\eta_\ell (1-P_\ell)^{\frac{1}{2}} P_\ell(\cos\theta)\Big)^2 + \Big(\sum_{\ell=0}^{\infty}(2\ell+1)\big[\cos 2\eta_\ell (1-P_\ell)^{\frac{1}{2}} - 1\big] P_\ell(\cos\theta)\Big)\Big]$$

where P_l, the opacity function, is given by

$$P_\ell = 1 - \exp(-4\varepsilon_\ell)$$

Various models of chemical reactions may then be simulated by a suitable choice of P_l (HOR 69), (ROS 67).

Calculation of elastic scattered intensity.

In general it is not possible to go direct from a measured scattering pattern to the associated intermolecular potential. Guided by theory, and intuition, an analytic

form for the potential is postulated. For this potential the scattering pattern may be calculated. The procedure is then to vary the parameters of the potential until the best fit of predicted and observed scattering patterns is obtained. A drawback of this procedure is that the potential so obtained may not be unique. Another danger is that if a potential containing too many adjustable parameters is used the procedure degenerates into a rather complicated curve fitting exercise of little physical significance.

The scattered flux was calculated using the method of partial waves outlined above. The phase-shifts were calculated using the J.W.K.B. approximation (MOT 65), this gives

$$\eta_\ell = \frac{1}{\lambda}\left[\int_{r_c}^{\infty}\left(1-\frac{b^2}{r^2}-\frac{V(r)}{E}\right)^{\frac{1}{2}}dr - \int_{b}^{\infty}\left(1-\frac{b^2}{r^2}\right)^{\frac{1}{2}}dr\right]$$

where λ is the wavelength given by

$$\lambda = 2\pi\left(\frac{\hbar^2}{2\mu E}\right)^{\frac{1}{2}}$$

and r_c is the classical turning point.

The J.W.K.B. approximation was used until η_ℓ fell below 10^{-2} radians, subsequent values of the phase shift were calculated using the Born approximation

$$\eta_\ell = -\frac{2\mu k}{\hbar^2}\int_0^{\infty} V(r)\left[j_\ell(r)\right]^2 r^2\,dr$$

For a potential of the form $V(r) = C/r^S$ then this reduces to MOT (65),

$$\eta_\ell = -\frac{4\pi^3 \mu C}{\hbar h^{2s}} \left(\frac{k}{2}\right)^{s-1} \frac{\Gamma(s-1)\,\Gamma(\ell - s/2 + 3/2)}{[\Gamma(s/2)]^2\,\Gamma(\ell + s/2 + 1/2)}$$

and hence for large l

$$\eta_\ell \propto 1/\ell^{s-1}$$

Having calculated I (θ), the scattered intensity in the centre of mass reference frame, it must then be transformed to $I'(\phi_L)$ the intensity in laboratory frame.

The relationships between the centre of mass and laboratory scattering angles in our case of out of plane scattering are shown in Fig. (2,3) (MOR 62). The situation is simplified somewhat by the fact that the angle between the beams is 90°.

The velocity of the main beam particle m_1 relative to the centre of mass is W_1

$$\omega_1 = (v_1^2 + v_2^2)^{1/2}\, m_2/(m_1 + m_2)$$

the velocity of the centre of mass

$$v_c = (m_1^2 v_1^2 + m_2^2 v_2^2)^{1/2}/(m_1 + m_2)$$

from the diagram

$$AC^2 = v_1'^2 + v_1^2 - 2 v_1' v_1 \cos\phi_L$$

also

$$AC^2 = \omega_1'^2 + \omega_1^2 - 2\omega_1'\omega_1 \cos\theta$$

and

$$\omega_1'^2 = v_1'^2 + v_c^2 - 2 v_1' v_c \cos\alpha_1'$$

and

$$\omega_1^2 = v_1^2 + v_c^2 - 2 v_1 v_c \cos\alpha$$

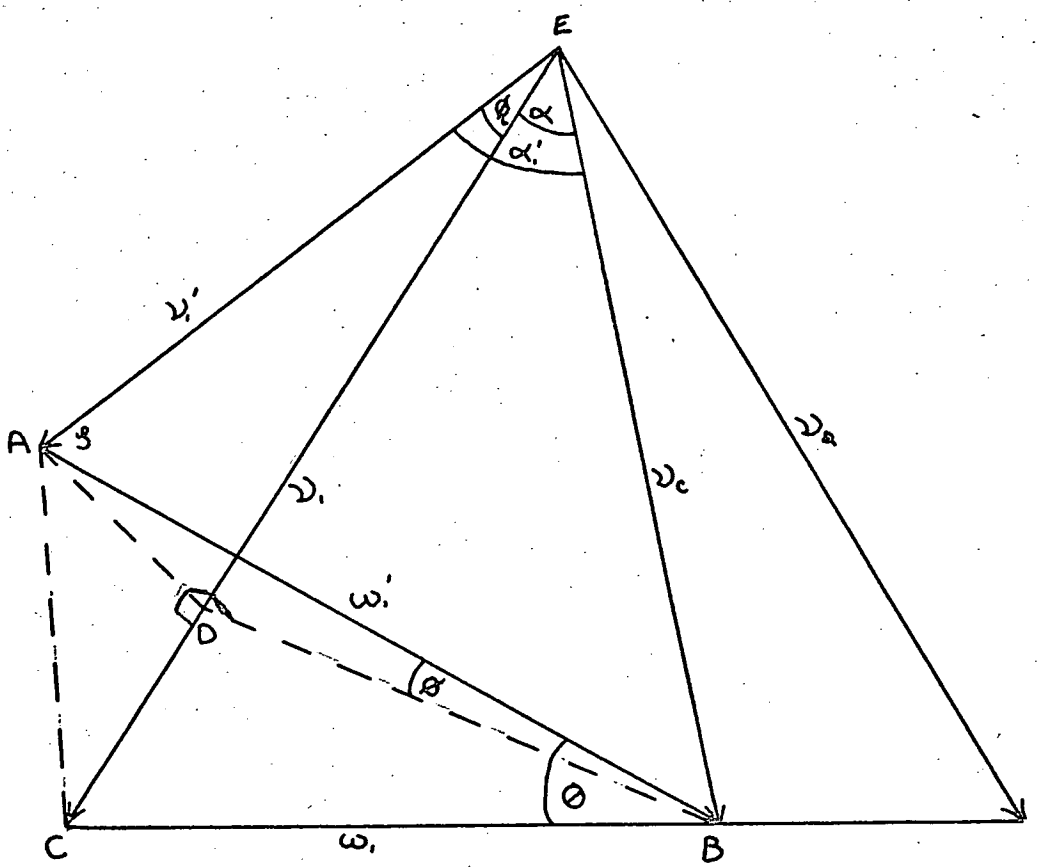

Fig. (2,3)

Centre of Mass to Lab transformation coordinates.

Now $$\cos\alpha_1' = \cos\alpha \cos\phi_L$$

$$\therefore \quad \cos\phi_L (v_1' v_c \cos\alpha - v_1' v_1)$$

$$= v_c^2 - v_1 v_c \cos\alpha - \omega_1' \omega_1 \cos\theta$$

but,

$$v_1' \sin\phi_L = AD = \omega_1' \sin\phi$$

$$\therefore \tan\phi_L = \frac{\omega_1' \sin\phi (v_c \cos\alpha - v_1)}{v_c (v_c - v_1 \cos\alpha) - \omega_1 \omega_1' \cos\theta}$$

which may be written as

$$\tan\phi_L = \frac{\omega_1' \sin\phi \; F}{G - H\cos\theta}$$

Now

$$AD = \omega_1' \sin\phi = DE \tan\phi_L$$

$$\therefore \quad DE = (G - H\cos\theta)/F$$

and

$$DC^2 = \omega_1'^2 \cos^2\phi + \omega_1^2 - 2\omega_1' \omega_1 \cos\theta$$

but

$$v_1 = ED + DC$$

$$\therefore \sin^2\phi = 1 - 2\frac{\omega_1}{\omega_1'}\cos\theta + \left(\frac{\omega_1}{\omega_1'}\right)^2 - \left[\frac{-Fv_1 + G - H\cos\theta}{F\omega_1'}\right]$$

Hence the centre of mass scattering angle θ may be related to the observed angle ϕ_L in the laboratory. It is also necessary to calculate the ratio of solid angle in the centre of mass to laboratory in order to transform the

differential cross sections in the centre of mass $\frac{d\sigma(\theta)}{d\omega}$ to those in the laboratory $\frac{d\sigma(\phi_L)}{d\omega_L}$

$$\frac{d\sigma(\phi_L)}{d\omega_L} = \frac{d\sigma(\theta)}{d\omega} \cdot \frac{d\omega}{d\omega_L}$$

where

$$\frac{d\omega}{d\omega_L} = \left(\frac{v_1'}{\omega_1'}\right) / |\cos\xi|$$

$$\cos\xi = (\omega_1'^2 + v_1'^2 - v_c^2)/2\omega_1' v_1'$$

General features of the scattered intensity

A useful model for the intermolecular potential is the Lennard-Jones (n,6) potential

$$V(r) = \frac{6\varepsilon}{n-6}\left[\left(\frac{r_m}{r}\right)^n - \frac{n}{6}\left(\frac{r_m}{r}\right)^6\right]$$

where ε is the well depth and r_m the equilibrium distance, n is frequently taken as 12. The scattering pattern was calculated for several reasonable values of e and r_m to obtain an idea as to which systems might be usefully studied. The results are shown in Figs. (2,4)-(2,6). Note that $I(\phi)\cdot\phi^2$ is plotted, this was done in order to remove the steep angular dependence.

It can be seen in Fig. (2,4) that the scattering pattern consists of two superimposed oscillations. The slower, frequency about 0.2^0, is the rainbow and supernumerary bows, on top of this can be seen much faster oscillations, frequency about 0.02^0, arising from diffraction effects.

Fig. (2,6) shows the scattered intensity from a much shallower well than that above. It will be seen that all structure is compressed into the first 0.1°. Clearly if any information is to be obtained about such a system a lower impact energy is required, Fig. (2,7), Fig. (2,8).

The following general conclusions may be drawn; the apparatus resolution must be about 0.15°, it was not practicable to attempt to resolve the faster oscillations. If it is considered that for useful measurements of the intermediate potential to be possible the rainbow angle must be greater than about 0.1°, then if a system of well-depth ϵ is to be studied, then the reduced energy E must be such that

$$E/\epsilon \leq 500$$

The variation of the scattering pattern with incident energy for a typical potential is shown in Fig. (2,6)-Fig. (2,8). It will be seen that as the energy decreases then the scattering pattern expands out along the ϕ axis. It will be realised, therefore, that different features of the potential may be studied by selection of the appropriate energy.

The differential cross-sections involved are typically in the range 10^{5}-10^{3} Å^2, it is shown in the next chapter that this corresponds to a scattered flux of from 100-1 particles/sec.

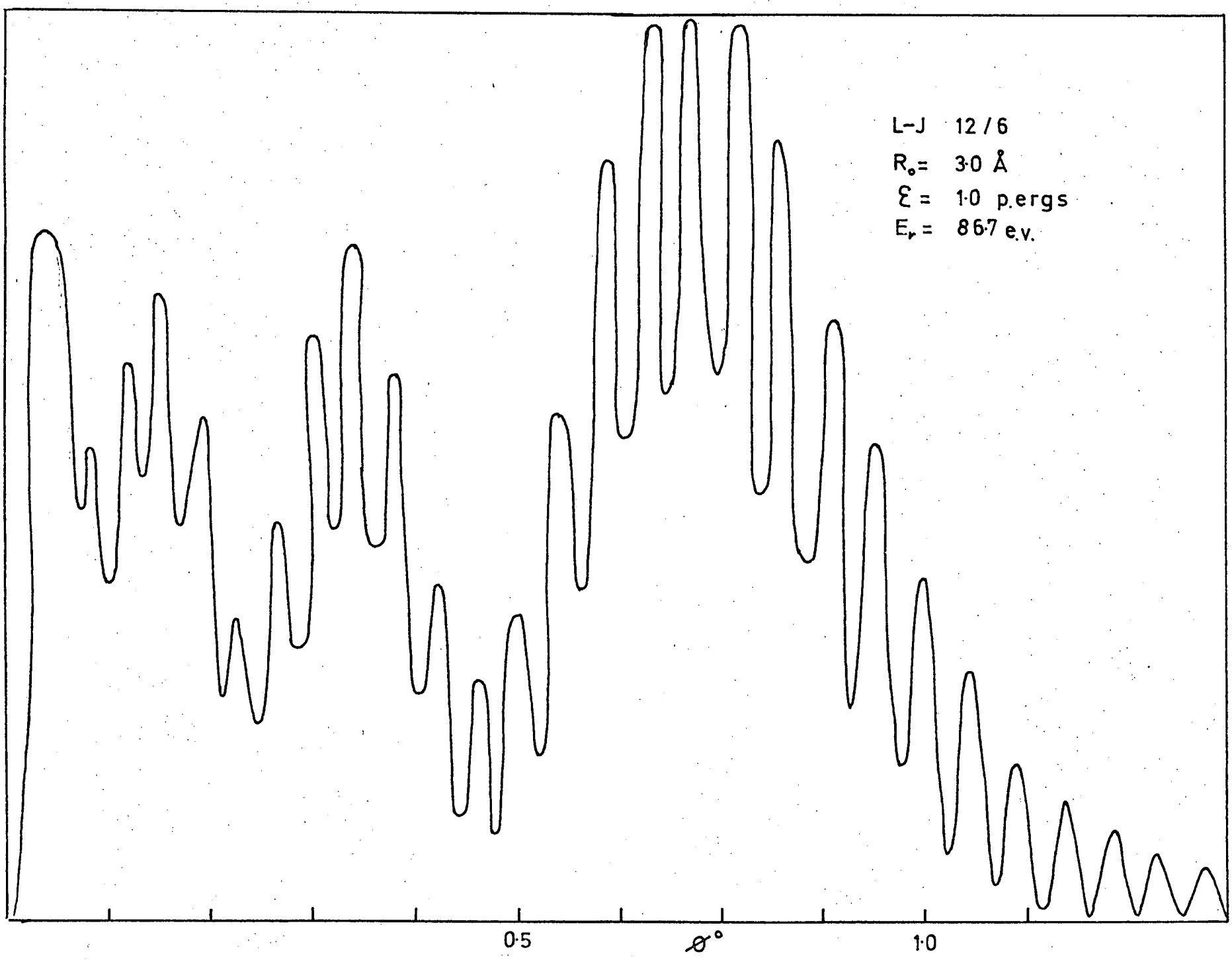

Fig. (2,4)

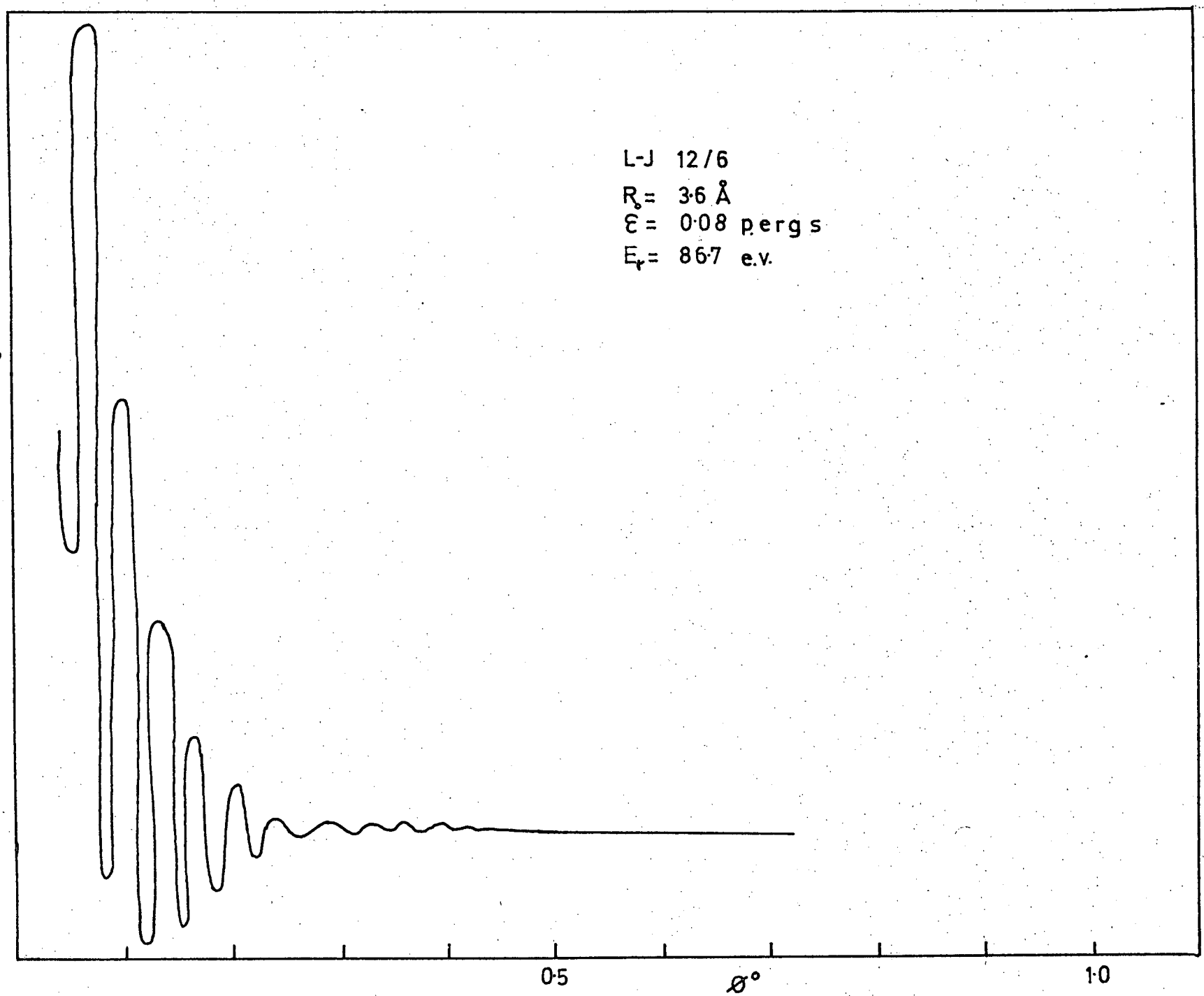
L-J 12/6
R_o = 3·6 Å
ε = 0·08 p.erg s
E_r = 86·7 e.v.
$I(\phi) \times \phi^2$
0·5
$\phi°$
1·0

Fig. (2,5)

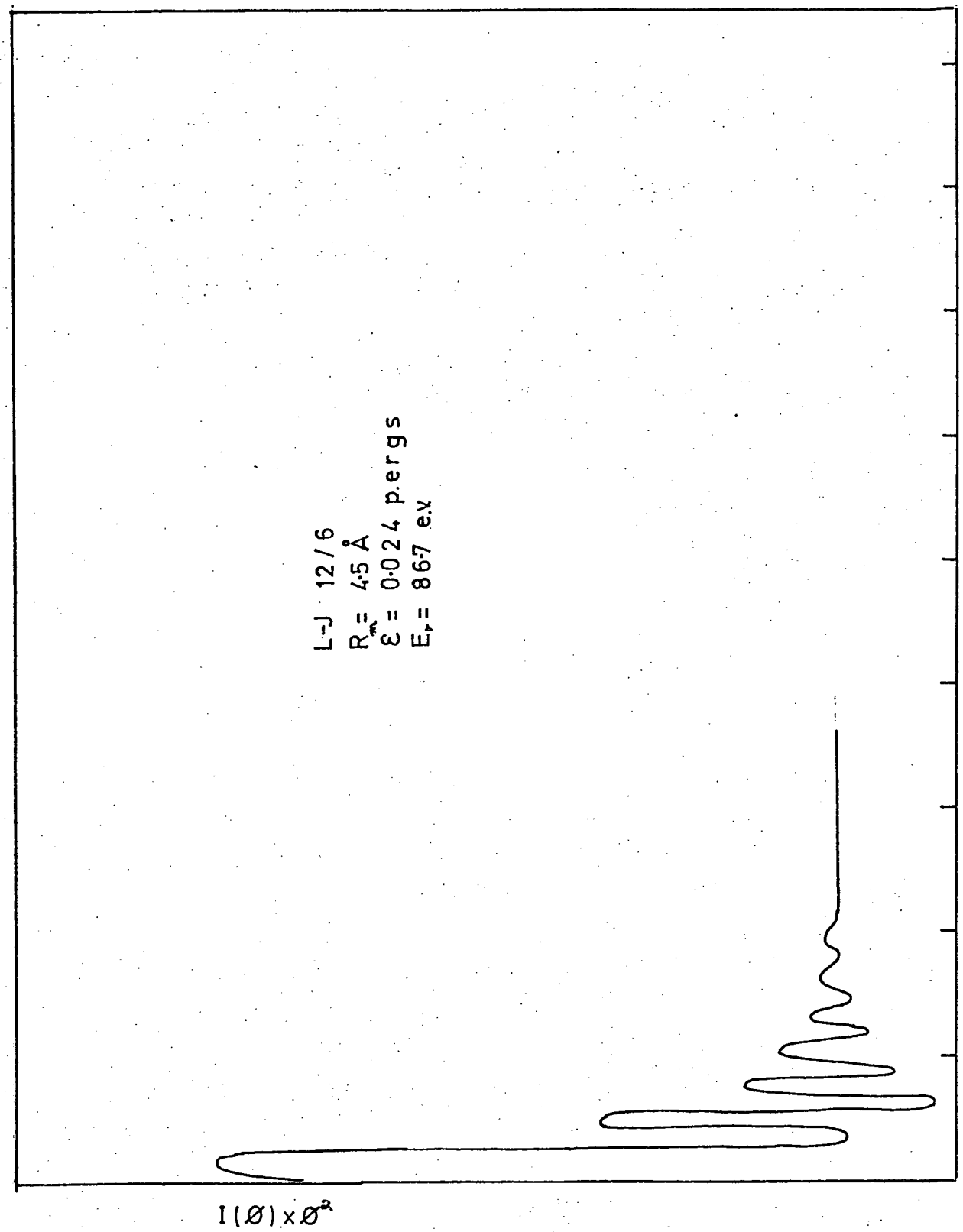

Fig. (2,6)

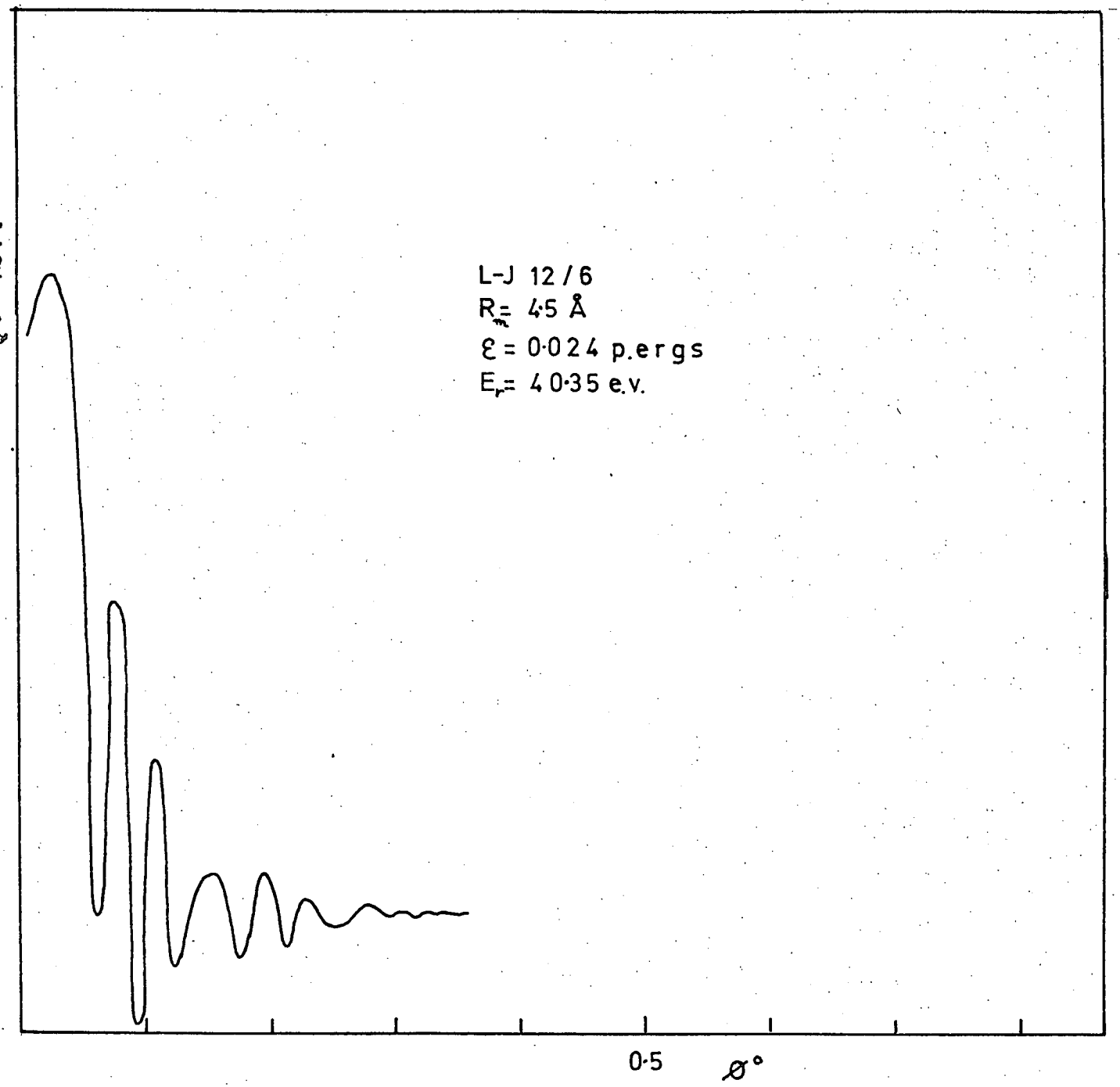

Fig. (2,7)

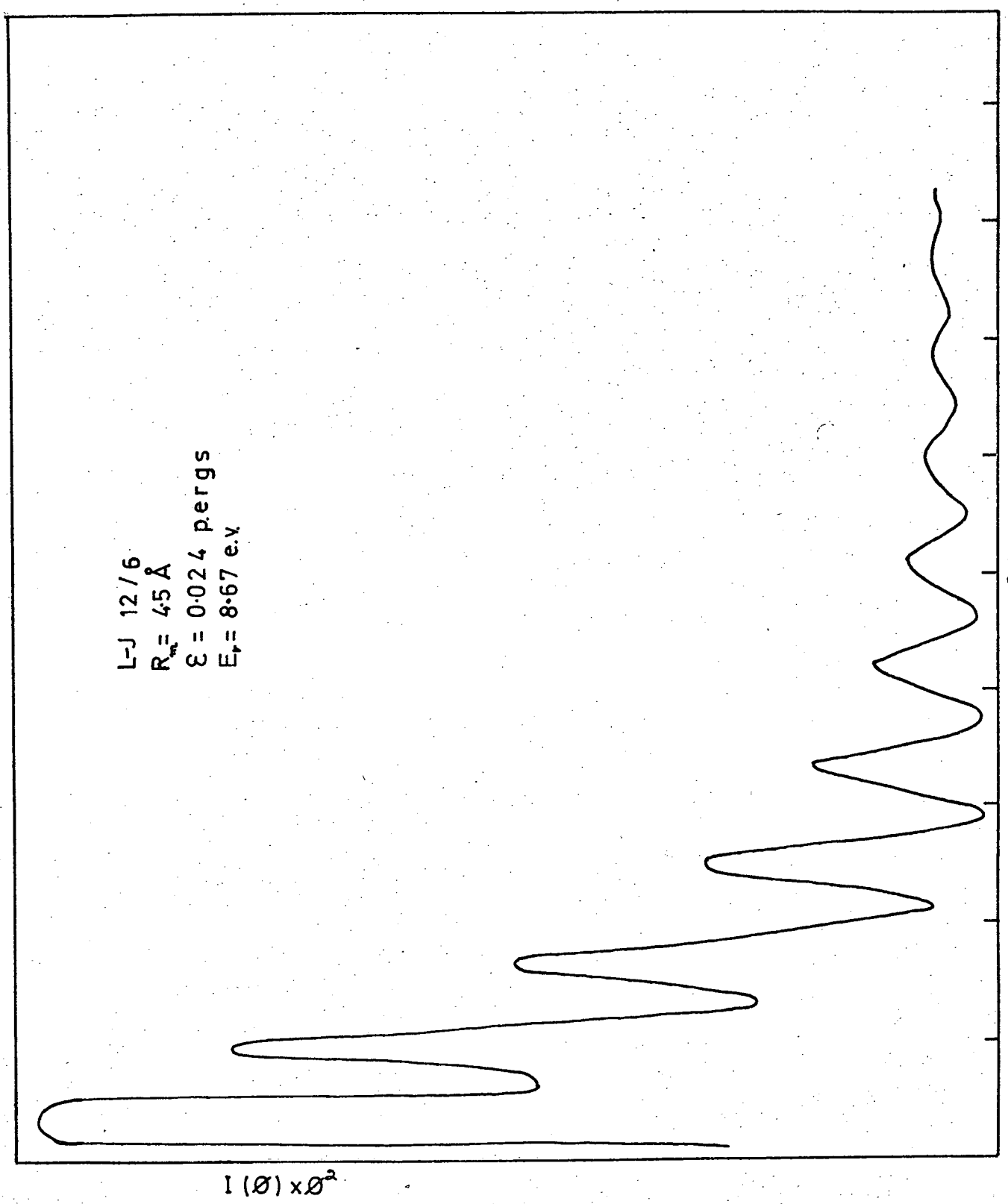

Fig. (2,8)

Electronic energies of KI and Na I

In its ground state an alkali halide is essentially ionic near the equilibrium distance, calculations based on such a model (RIT 51) agree well with experiment. However the products of the adiabatic dissociation of an alkali halide molecule are two ground state atoms, hence the potential curve of the ionic state must cross that of a covalent state at some point R_c . Where

$$\frac{e^2}{R_c} = I(m) - E(x)$$

Where I(m) is the ionisation potential of the alkali and E(X) the electron affinity of the halogen. If the covalent state has the same symmetry as the ground state than the non-crossing rule applies (COU 52) and the potentials will have the form shown in Fig. (2,9). Curve (1) corresponds to the ionic state for $R > R_c$ and the covalent state for $R < R_c$, curve (2) corresponds to the covalent state for $R > R_c$ and the ionic state for $R < R_c$.

If the system is initially in state (2) with $R > R_c$ say, then if R is decreased at a finite rate there is a finite probability that a transition to state (1) occurs and the system follows the dotted path, Fig. (2,9). Such behaviour is of importance in spectroscopy (BER 57) and collision processes (CHI 69), (HOR 69). The system originally in state (2) may interact by either of the two potentials (1) or (2), the scattering from each will be coherent and hence interference effects will appear in the scattering pattern. Observation of such interference gives

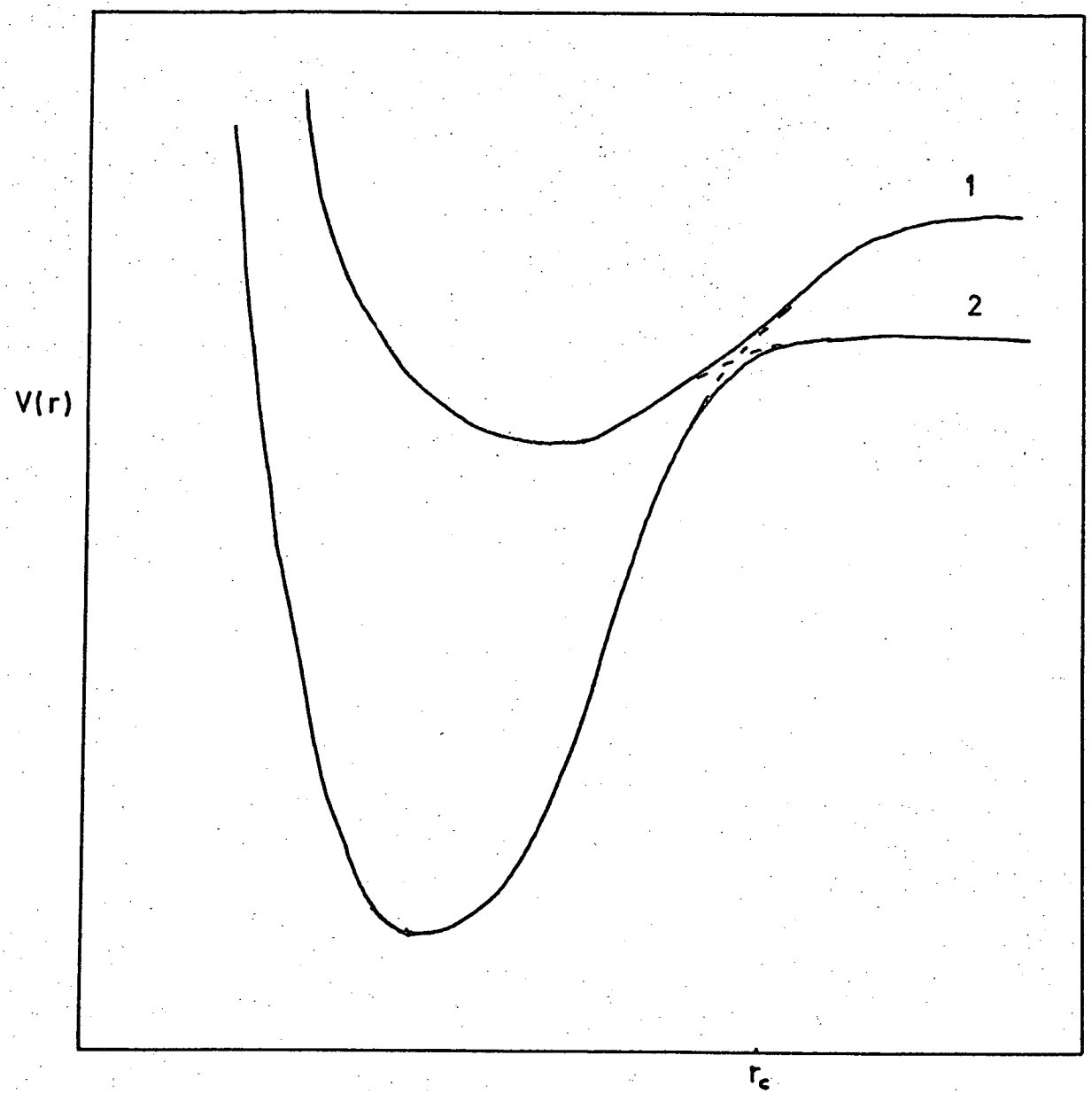

Fig. (2,9)

Alkali halide potentials.

details of the potentials in the region of R_c.

Following the argument of Zener (ZEN 32) it is expected that transitions between the two states will occur in a small region around R_c, the probability of transition depending on the energy difference between the two potentials and the relative velocity of the particles. The probability P of remaining in the same state on passing the crossing point, IE electron transfer occurs, is

$$P(b) = 1 - \exp(-\omega)$$

where $$\omega = \frac{2\pi |H_{1a}|^2 R_c^2}{\hbar v e^2}$$

and the separation between the potentials at R_c is $2/H_{12}/$. v is the radial velocity and is hence a function of the impact parameter b. It is important therefore to have some knowledge of the potentials in the region of R_c.

As a first approximation the system may be considered as a two state one electron problem, I.E. exchange interaction with the five p electrons of the halogen are ignored. The electronic wave function may be written as

$$\Psi(R,r) = C_1(R)\psi_1(r_1) + C_a(R)\psi_a(r_a)$$

where R is the internuclear separation and ψ_1 and ψ_a the alkali metal valence s electron and halide ion p electron wave-functions respectively. Following the standard variational procedure (COU 52) a quadratic in the system energy E(R) is obtained.

$$(1-S^2)E^2(R) + 2(h_{1a}S - E_1 - E_a)E(R) + E_1E_a - h_{1a}^2 = 0$$

where

$$S = \int \psi_1 \psi_a \, d\tau$$

$$h_{1a} = \int \psi_1 H \psi_a \, d\tau$$

$$E_1 = \int \psi_1 H \psi_1 \, d\tau$$

$$E_a = \int \psi_a H \psi_a \, d\tau$$

H being the electronic Hamiltonian

$$H = E_1 + E_2 + V(r_1) + V(r_2)$$

E_1 and E_2 being the eigen-energies of the isolated particles, $V(r_1)$ and $V(r_2)$ are the potentials experienced by the electron due to the alkali metal core and the halide atom respectively.

Calculations were performed for the systems K/I and Na/I, these are of particular interest having been studied extensively spectroscopically (BER 57). Marked differences in the spectra, attributed to the "crossing" of the potentials, have been observed. The systems have also been studied using crossed thermal beams (HOR 69).

The basis wave-functions $\psi_1(r_1)$ and $\psi_a(r_2)$ were of the Hermann and Skilman type, those of Na and K were obtained from Hermann and Skilman's book (HER 63), that for I^- was calculated by Narasimhan (NAR 69). The potentials $V(r_1)$ and $V(r_2)$ were of the Hartree type and were calculated from the tabulated wave functions. The various integrals involved were evaluated numerically using Simpson's rule. It was assumed that the axis of quantisation lay along R.

The calculated crossing distances were 12.1 Å and 6.4 Å for K/I and Na/I respectively, this compares with 11.3 Å and 6.9 Å calculated using the known ionisation potentials and electron affinities. The separation of the potentials at the crossing point was 5.2×10^{-15} ergs and 2.4×10^{-13} ergs for K/I and Na/I respectively. The difference between the two systems is very striking.

Recent experimental work by Moutinho on the inelastic scattering of K/I and Na/I gave H_{12} as 4.4×10^{-15} ergs for K/I and 8×10^{-14} ergs for Na/I (MOU 71). Fluendy's (FLU 70) work on the elastic scattering of K/I gave a value of approximately 6×10^{-15} ergs. Having obtained R_c and H_{12} the transition probability for the two systems was calculated using the Landau-Zener approximation. The results obtained can serve as a qualitative guide only however. If p is the probability of adiabatic behaviour on one traversal of the crossing point then the probability of the system, having started in state (2), being in state (1) after a collision is

$$P(b) = 2p\,(1-p)$$

The variation of p and P(b) with b is shown in Fig. (2,10) and Fig. (2,11). It will be seen that K/I is essentially diabatic at all but the lowest energies. The total cross-section for the system finishing in state (1) is

$$Q = 2\pi \int_0^{R_c} P(b)\, b\, db$$

If comparison is to be made with experimentally determined cross-sections then account must be taken of the

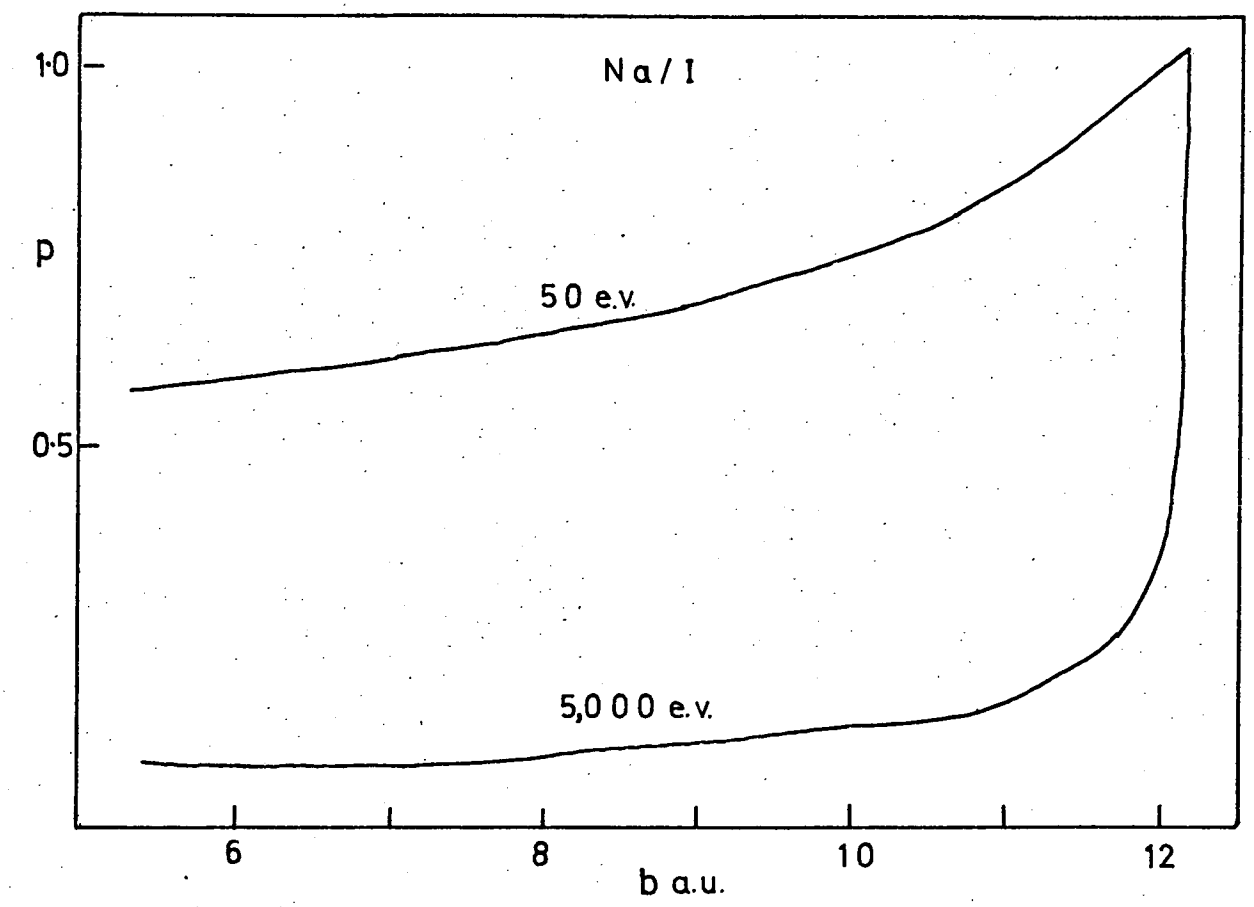

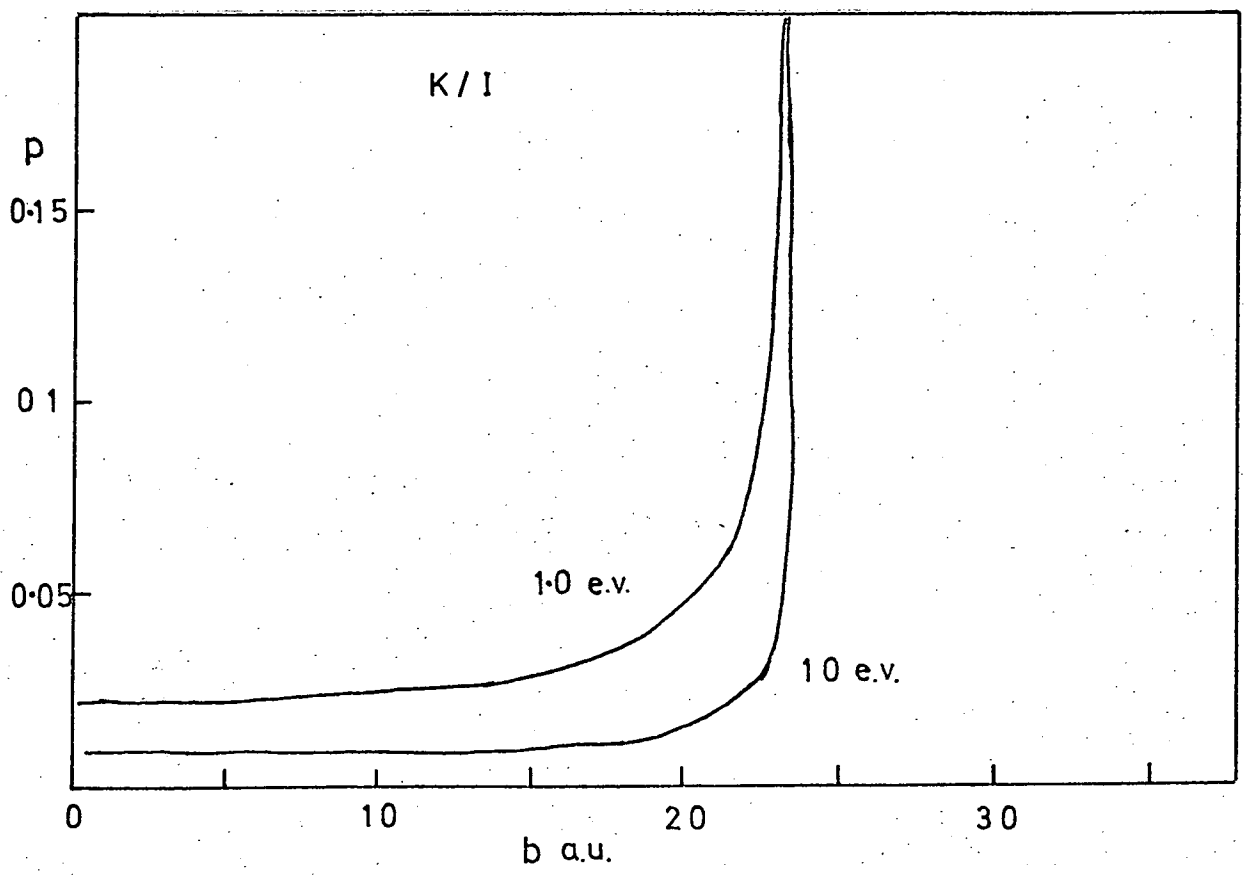

Fig. (2,10)

Probability of adiabatic behaviour as a function of impact parameter.

Probability of ion-formation, Landau Zener.

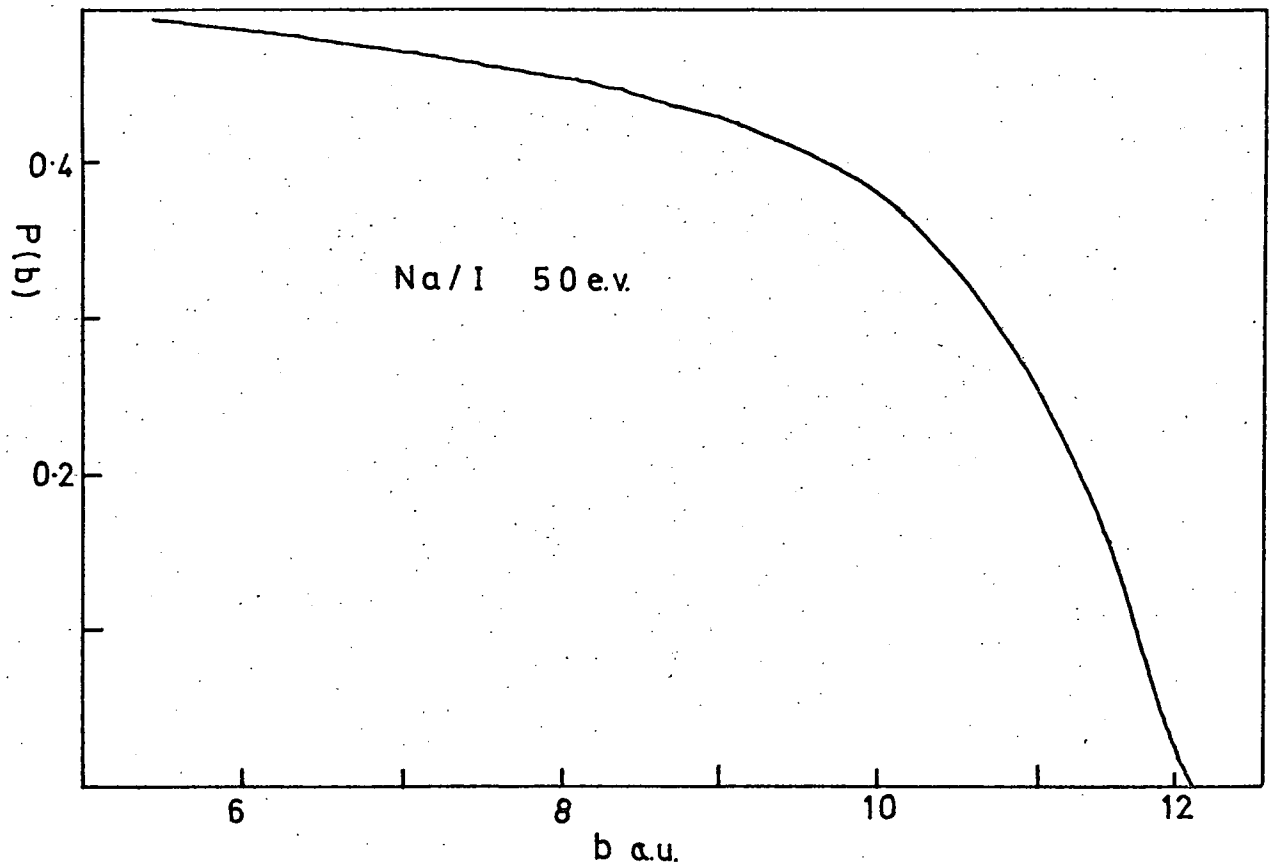

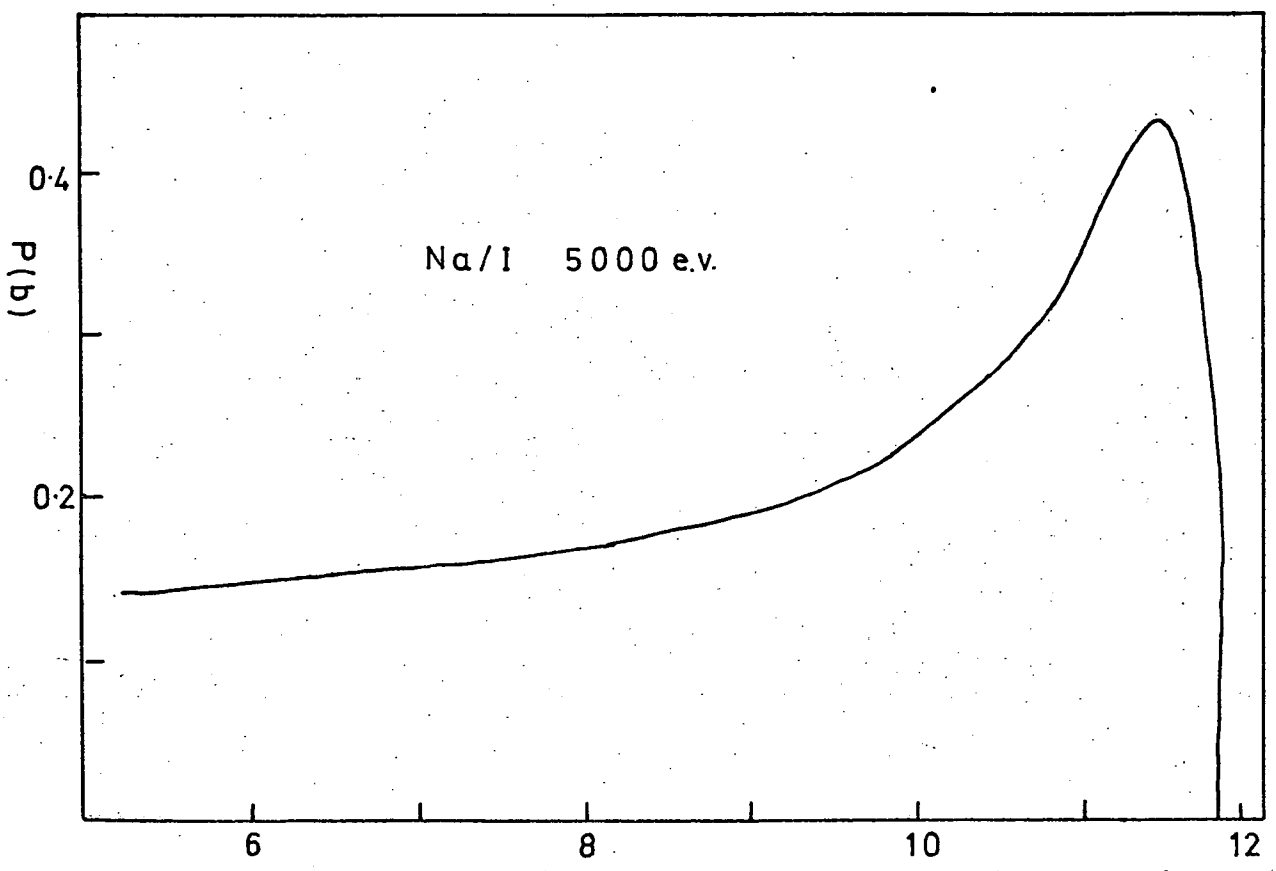

Fig. (2,11)

statistical weights of the states. (HOR 69).

The variation of Q with energy is shown in Fig. (2,12).

As the Landau-Zener approximation is known to have serious limitations (COU 62), (BAT 60) a more rigorous approach was attempted. The method used was a modification of that developed by Bates, Johnston and Stewart (BAT 64), and is similar to the well known variation of constants.

The nuclei M and X were treated as classical particles moving with a constant velocity V. R was taken as the position vector of M relative to X and Z = $\underline{R}.\underline{V}$. It was assumed that an electron was transferred from state 1 associated with the alkali metal M to state 2 associated with the halogen X. For simplicity the electronic wave functions for states 1 and 2 were identified as the atomic eigen-functions. $V(r_1)$ and $V(r_2)$ were taken as the potentials experienced by the electron in states 1 and 2 respectively. The complete electronic wave-function may be written as

$$X = C_1 \psi_1 (r_1) + C_2 \psi_a (r_2)$$

where $\psi_1 (r_1)$ and $\psi_a (r_2)$ are the atomic eigen-functions. It should be noted that the coefficients C1 and C2 have no connection with those appearing in the L.C.A.O. calculation above. The use of such diabatic potentials has been justified by Dykne and Chaplik (DYK 63). The variatiations of the coefficients during a collision are given by

Fig. (2.12)

Total ion-production cross-sections.

$$i v \frac{dC_1}{dZ} = C_2 \bar{K}(R) \exp(i I(Z)/v)$$

$$i v \frac{dC_2}{dZ} = C_1 \bar{K}(R) \exp(-i I(Z)/v)$$

where

$$\bar{K}(R) = \frac{h_{12} + h_{12} - S(h_{11} + h_{22}}{2(1-\bar{S}^2)}$$

$$I(Z) = \int_{Z_0}^{Z} g(R)dZ$$

$$g(R) = E_1 - E_2 + \frac{h_{11} - h_{22} + S(h_{12} - h_{21})}{1 - S^2}$$

$$h_{12} = \int \psi_1 V(r_1) \psi_2 \qquad h_{21} = \int \psi_2 V(r_2) \psi_1$$

$$h_{11} = \int \psi_1 V(r_2) \psi_1 \qquad h_{22} = \int \psi_2 V(r_1) \psi_2$$

$$S = \int \psi_1 \psi_2$$

E_1 and E_2 being the atomic eigen energies and Z_0 being arbitrary (BAT 59). Clearly C_1 and C_2 are dependent on the impact parameter b.

Writing

$$C_1 = a + ib \text{ and } C_2 = C + id$$

substituting in the above equations and equating real and imaginary parts, the following four real equations are obtained.

$$\dot{va} = \bar{K}(c \sin I + d \cos I)$$

$$-\dot{vb} = \bar{K}(b \cos I - d \sin I)$$

$$\dot{vc} = \bar{K}(b \cos I - a \sin I)$$

$$-\dot{vd} = \bar{K}(a \cos I + b \sin I)$$

where $I = I(Z)/V$

The probability of the system being in state 1 is $a^2 + b^2$ and in state 2 $c^2 + d^2$. It can be shown that probability is conserved I.E.

$$a^2 + b^2 + c^2 + d^2 = 1$$

Taking the initial conditions as

$$a^2 + b^2 = 1$$

$$c^2 + d^2 = 0$$

the equations were solved using the Runge-Kutta method. Computational difficulties limited the impact parameter to being greater than about 5 a.u. It was not considered that this would have a serious effect on the total cross-section.

The probability of ion-formation I.E. $c^2 + d^2$, as a function of impact parameter for the system Na/I is shown in Fig. (2,13), the maximum will be seen to occur around $b = R_c$. In the case of K/I behaviour was found to be essentially diabatic in the energy range considered. The total ion-production cross-section for Na/I was calculated as above I.E.

$$Q = 2\pi \int b\, P(b)\, db$$

The variation of Q with energy is shown in Fig. (2,14), it was found that

$$Q \propto E^{-.47}$$

in agreement with the limiting behaviour of the Landau-Zener formula (BAT 54). In general however the Landau-Zener formula predicts much larger cross-sections, Fig. (2,12).

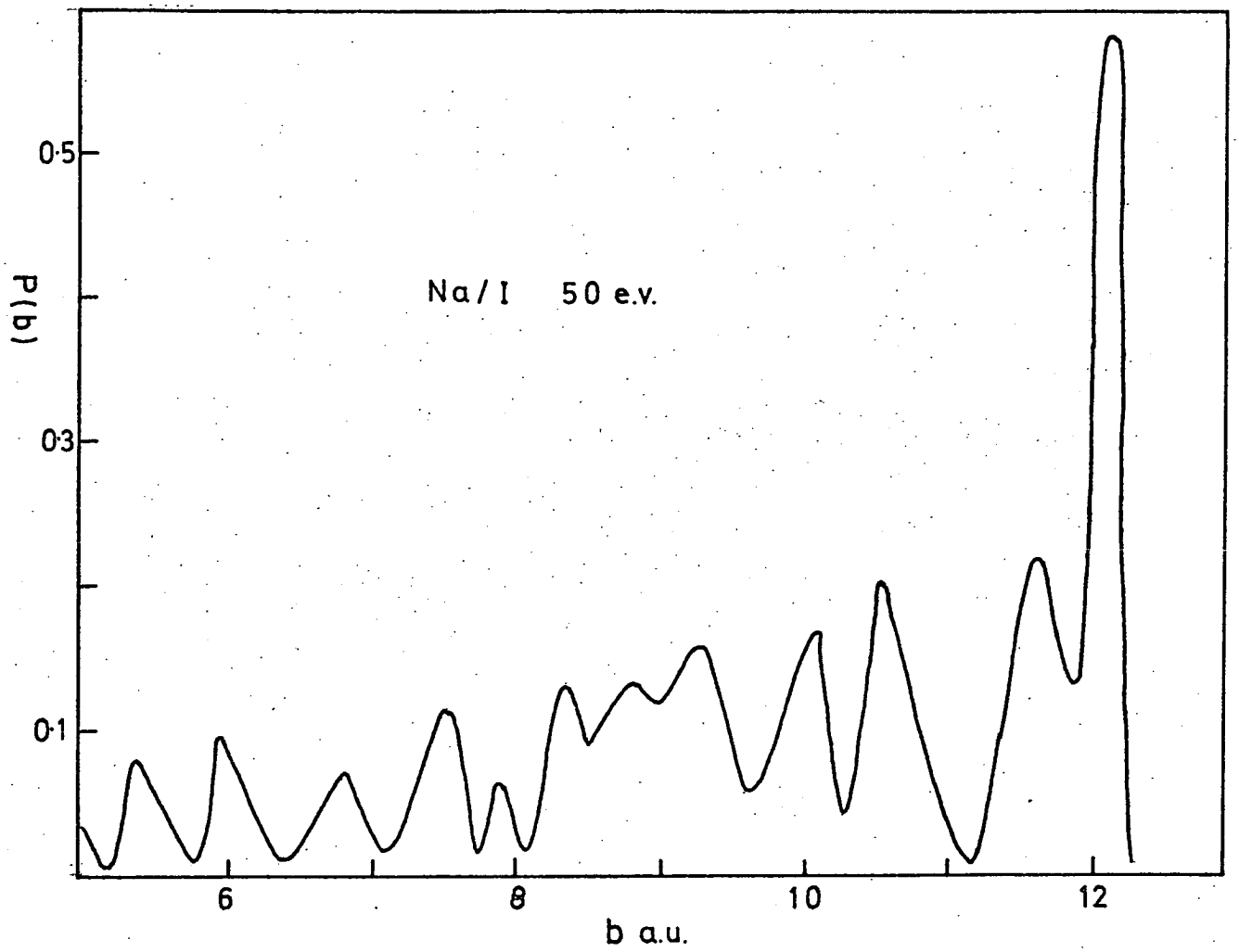

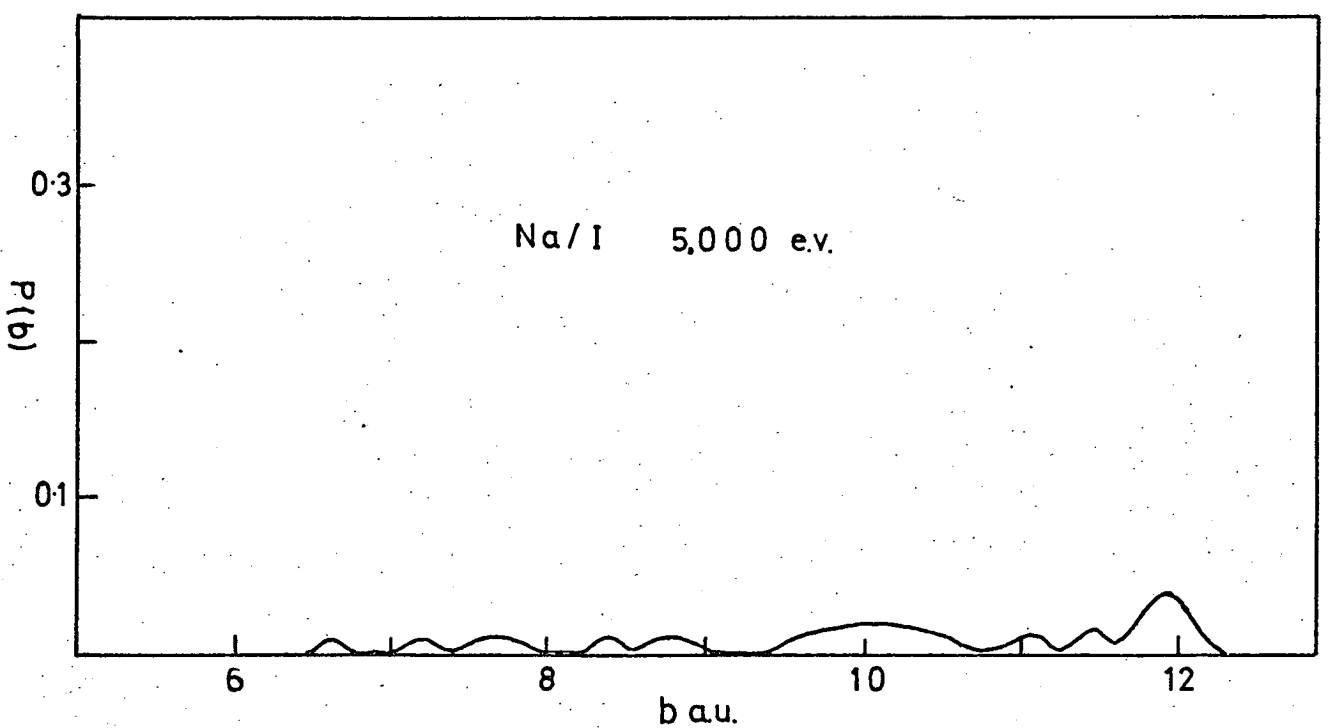

Fig. (2,13)

Probability of ion-formation.

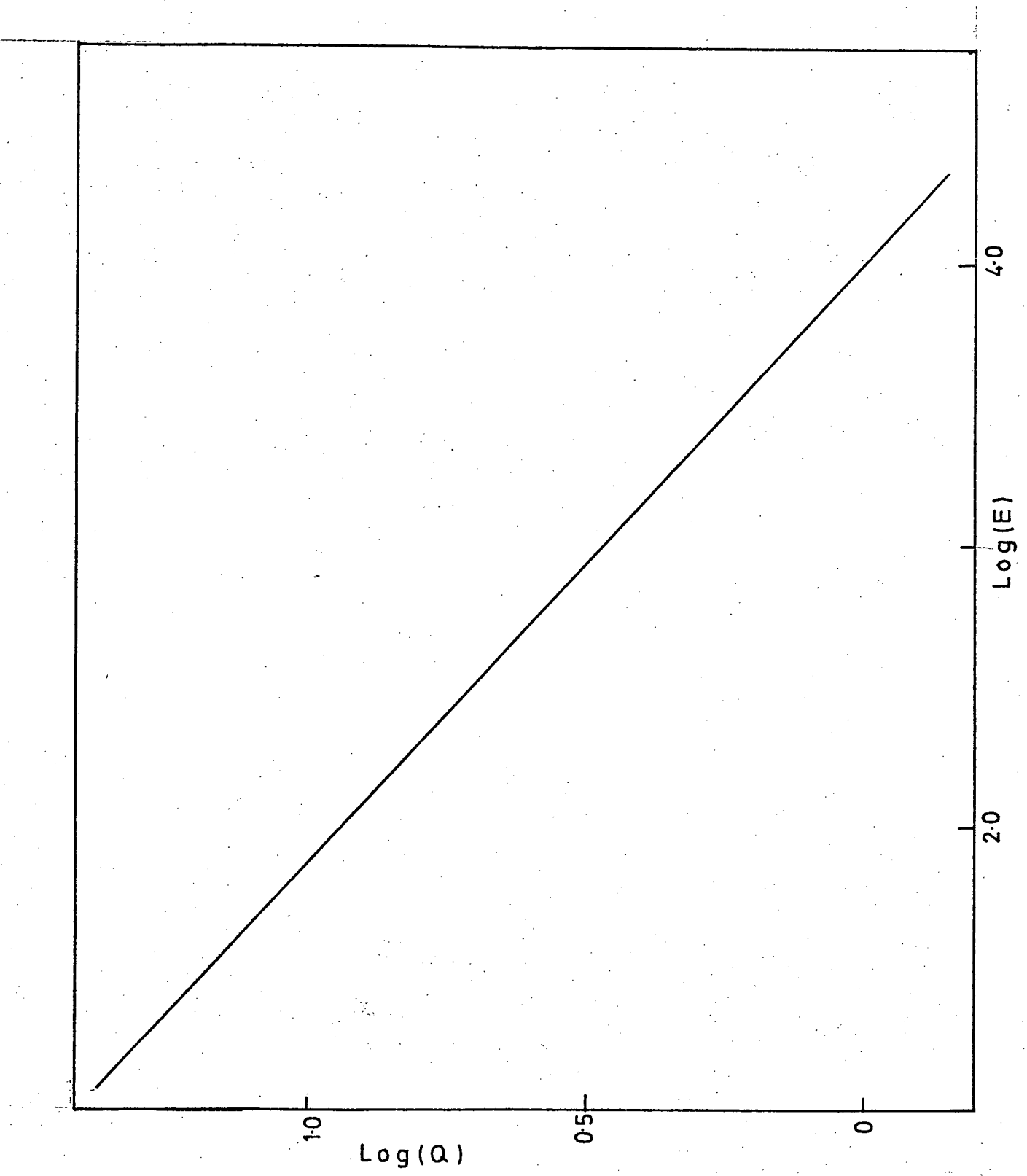

Fig. (2,14)

Total ion-production cross-section.

The total ion-production cross-section for the alkali metal/halogen atom systems has been calculated by Bandrauk (BAN 69) using the distorted wave approximation. He obtained the expression

$$Q = 7 \times 10^6 \frac{S^2}{\Delta E^2} \left(\frac{2\mu}{E} \right)^{\frac{1}{2}} \text{Å}^2$$

where S is the overlap at R_c and ΔE the difference between the alkali metal ionisation potential and halogen electron affinity. Both E and ΔE are in electron volts. It will be seen that again it is predicted that

$$Q \propto E^{-\frac{1}{2}}$$

For Na/I E = 2.06 e.v. Using Slater type orbitals Berry (BER 57) estimated the overlap in Na/I to be 3.2×10^{-3}, however using Hermann-Skilman wave functions a value of 5.9×10^{-3} was obtained. Using these values of S total cross-sections of 10.6 Å^2 and 34.9 Å^2 at 100 e.v. were calculated. Clearly the absolute magnitude of the total cross-sections must remain in doubt until experimental data are available.

It is expected that the approximation outlined above will break down at both high and low energies. The reason for failure at low energies is clear enough, the relative velocity can not be considered constant under such conditions. It is therefore not possible to obtain any information for energies near the ionisation threshold. This sets a lower limit of around 5 e.v. The upper energy

limit arises in a rather more subtle way; when the electron "jumps" from one atom to the other, as one atom is moving faster than the other, the electron experiences a change in momentum, this has been neglected in the above. As the relative energy of the two particles increases so the effect becomes more important. Bates and McCarroll (BAT 58) have shown that the change in the electrons momentum may be ignored if

$$VZ \ll 1$$

where V is the relative velocity and Z the extent of the smaller wave function in atomic units. Taking Z = 7 a.u. then for the approximation to be valid

$$V \ll 3 \times 10^7 \text{ cms/sec}$$

which in the systems considered corresponds to an energy of about 20 k.e.v. In the energy range considered the change in the electrons momentum may be neglected.

Unfortunately it was not possible to extend these calculations to the systems K/I_2, Na/I_2. The crossing distances R_c for these systems are 5.5 Å and 4.1 Å respectively hence behaviour similar to Na/I might be expected i.e. essentially adiabatic.

Classical trajectories for the K/I_2 system.

When a potassium atom collides with an iodine molecule a number of processes may occur. In order to obtain a qualitative picture of the collision a model was postulated and the classical trajectories calculated. The model used as based on the spectator model of chemical reaction (HER 66).

It was assumed that when the K/I_2 separation reached a value R_c given by

$$\frac{e^2}{R_c} = I_K - E_I$$

where I_K and E_I are the potassium ionisation potential and iodine electron affinity, then the potassium valence electron transferred to the iodine molecule. Three different channels were then open to the system

$$K + I_2 \longrightarrow KI + I \qquad (1)$$

$$K + I_2 \longrightarrow K + I_2^* \qquad (2)$$

$$K + I_2 \longrightarrow K + I + I \qquad (3)$$

Cross-sections for the three processes have been estimated for a range of energies.

It was assumed that the I_2 molecule was initially at rest and had zero vibrational and rotational energy. It was also assumed that after electron transfer I_2^- behaves as I^- I with no interaction between the two particles, the I atom therefore remains fixed in space.

The electron affinity of I_2 is uncertain, values ranging from 1.2-2.6 e.v. have been reported. In order to simplify calculation the following procedure was used to estimate E_{I_2}. The electron affinity of I is accurately known, 3.2 e.v., as is the bond energy of I_2, 1.5 e.v., the electron affinity of I_2 was taken as 3.2-1.5 e.v. this is in good agreement with Person's value (PER 63).

The results are shown in Figs. (2,15), perhaps the most striking feature is the cross-section for reactive scattering, the model predicts that for energies greater than about 2.5 e.v. no KI is formed.

As the energy is increased above 2.5 e.v. the dominant process is the dissociation of the iodine molecule. At energies above 10 e.v. vibrational excitation becomes more important than dissociation; the I ion is simply not able to respond in the time of the collision and the energy transferred to the iodine molecule decreases.

As the energy is increased still further the situation is reached in which the I remains virtually stationary during the collision and there is almost no transfer of energy, the collision is therefore essentially elastic.

Clearly the results derived from this crude model can not be taken too seriously but a qualitative picture is obtained. The most serious weakness of this model is the neglect of the I.I interaction. I_2 has a well depth of

Classical reactive and inelastic total cross-sections.

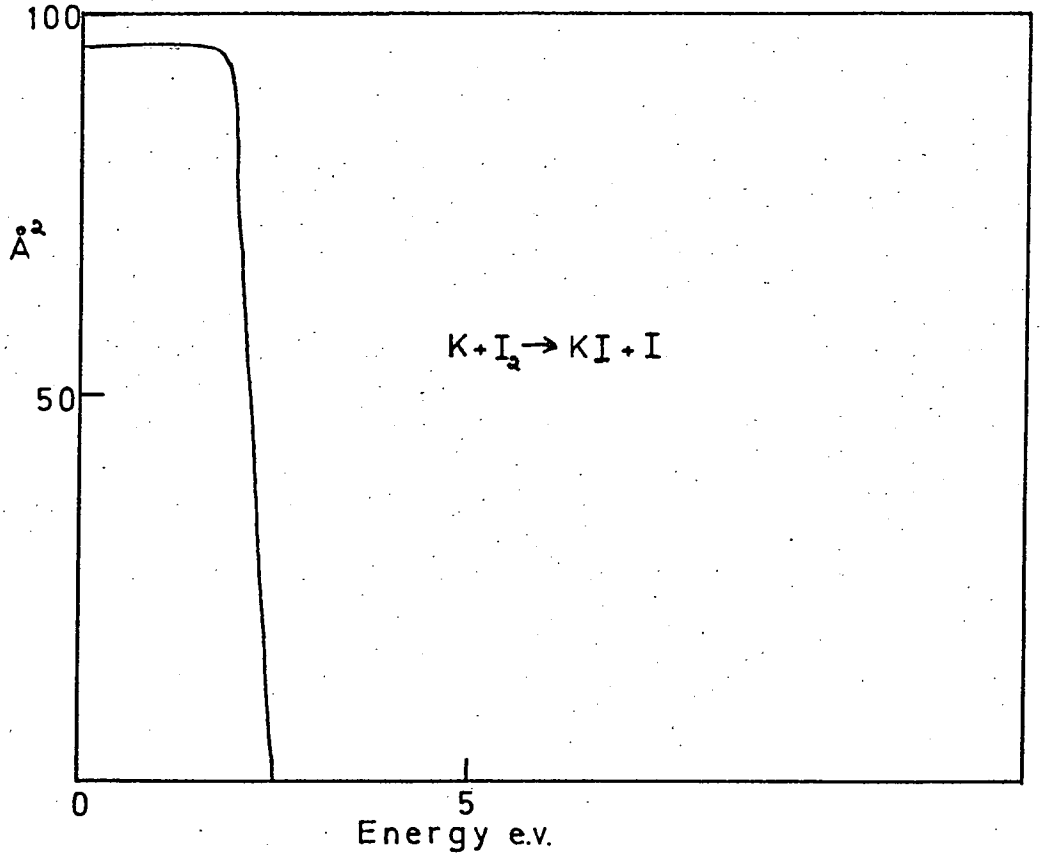

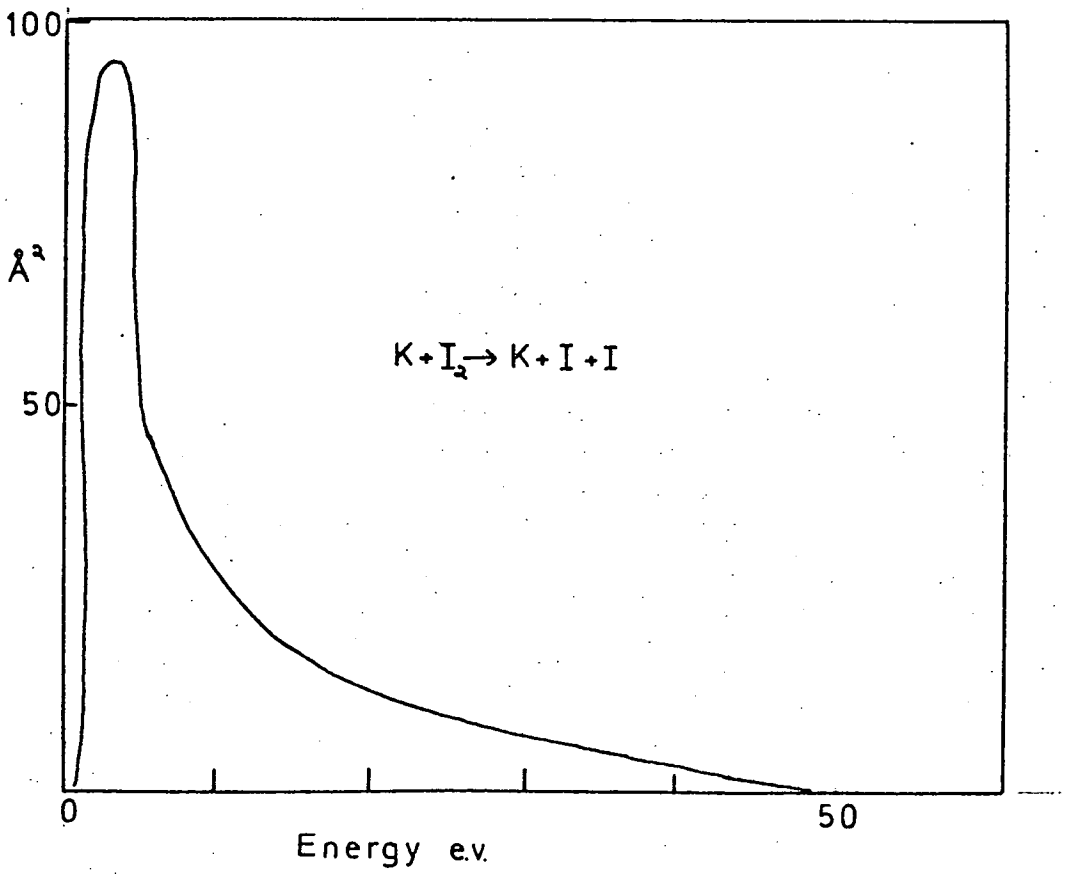

Fig. (2,15).

about 0.8 e.v and an equilibrium bond distance of about 3.2 Å (PER 63). This will certainly modify the assumed coulombic $K^+I_2^-$ potential. Work is at present in hand in this laboratory to calculate classical trajectories, account being taken of all interactions, the effect of varying the I_2^- potential may then be examined.

CHAPTER III

EXPERIMENTAL.

Aim of Experiments.

Superthermal molecular beams may be used to study a great variety of elastic and inelastic processes. Flexibility is therefore an important criterion in the design of an apparatus.

In designing the apparatus several possible applications were anticipated. These were; to obtain intermolecular potentials by elastic scattering studies, to measure energy loss spectra by time of flight and hence obtain details of vibrational-translational energy transfer and finally to measure the intermolecular potential in chemically reactive systems with a view to extending our understanding of chemical dynamics.

It was shown in the previous chapter that an apparatus resolution of about 0.15° is required to study elastic scattering. It should also be possible to make measurements out to about 5° from the main beam. The expected scattered signal is small hence counting techniques must be used. Care must also be taken to reduce background noise to a minimum. If energy loss spectra due to vibrational excitation are to be measured then an energy resolution of better than 0.5 e.v. is required. A monochromatic source, or some form of velocity selector, would be necessary. As the scattered signal will be very small a very efficient data collection system will be required e.g a multichannel analyser or on-line computer.

The requirements for the study of chemically

reactive systems are similar to those outlined above. In addition it should be possible to distinguish between reactants and products either by conventional mass-spectrometry or by time of flight.

This chapter is an account of the design, construction and operation of an apparatus to meet the above requirements. To date the apparatus has been used primarily for the study of elastic collisions although time of flight facilities have been partially developed and tested.

Introduction

The apparatus was designed to measure differential cross-sections at superthermal energies for a variety of systems, the major design requirements have been outlined above.

For reasons which will be considered in the next section the alkali metals were chosen as the main beam material. A variety of materials could be used as the collision partner.

The main features of the apparatus are shown in Fig. (3,1). There were four separately pumped chambers, the first two contained the main-beam source and the third the cross-beam source. The detector chamber was connected to the third chamber by means of flexible bellows and could be rotated by $\pm 10^{\circ}$ round the main beam. The detector could be rotated by increments as small as 0.002°, increments less than 0.01° were not normally used however.

The detector was of the surface ionisation type and was followed by a quadrapole mass-spectrometer and an electron multiplier. Pulse counting techniques were used to permit the measurement of very weak signals and also to eliminate noise due to drift in the multiplier gain.

The scattered signal, detector position and other relevant data were recorded on paper tape and subsequently analysed by computer.

The rest of this chapter divides into four sections, the vacuum chambers etc., the sources, the detector and data handling system and finally the experimental procedure.

Apparatus.

In discussing the design of the apparatus three major points must be dealt with, the vacuum system itself, the internal location and alignment of components and finally the means by which the detector and the main beam may be rotated relative to each other.

To reduce noise arising from spurious scattering it is desirable that the detector and each of the two sources be separately pumped. In order that the mean free path of beam particles be greater than the apparatus dimensions background pressures should be 10^{-6} torr or better.

The correct alignment of components such as sources and slits etc. is of great importance in this type of work. Not only is it important that the apparatus may be aligned to start with it is a great help if on dismantling and subsequent reassembly as little as possible is disturbed. The main frame, on which the apparatus sits, consists of $1\frac{1}{2}$" square mild steel tube arc welded to form a bed 10' x 3' x 26". The legs were provided with adjustable feet for levelling. Two flat and parallel mild steel bars were bolted along the length of the frame. These bars provided the datum to which all measurements were referenced.

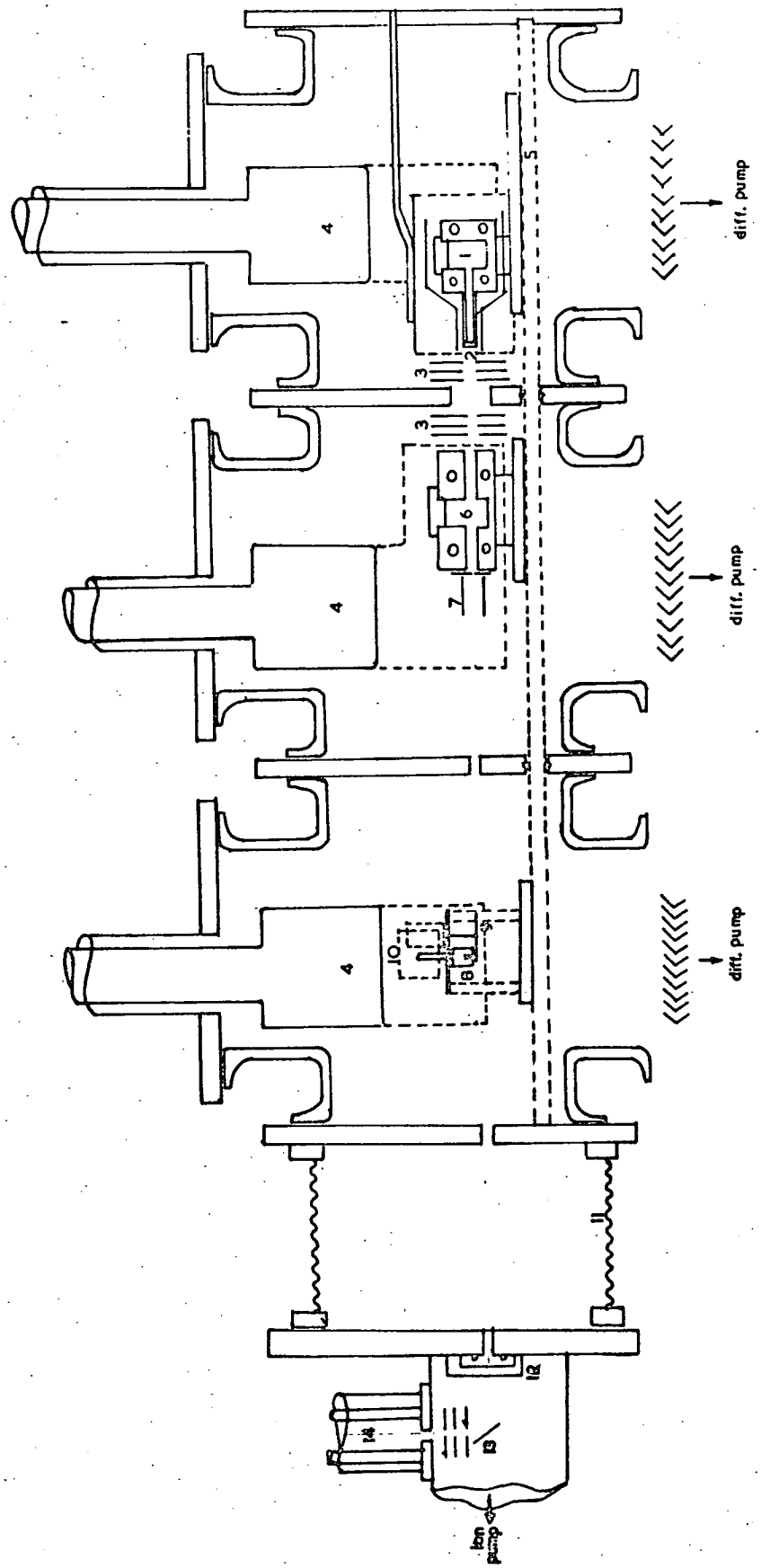

Fig. (3,1)

Schematic of Apparatus.

1. Alkali metal supply oven
2. Ioniser
3. Lens
4. Cold traps
5. "Optical" Bench
6. Charge exchange chamber
7. Ion collector plates
8. Cross-beam dissociation chamber
9. Chopper Disc
10. Cross-beam supply oven
11. Stainless steel bellows
12. Gate valve
13. Detector
14. Quadrapole mass spectrometer

An "Optical" bench on which the main-beam and cross-beam could be located was built up as follows: The bulkhead separating the detector and scattering chambers Fig. (3,2), was located perpendicular and square to the datum bars and bolted to them. The bulkhead closing the end of the vacuum system was similar in construction but was located in guide rails to allow some adjustment along the length of the apparatus. Running between the two bulkheads were two 1" diameter stainless-steel bars, these were a tight fit in locating holes in each bulkhead. The bars therefore provided a fixed bench on which the beam sources could be placed. Each component was mounted on a special kinematic base plate which had two grooves machined in it, Fig. (3,3), these provided accurate location on the bars. The vacuum system can now be imagined as being built round these fixed bars.

The vacuum system divides conveniently into two parts, that containing the sources, and the detector chamber. The source chambers consisted of three Q.V.F. P X 6 glass cross pieces separated by stainless-steel bulkheads Fig. (3,2). The cross pieces sat on dural plates, adjustable for height and inclination by means of corner screws. The components were held rigidly together by means of clamping rings. Great care had to be taken on assembly to ensure that no part of the system was under stress. All vacuum seals were made by means of "O" rings.

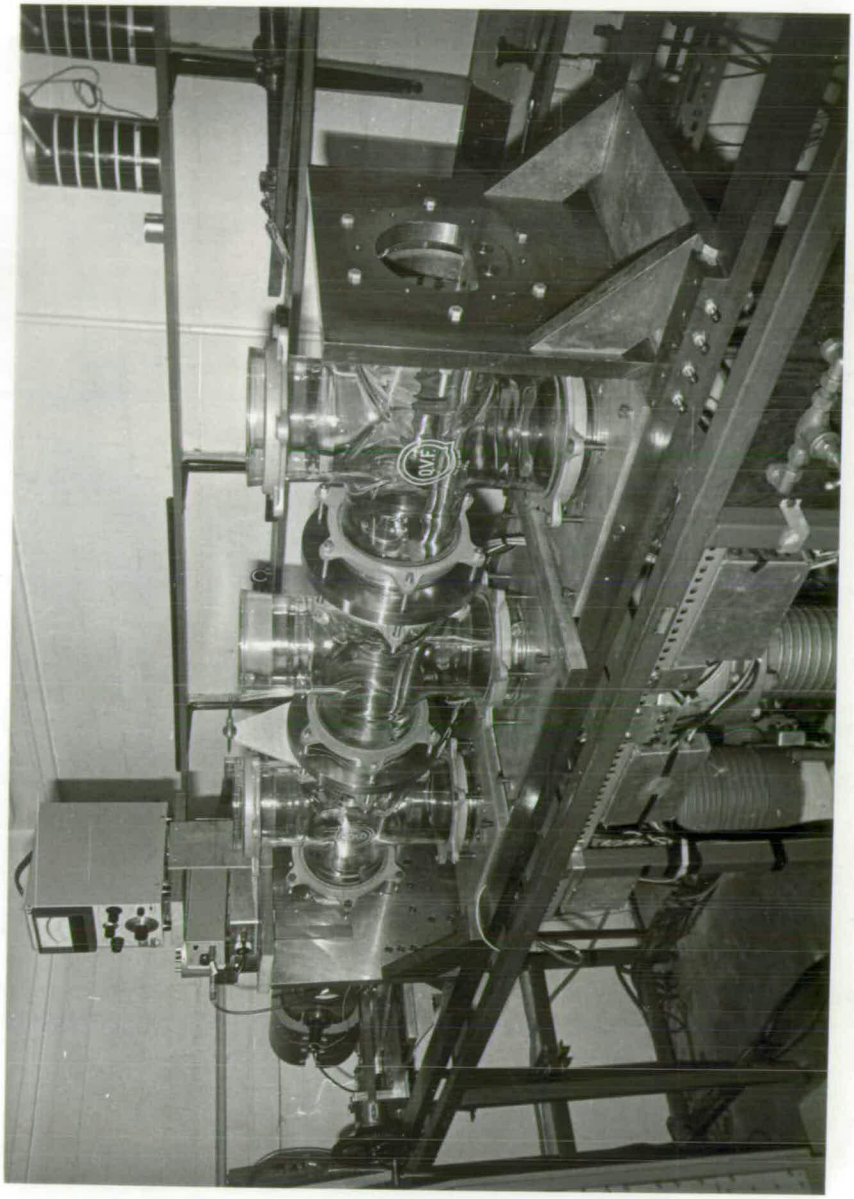

Fig. (3,2)

Superthermal Apparatus.

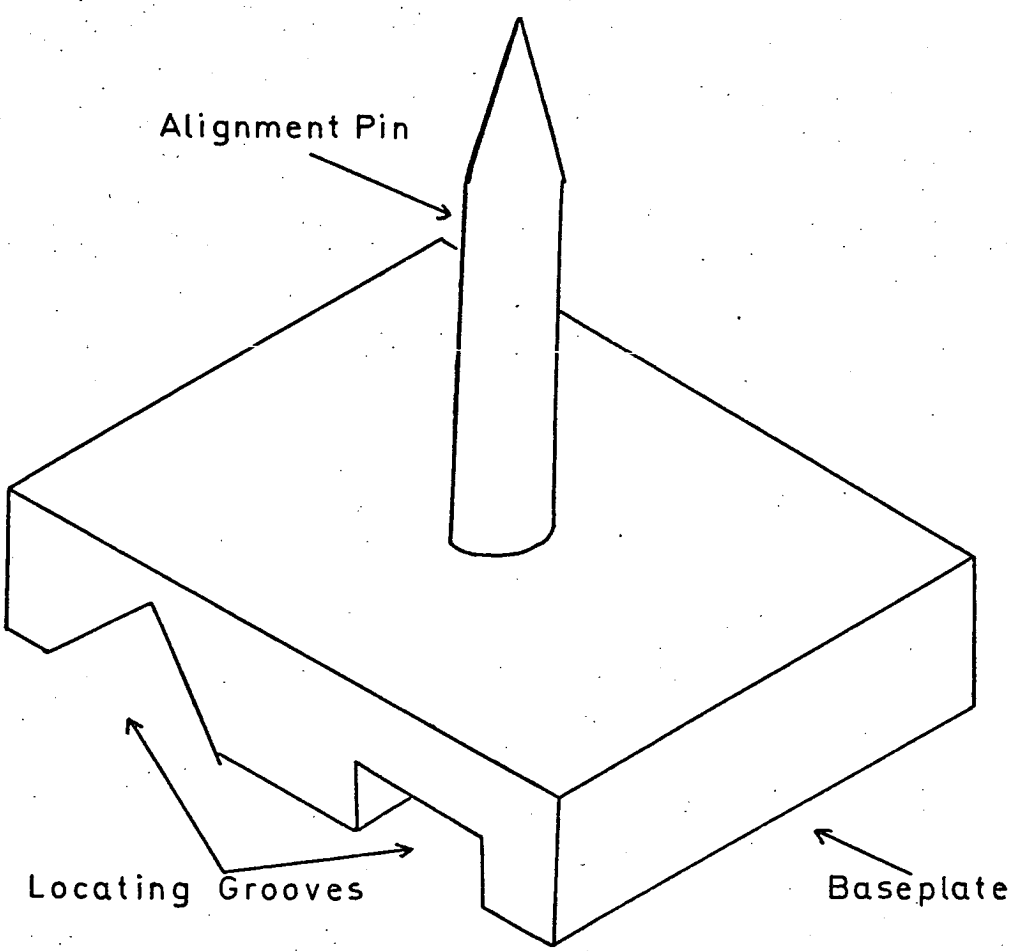

Fig. (3,3)

Base Plate and Alignment Jig.

Vacuum Pumps and Cold Traps

The main beam source chambers were pumped by Leybold DPL 150 oil diffusion pumps, these have a pumping speed of about 1000 litres/sec. The pumps were baffled by water cooled ring baffles, Leybold 12772, and a liquid nitrogen cooled baffle, Leybold 12845. These precautions were taken to minimise the amount of hydrocarbon oil back-streaming into the experimental chambers. The third chamber, the scattering chamber, was pumped by an N.R.C. VH 6 oil diffusion pump having a pumping speed of approximately 2000 litres/sec. This pump was baffled by an NRC VH 6 liquid nitrogen cooled baffle. The diffusion pumps were backed by three rotary pumps, two Leybold S12's and a D12, linked in parallel. Liquid nitrogen cooled cold traps were placed between the rotary and diffusion pumps. These served two purposes, they prevented any volatile corrosive substances, such as iodine, from entering the rotary pumps also, in the event of a mains failure, they prevented rotary pump oil being sucked back into the diffusion pumps.

Each chamber was also fitted with a liquid nitrogen cooled cold trap. These have a very high pumping speed for condensibles. The cold traps were made from 1/16" copper sheet brazed and welded in the form of a D. The traps had a capacity of about 4 litres and a consumption of around 1.5 L/hr under normal running conditions.

Pressure measurement

The backing pressure was measured at the exit of each diffusion pump by means of a Pirani gauge, the gauge was also connected to the vacuum interlock. Pressures in the experimental chambers were measured by A.E.I. VH 9 ion-gauges mounted on the top flanges of each chamber.

Normally the pressure in the backing line was around 50 μ and in experimental chambers 2×10^{-6} torr.

Detector Chamber

The detector chamber was made from 3/32" stainless steel sheet folded and arc-welded to form a box 6" x $4\frac{3}{4}$" x $6\frac{3}{4}$". Connections were made by means of conflat flanges welded to the basic box, Fig. (3,1) and Fig. (3,4). The chamber was pumped by means of a 70 litres/sec ion-pump, this was used in preference to a baffled diffusion pump as when an electron impact detector is used the latter gives rise to a background noise due to backstreaming. It was also more convenient to fit an ion-pump into the apparatus. The normal pressure in the detector chamber was 6×10^{-8} torr. The detector assembly itself hung down into the chamber from the top, Fig. (3,1). In order that the detector could be rotated about the main beam the detector and scattering chambers were connected by means of stainless steel bellows. Initially Varian pressure formed seamed bellows were used, it was found, however, that these had insufficient flexibility and were prone to leak

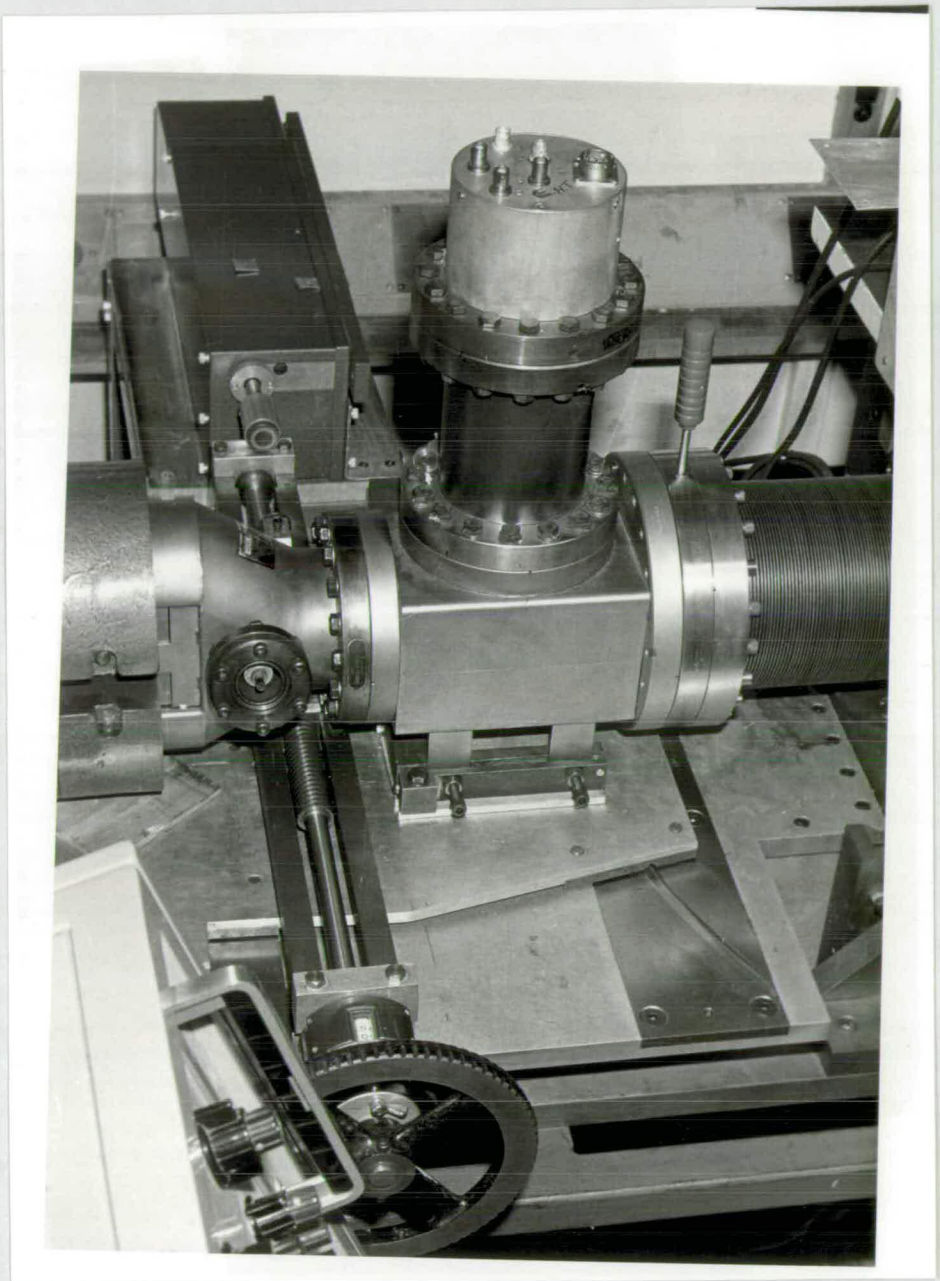

Fig. (3.4)

Detector Chamber.

after a short period in use. These bellows were then replaced by edge welded bellows which were found to be vastly superior.

In order that the detector chamber could be kept under vacuum when the rest of the apparatus was up to atmosphere a gate valve was placed between the detector chamber and the bellows. The basis of the gate-valve was a standard 8" flange. Half the centre portion was machined out and a ¼" hole drilled to allow the beam to pass, a ½" "O" ring groove was cut concentric with this hole. A stainless steel plate sliding between rails was used as a seal, see Fig. (3,5). The valve was operated by means of a ¼" diameter rod which passed through the side of the flange, a vacuum seal was obtained by means of an "O" ring. The region seen by the detector was limited by means of 0.030" slits mounted on the gate valve.

Rotation of the detector.

The detector chamber was bolted to a dural plate which was free to rotate on a lower fixed platform, the radius of rotation being fixed by ball-races. The arrangement is shown in Fig. (3,6). Set into the plate and the platform were two rectangular steel sections, those on the upper plate had radial V grooves machined in them, the lower platform had one V locating groove and a U guide groove, the grooves being 34" and 20" radii respectively. All grooves were hard chromium plated to reduce wear. Ball-bearings, ⅜" in diameter, were located

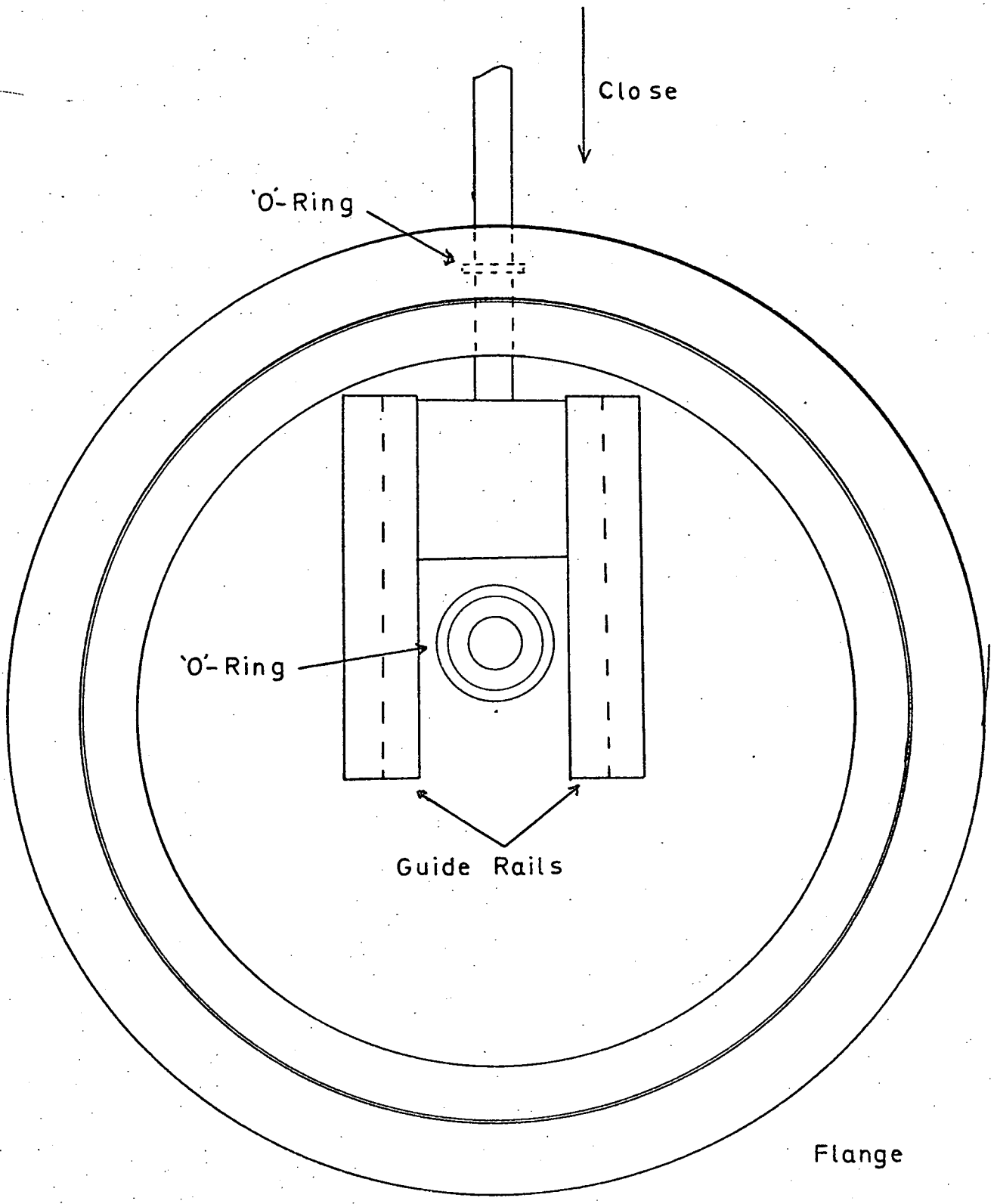

Fig. (3,5)

Gate Valve.

in the grooves thus allowing the plate to rotate relative to the platform. An angular displacement of up to $\pm 10^{o}$ about the mid-point was possible. The centre of rotation was approximately in the middle of the scattering chamber. The lower platform was adjustable in height thus allowing the detector to scan out of the plane of the main beam.

The detector assembly was rotated by means of the screw arrangement shown in Fig. (3,6). On rotating the lead screw the drive-block moves along its guide rails, the lower part of the drive-block is a tight sliding fit in the channel which is bolted to the plate carrying the detector. The plate is therefore forced to rotate on its ball races. The detector was prevented from moving forward when the scattering chamber was pumped down by a spring attached to the main frame of the apparatus.

Measurement of detector position.

Two solutions were considered to the problem of finding the angular position of the detector; a direct angular measurement could be made on the platform or a linear measurement made on the drive mechanism. The latter method was chosen for its simplicity. Two choices were again open, to measure the rotation of the lead screw or the linear motion of the drive block. The first method was rejected because of the likelihood of errors arising from backlash and non-uniformity of the thread.

The linear displacement of the drive block was measured with a "Teletrak" linear transducer. The transducer

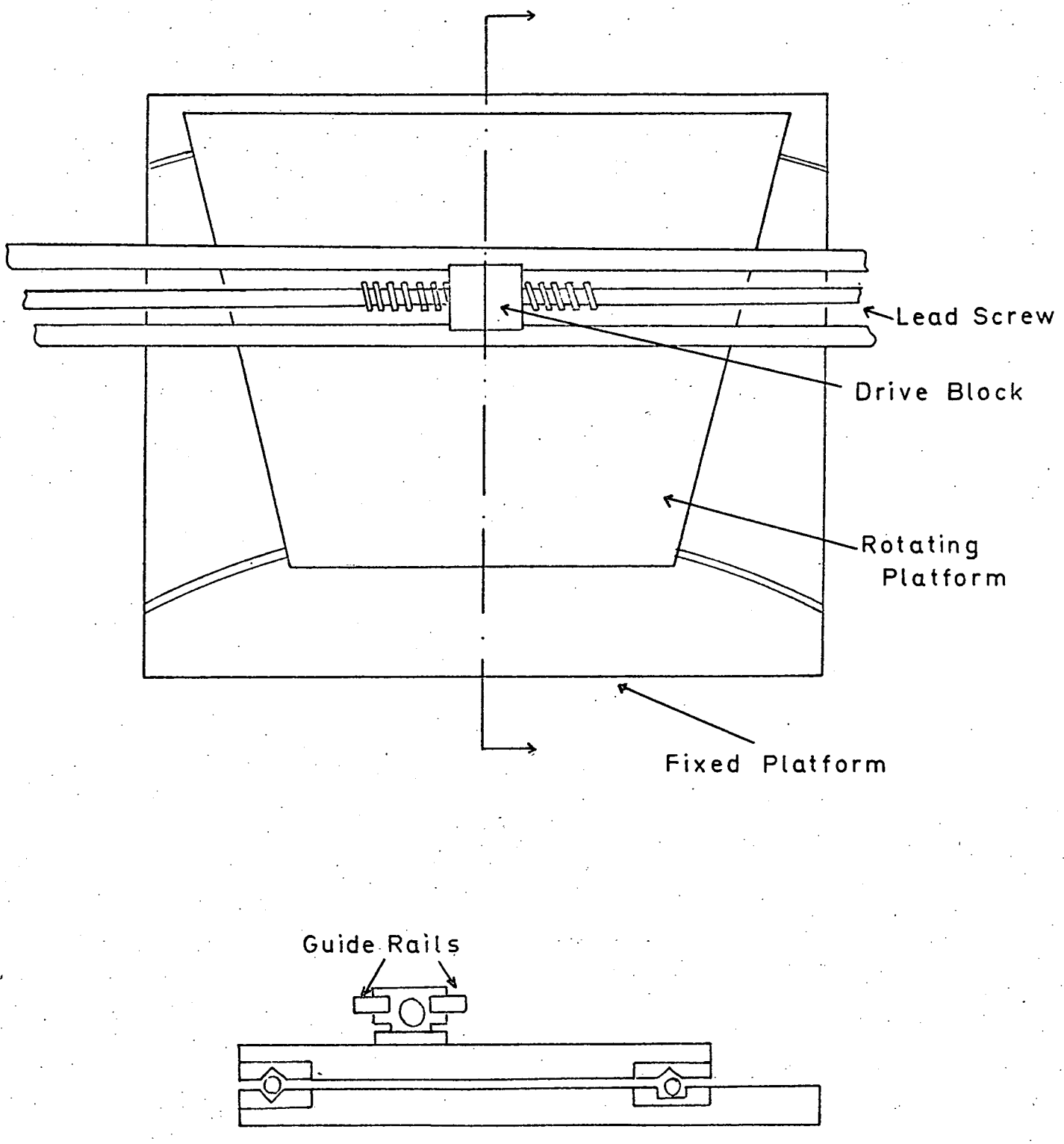

Fig. (3,6)

Detector Platform.

was mounted on a separate sub-frame and its sensor coupled to the drive block with a magnet. This system has many points to recommend it; both digital and B.C.D. outputs are immediately obtained, the measurement is absolute and is not therefore affected by temporary power failure or an excessive rate of change of position. The position can be measured to high accuracy and with high precision.

The only likely source of error in the measurement of the scattering angle was if the centre of rotation of the detector and the scattering centre did not coincide. The magnitude of this error could be easily estimated. If L was the distance from scattering centre to detector, then at an angle θ if the angular error is not to exceed $\delta\theta$ the scattering centre must be located to better than δ L where

$$\delta L = \frac{L\,\delta\theta}{\sin\theta}$$

Taking $\theta = 5^{\circ}$, $\delta\theta = 0.05^{\circ}$ and L = 51 cms then

$$\delta L \lesssim 0.5 \text{ cms}$$

This could be easily achieved.

Main beam source

Introduction

It has already been mentioned that prior to 1965 the great majority of beam scattering studies had been in the thermal energy range, I.E. less than 0.5 e.v. or the high energy, greater than 200 e.v. The only real exception was the experiment of Bull and Moon (BUL 1954). In this work molecules of $C Cl_4$ were accelerated by means

of a rapidly revolving paddle wheel which produced bursts of molecules with energies around 1 e.v. The apparatus was used to study the reaction

$$Cs + C Cl_4 \longrightarrow Cs Cl + C Cl_3$$

but the results obtained were not conclusive and no further work appears to have been done.

In the last decade various sources have been developed to bridge, in part at least, the energy gap. These fall into three broad groups, ion sources similar to those used at high energies, sputtering and nozzle sources. The different sources are discussed in detail by Anderson, Andres and Fenn (AND 66) and Fenn (FEN 68).

A useful sputtering source has been developed by Los and coworkers (LOS 68). In this method a beam of high energy, 6 keV, argon ions are directed at a block of potassium. Neutral potassium atoms with energies in the range 0.5-45 e.v. are ejected, these are then collimated and mechanically velocity selected. Several experiments have been performed with this source (LOS 69A) but it does suffer from several drawbacks; it is restricted as to the beam materials, and the problems of constructing and maintaining a mechanical velocity selector capable of operating at the required speeds are acute.

Several types of nozzle source, which operate in different energy ranges, have now been developed; namely the binary mixture nozzle (AND 66), the shock-tube nozzle (SKI 61) and the arc-heated nozzle (YOU 69). In the binary

nozzle a mixture, consisting in a large part of a light driver gas and a small amount of heavy gas, is expanded through a nozzle, the energy of the heavy gas is increased by collisions with the faster light molecules. In the shock-tube nozzle gas is heated by means of a shock wave, which is restricted to a short pulse of material. In the arc-heated nozzle a combination of arc-heating and aerodynamic acceleration is used.

The maximum beam energy which can be obtained is about 10 e.v. by the first two methods and 20 e.v. by the last. It is limited in the case of the binary mixture by the molecular weight of the working gas, in the case of shock wave heating by the shock strength and in the arc-heated nozzle by the materials of the nozzle.

The "classic" technique of ionisation, acceleration and neutralisation has now been advanced so that beams having energies of less than 10 e.v. can be produced (CRO 70). It is worth examining the limitations of a source of this type.

The current which can be drawn from an ion source is limited by the mutual repulsion of the ions. It has been shown (WAT 27) that the maximum current obtainable in a beam of charged particles of mass M, energy V and convergence γ is

$$I_{max} = 4.67\,\pi\, E_0\, (e/2M)^{\frac{1}{2}} V^{3/2} \tan^2\gamma$$

Unfortunately there exists another restriction such that not only is the maximum current that can be obtained limited, but also it is not always possible to achieve this maximum.

It was shown by Simpson and Kuyatt (SIM 63A) that in order to attain the current densities for space charge saturation, in the presence of thermal effects at the emitter surface, one would have to exceed the space charge limitations imposed by the diode nature of the ion-gun. It was this restriction which defined the lower energy limit of previous work. To work outside these limits it is necessary to decouple the thermal energy and space charge effects by first accelerating the ions to a fairly high energy, several hundred volts, and then decelerating to their final low energy. Simpson and Kuyatt (SIM 63 B) designed an electron gun using this multistage principle, this was later adapted by Haskell and Heinz (HAS 66) for use with low energy ions.

The source used in this work was of the ionisation/ neutralisation type incorporating a multistage lens system.

The main beam source falls naturally into three parts, the ioniser, the lens system and the neutraliser.

The ioniser.

There are two main methods by which ions may be formed; electron impact, either directly or in a discharge, and surface ionisation. The advantages and disadvantages of the two methods are as follows. Electron impact has a low efficiency, $\sim 10^{-4}$, some form of selector is required to remove excited species and, in the case of molecules, fragments of the parent species. The method does, however, have the advantage of being applicable to all substances. Surface ionisation is highly efficient, $\sim 100\%$, but is almost entirely restricted to the alkali metals.

As there is a great wealth of experimental results on alkali metal systems at thermal energies it was decided to try to extend the data to higher energies. A surface ionisation source was therefore chosen for this work.

It has been found that if atoms strike a hot filament, of work function W, then the ratio of emergent ions n^+ to neutrals n is given approximately by

$$\frac{n^+}{n} = c \exp(\phi - W / kT)$$

where ϕ is the ionisation potential of the incident atoms. The variation of ion-current with temperature is shown in Fig. (3,7) (HUS 63). It will be seen that above a critical temperature T_c, about 1100°C, the ionisation efficiency is almost independent of temperature.

In this work ions were produced by allowing alkali metal vapour to diffuse through hot porous tungsten. Ionisers of this type have been extensively developed in America for use in space as rocket motors (KUS 65). A simpler system in which alkali metal vapour is directed at a hot filament (DAT 68), (PAU 66), (ROT 68) was considered but not used.

The ionisation potentials of the alkali metals are

Li	5.4 e.v.
Na	5.1 e.v.
K	4.3 e.v.
R_b	4.2 e.v.
Cs	3.9 e.v.

The work function of tungsten is approximately 4.7 e.v. hence lithium could not be used in this ioniser and sodium with only limited efficiency. It would be possible to use these materials if rhenium, work-function 5.2 e.v. was used instead of tungsten (H&I 68). To date the majority of the work has been with potassium.

The ioniser is shown in Fig. (3,8), it consists of two parts, the alkali metal supply oven and the tungsten ioniser. The supply oven was made of stainless steel, the heaters consisted of 0.020" nichrome wire threaded through fused alumina tubes. The oven temperature was measured with a NiCr/NiAl thermo-couple. The oven was sealed by means of an annealed copper gasket. On the base of the oven were machined two $\frac{1}{8}$" V grooves mutually at right angles. The oven sat on three rounded tungsten pegs 1/16" in diameter, these engaged in the V grooves hence fixing the oven position. The oven and tungsten locating pins were insulated from earth.

The ioniser section consisted of a molybdenum tube 3" x .25" x 0.030" on the end of which was welded a 0.030" thick disc of porous tungsten, 75% dense. Initially it was attempted to electron-beam weld the tungsten disc to the molybdenum tube but this proved unsuccessful. The two parts were finally heli-arc welded and have given no trouble during several hundred hours of operation. The method of attaching the ioniser tube to the supply oven is shown in Fig. (3,9), when the nut is tightened, the annealed copper ring distorts and grips the molybdenum tube; in order to avoid crushing the walls of the molybdenum tube a short length of thick walled stainless-steel tube was placed inside.

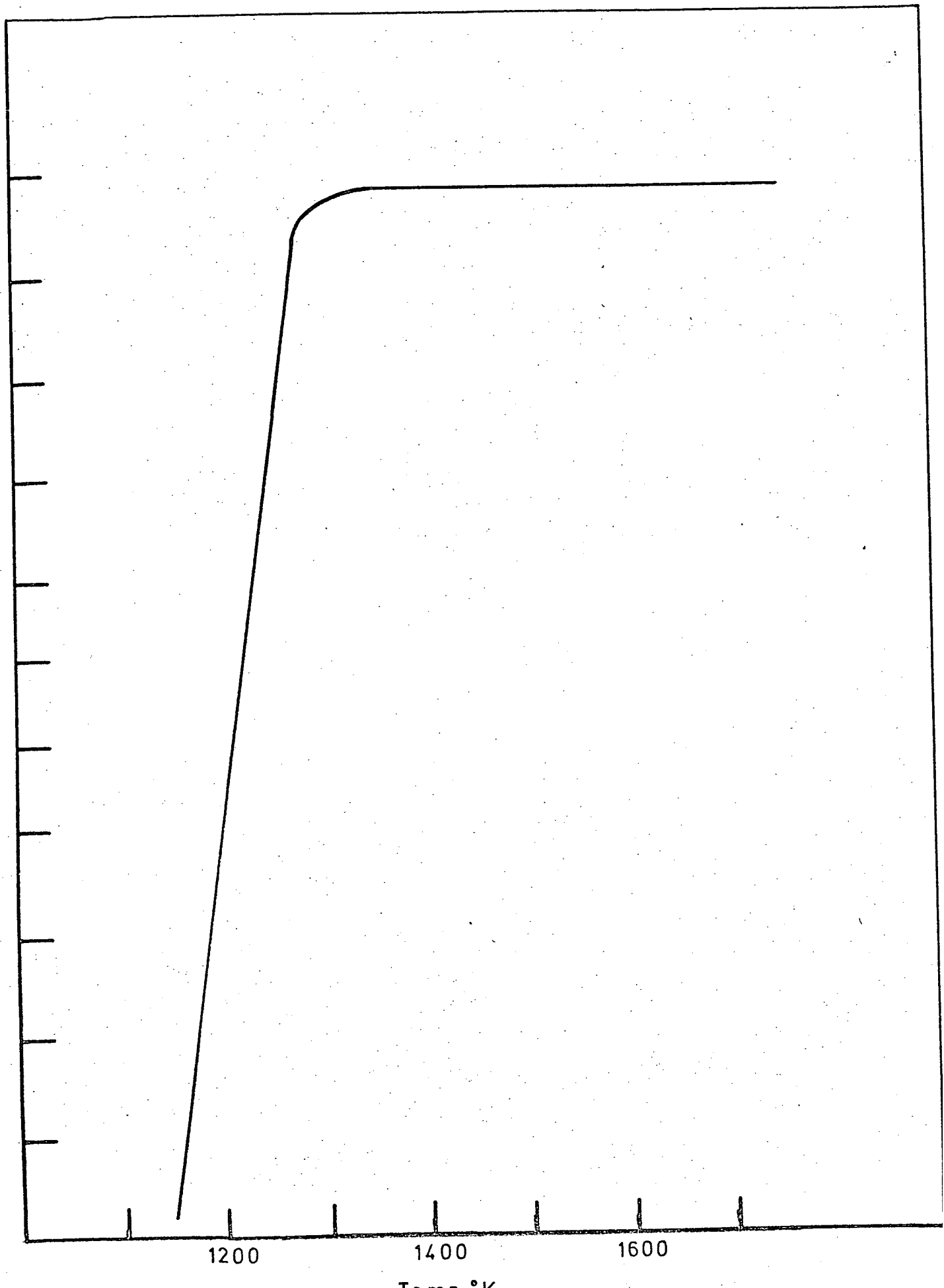

Fig. (3.7)

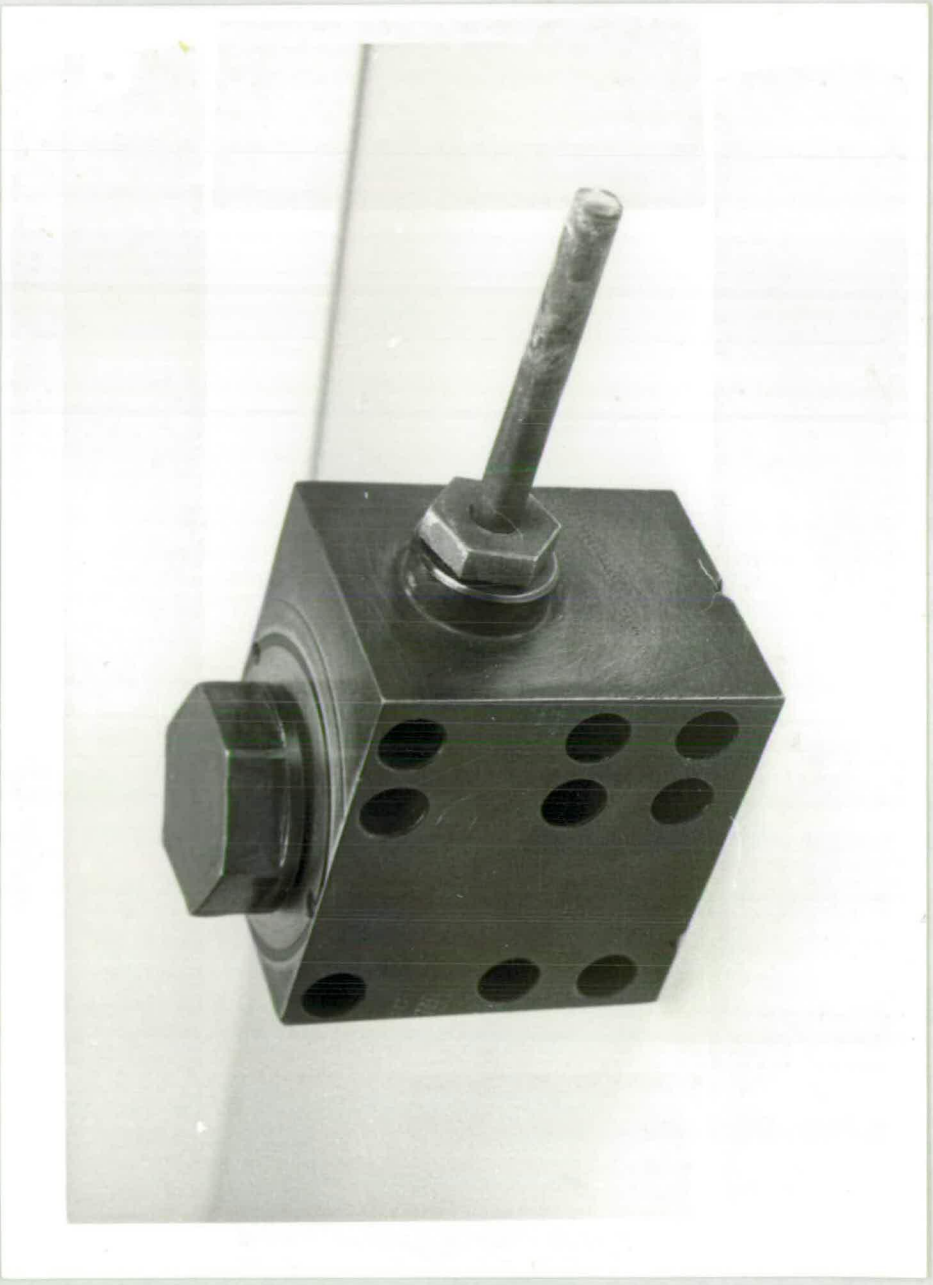

Fig. (3.8)

Ioniser and Supply Oven.

This system worked very well though if thermally cycled a leak was liable to develop. It has been already mentioned that the ioniser operating temperature must be in the region of 1200°C, the actual temperature is not important provided it exceeds the critical temperature T_c. Attaining this temperature proved quite a problem, the solution adopted was a high current radiation heater.

The heater consisted of a 1½" x ½" x 0.060" molybdenum tube concentric with the ioniser, the tube was slit for most of its length and then welded to two molybdenum plates (Fig. (3,10). The heater was then clamped, by means of the molybdenum plates, to heavy copper supports which carried the heater current. Power was taken to the copper supports by means of 5/16" copper pipes, these also carried cooling water. The heater carried a current of approximately 550 amps, the ioniser was then heated by radiation. In order to minimise heating of the surroundings the heater was enclosed in a radiation shield, this consisted of three concentric thin walled tubes 1⅛" long, the inner, which had a diameter of 1", was made of molybdenum, the outer two tubes were 1¼" and 1½" in diameter and made of stainless steel. The radiation shield was itself surrounded by a water cooled copper shield.

The ioniser has proved very reliable.

<u>The lens system.</u>

That charged particles could be focused by electrostatic fields was first recognised in 1931 by Davisson and Colbick (DAV 31) and an extensive development of electro-

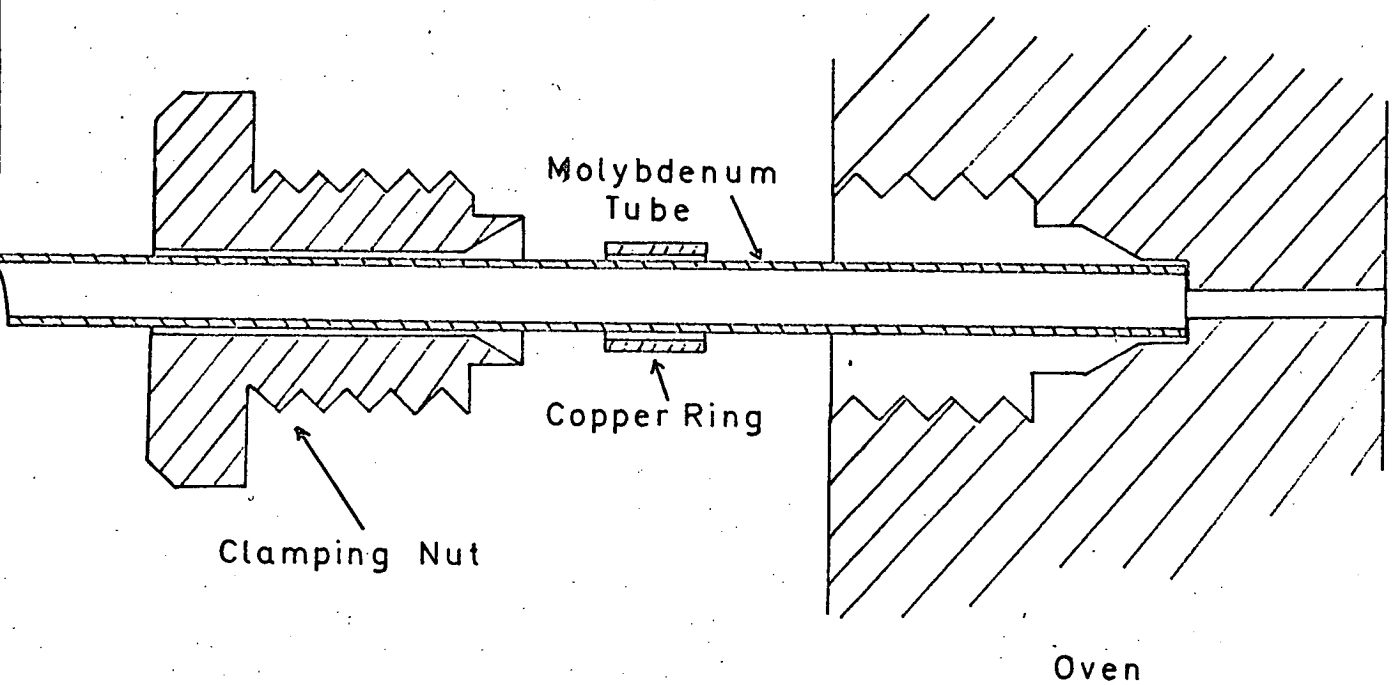

Fig. (3.9)

Method of attaching the ioniser to the supply oven.

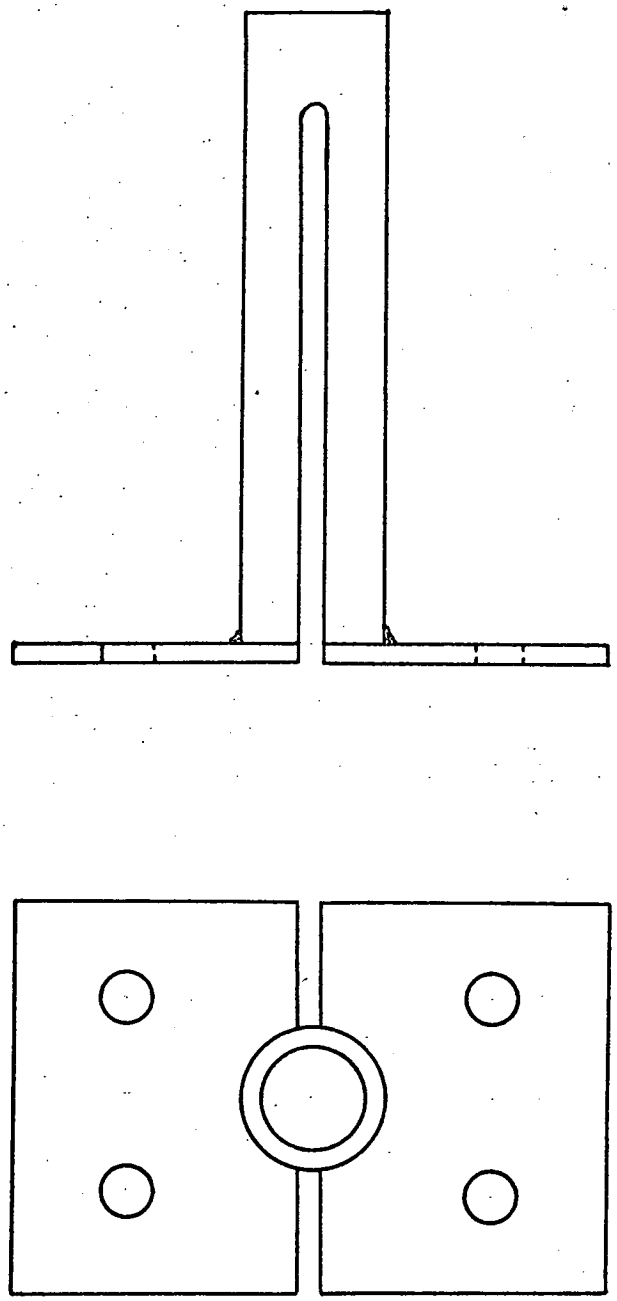

Fig. (3.10)

Ioniser Heater.

optical devices has followed.

The motion of a charged particle in an electric field is governed by the Lorentz equation.

However no general solution in terms of lens parameters is available. Lens characteristics are, therefore, usually determined experimentally or indirectly by a modelling procedure (KLE 53). It is difficult therefore to determine a priori the optimum values of the lens parameters.

The lens system used in this work was based on that developed by Simpson and Kuyatt (SIM 63B) and Haskell and Heinz (HAS 66), the lens is shown in Fig. (3,11). The extraction stage was a standard Soa immersion lens the properties of which are known (SOA 1959). The grid and accelerating electrodes, which were made of molybdenum and stainless steel respectively, were mounted on alumina rods and secured with tungsten springs. The defining aperture was mounted on the bulkhead separating the first two chambers and was insulated from it with pyrophyllite. The deceleration stage was a two element lens the focal properties of which have been measured by Spangenberg and Field (SPA 43). The lens was mounted on a separate base-plate in the second chamber. No provision was made to allow variation of the inter-stage distance from outside the vacuum system. This restriction means that the ion-beam can not be truly optimised but it was not thought to be a serious disadvantage. To reduce the effect of spurious surface charges the lens elements were coated with colloidal graphite before each run. Mounted on the same base-plate as

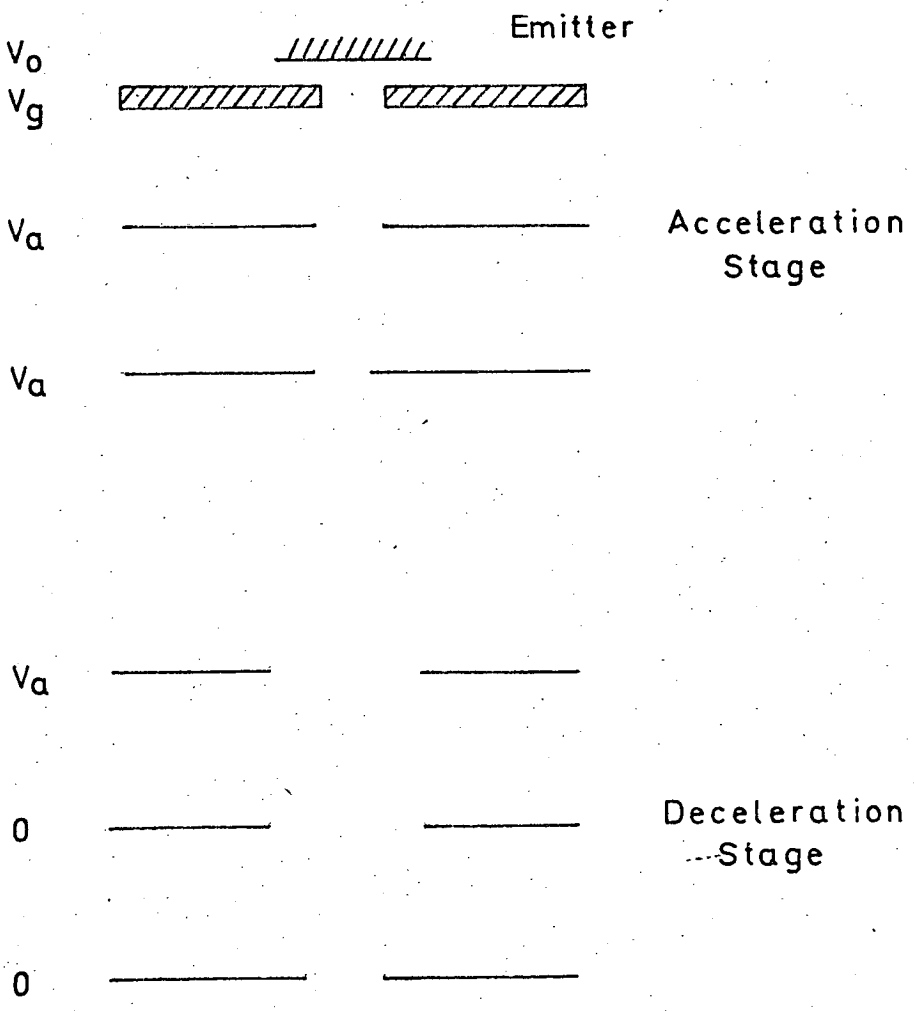

Fig. (3.11)

Lens System.

the lens were X, Y deflector plates, to correct any misalignment of the ion beam, and a device for locating the ion-beam. This consisted of four 1/16" rods mounted mutually at right angles round the main beam axis, the ion-current at each rod could be measured with an electrometer hence the centre of the ion-beam could be found.

Performance

The performance of the lens system was difficult to estimate as there was no way of determining, experimentally, the focus of the lens or the ion-beam profile. The ion-current passing through the charge-exchange chamber when it contained no vapour was measured. The charge exchange chamber slits and the final lens element define a minimum value of the convergence angle δ, using this it was possible to estimate the ion-current and compare with experiment, this is shown in Fig. (3,12).

It will be seen that at higher energies the ion-current is over estimated by a factor of about six. However in the circumstances the agreement was considered quite good. In similar work Haskell and Heinz (HAS 66) found discrepancies up to a factor of about thirty.

Although the lens system appeared to function quite well it was considered worthwhile experimenting with different systems. A deceleration lens of the Lyndholm multi-element type is at present under construction. This lens has been used with success in the production of ion beams (WOL 69) and is more flexible than the two element lens in use at present. It is hoped that the properties of

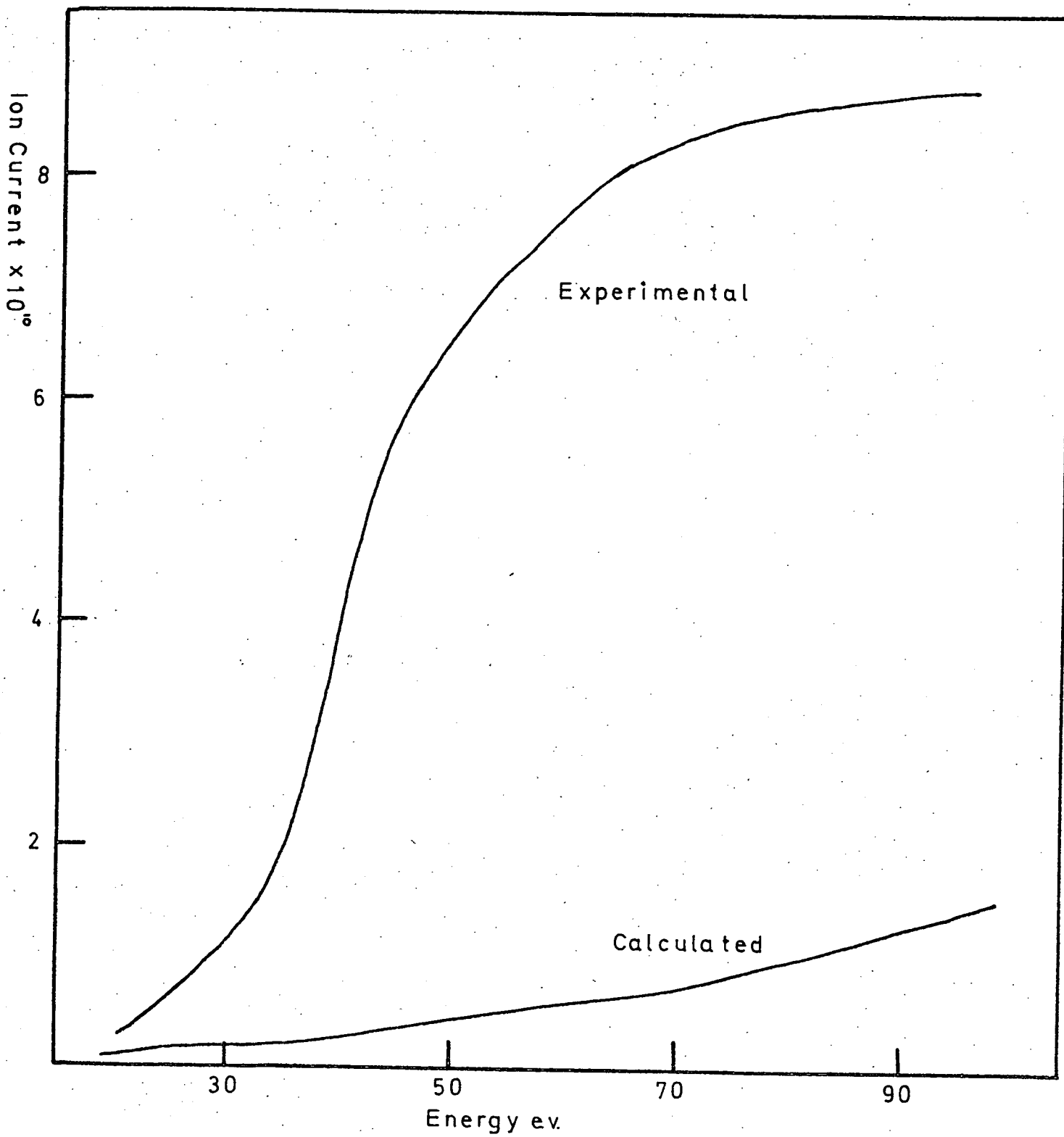

Fig. (3,12)

Ion current vs Energy.

the lens will be calculable using the program developed by U.K.A.E.A. Culham (BAT 65).

The Neutraliser

After passing through the final lens the ions were neutralised by resonant charge transfer.

$$M^{+}_{Fast} + M \longrightarrow M_{Fast} + M^{+}$$

as the mass of the electron is so much smaller than that of the atom there is little momentum transfer and hence the fast neutral is little deviated from its path. A discussion of the subject will be found in the review by Hasted (HAS 62).

The ions passed through a chamber containing potassium vapour; if the length of the chamber is l and the number density of the potassium vapour n then the fraction of ions neutralised is given by the familiar Beer-Lambert law

$$I/I_0 = \exp-(n\sigma l)$$

where σ is the charge transfer cross-section. In the case of potassium in the energy range considered 6-200Å^2 (MAH 68).

It is clear that a given attenuation may be achieved by varying n or l independently. On the grounds that the sooner the ions are neutralised the better to prevent spreading of the ion beam by mutual repulsion it would appear that l should be as small as possible. On the other hand if the vapour pressure of potassium is increased then the background pressure of potassium in the system will also rise. This is undesireble as ions may then be neutralised in the lens system before deceleration. A compromise between these two conflicting

considerations must be found.

The charge exchange chamber is shown in Fig. (3,13) the neutralisation region is seven cms. long. Emergent fast neutrals are collimated by means of slits to form a narrow ribbon 0.125" x 0.009".

The chamber was heated by means of 0.020" nichrome wire threaded on fused alumina tubes, the temperature was measured by a Ni Al/Ni Cr thermo-couple. Unneutralised ions leaving the charge exchange chamber were deflected on to a collector plate, the ion current was measured by means of an electrometer.

Having fixed the length l it still remained to determine the optimum value of n, I.E. that which maximises the fast neutral flux. Clearly n may not be increased indefinitely as elastic scattering would become important. Following the argument of Hollstein and Pauly, (PAU 66) the optimum value of n is such that

$$n\,6\,l \lesssim 1$$

In this case an operating temperature of 150°C was predicted. This was verified experimentally, the neutral flux being measured as a function of charge exchange chamber temperature Fig (3,14).

Under certain circumstances, see next section, it would be advantageous if the material of the main beam and the charge exchange vapour were different. It was considered that if the ionisation potential of the two materials were similar then it should be possible to produce a fast neutral beam.

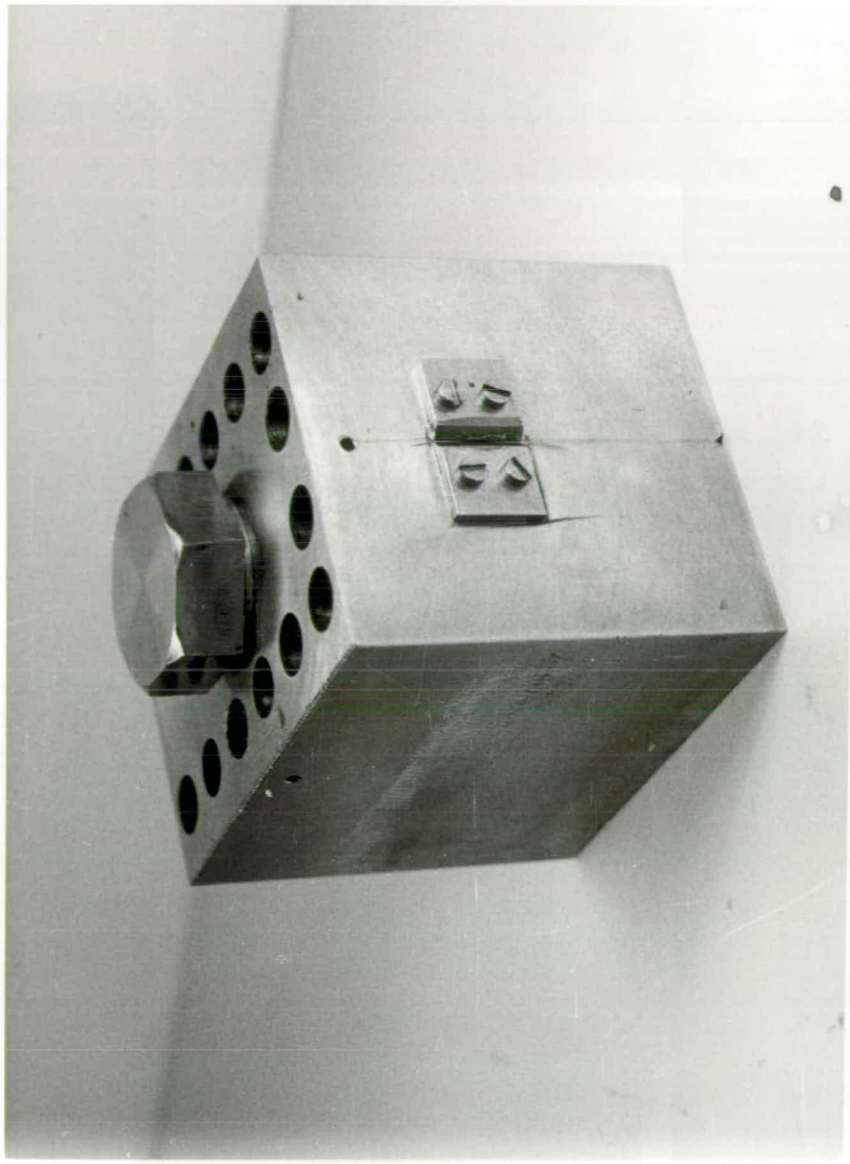

Fig. (3.13)

Charge Exchange Chamber.

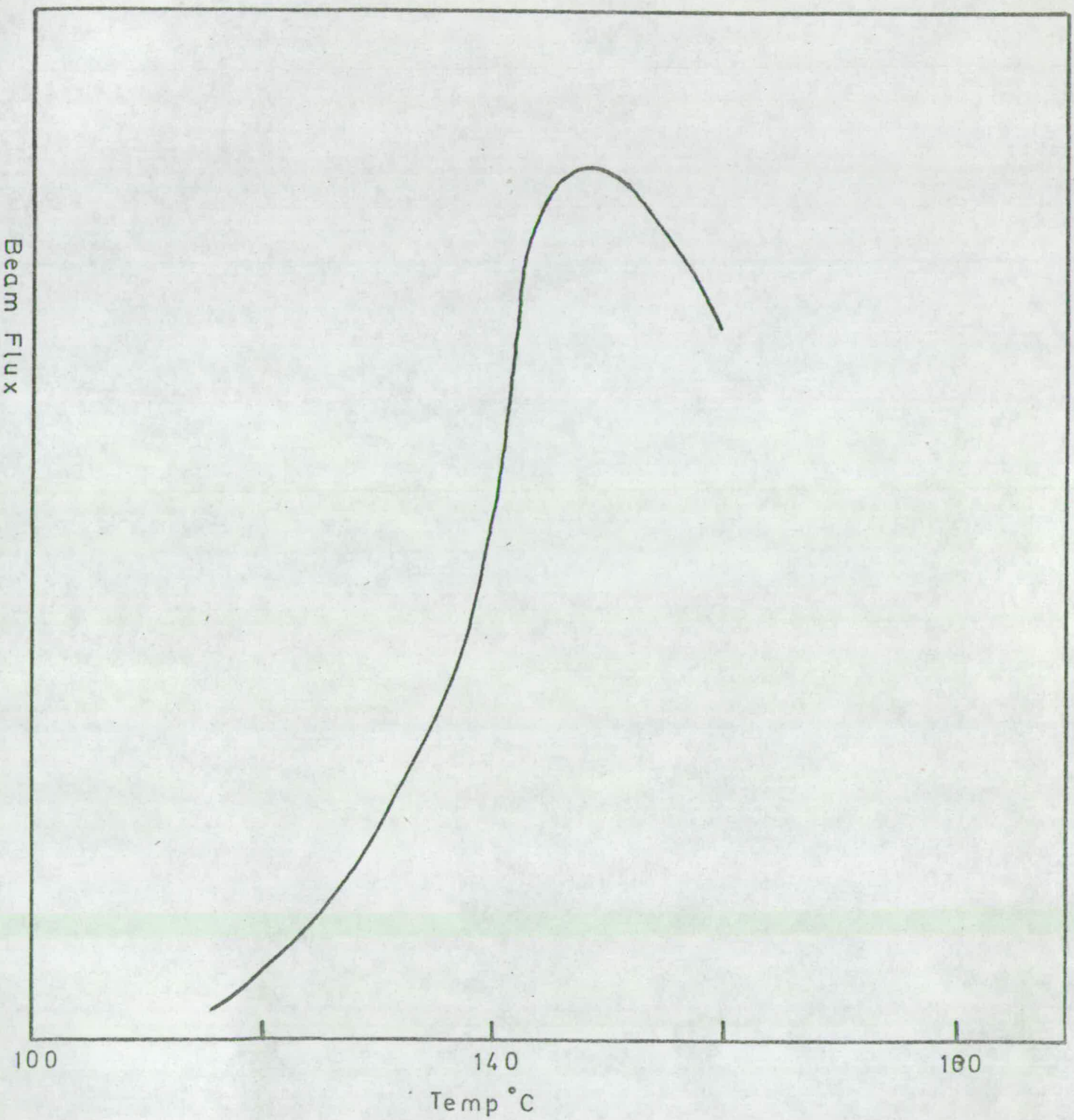

Fig. (3,14)

Beam Flux versus Charge Exchange Chamber temperature.

An attempt was made to produce a beam of caesium by charge exchange between caesium ions and potassium atoms, the ionisation potentials of caesium and potassium are 3.9 e.v. and 4.3 respectively. Caesium was produced by heating an equimolecular mixture of caesium chloride and sodium to about 250°C in the supply oven. Although caesium ions were produced without any difficulty no fast neutrals were detected. It is possible that more success would be had with a rubidium/potassium mixture, the ionisation potential of rubidium is 4.2 e.v. This has not yet been tried.

Oven Power Supplies

The supply oven and charge exchange chambers were both supplied by 30 V 5A D.C. power units. The A.C. input to the power supplies was controlled by ether temperature control units, the oven temperatures being monitored with NiCr/NiAl thermocouples. Initially the charge exchange chamber temperature was controlled by an Ether type 2006 three term controller, this fed, in turn, a magnetic amplifier and a saturable reactor. Although great accuracy was claimed for this unit it never worked satisfactorily and was eventually replaced with the Ether type 991 which had controlled the supply oven. The 2006 was then put on the supply oven the temperature of which was not critical.

Lens Power Supplies

Two separate groups of power supplies were used, a high current supply for the lenses themselves and a low current supply for the deflector plates. The lens voltages were supplied by three Keithley 240A 0-1200 volt supplies.

The low current supply consisted of two Kingshill power supplies, a 5300 20 volt supply and a M1510 150 volt supply, these fed a resistor chain from which the various voltages could be tapped. All supply lines were A.C. decoupled.

The Detector.

The detection system was based on an E.A.I. Quad 250 quadrapole mass-spectrometer. The original electron impact ioniser was replaced by a surface ioniser, Fig. (3,15). The ioniser consisted of a platinum/tungsten filament 0.020" x 0.001". Ions produced at the filament were focused into the mass-spectrometer by means of a lens. Beam material missing the filament passed straight on into the ion-pump and hence could not contribute to background noise. Surface ionisation of fast neutrals is not as simple as the thermal case, as the ionisation efficiency depends not only on the surface temperature but also on the energy of the incident neutrals. Broadly speaking two types of behaviour may be identified, these depend on whether the filament temperature is greater than the critical temperature Tc, about 900°C in our case. Hulpke and Schlier have found that for temperatures greater than T_c then the ionisation efficiency for potassium on platinum/tungsten is nearly 100% for energies up to 3 e.v. but falls off above this energy due to reflection (HUL 67). A detector has been designed (LOS 69B) which overcomes this problem but is not suitable for our application. This situation could be tolerated but for a further complication, namely that at temperatures greater than Tc thermal potassium effusing from the charge exchange chamber and filament impurities are ionised. This noise would swamp the

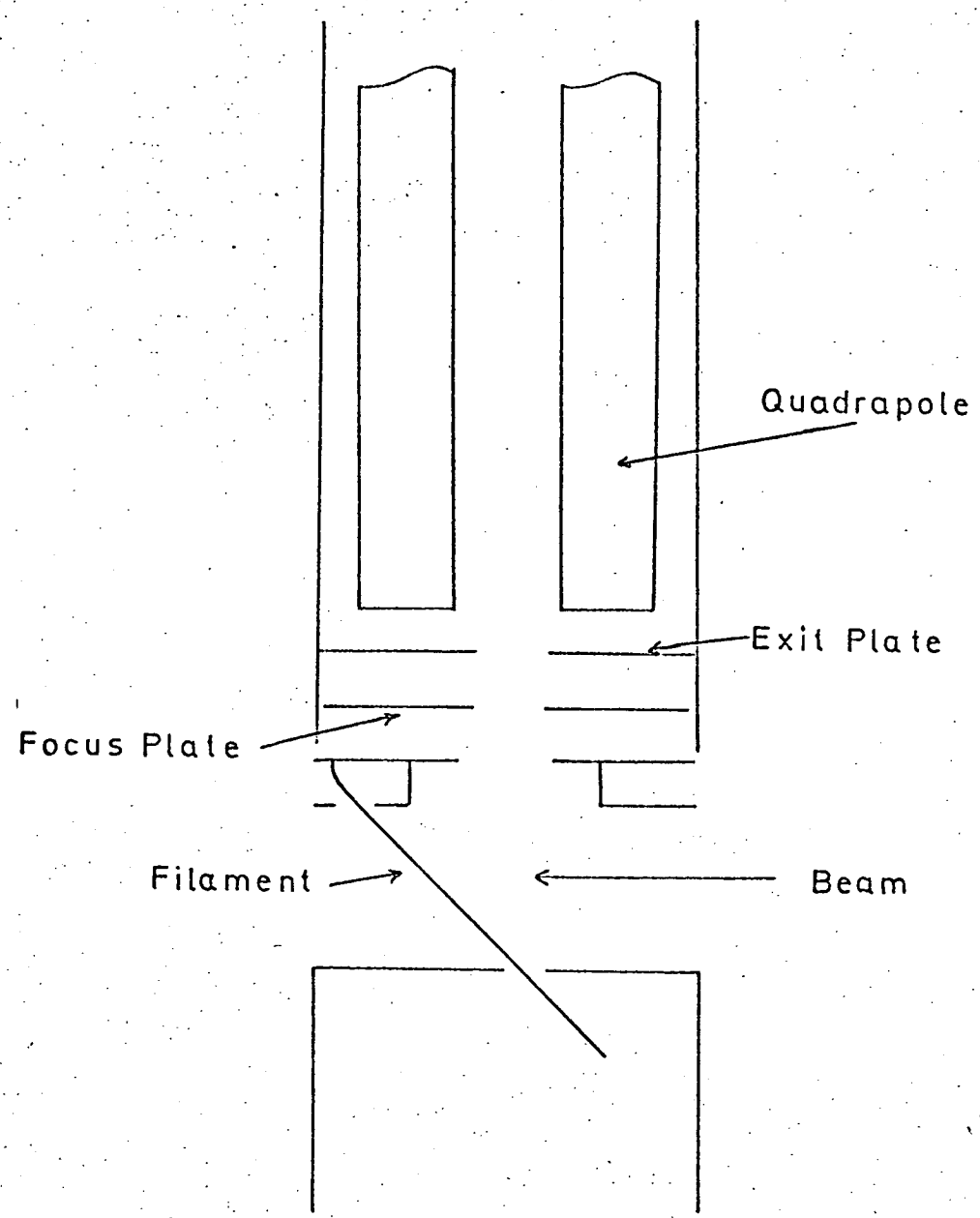

Fig (3,15)

Detector.

signal due to the beam. The first effect could be avoided by using a material other than potassium in the charge exchange chamber, this was discussed in the previous section. Little is known of the processes occurring at temperatures below Tc. The ionisation efficiency appears to increase steeply with increasing incident energy (Fig. (3,16) (ROT 69) but presumably reaches a plateau or maximum as reflection increases. In this work the filament current was adjusted to a point just below that at which thermal potassium was ionised. It was not possible to measure the filament temperature directly as the defining slits were too small to allow accurate pyrometer readings.

After mass selection in the quadrapole the ions were accelerated into an electron multiplier. The measured transmission of the lens and quadrapole was in the region of 8%. Initially a fourteen stage copper/beryllium multiplier was used, this had a gain of about 10^6 when new. However after exposure to the atmosphere the gain fell drastically to around 10^3. It was, however, found possible to reactivate the multiplier by baking at 350°C in hydrogen at one atmosphere then in dry oxygen under similar conditions for three hours. After this treatment the gain returned to its previous value and proved quite satisfactory. However a vacuum failure when the E.H.T. was on deactivated the multiplier permanently.

As a replacement it was decided to use a Mullard type 419 BL channel electron multiplier, C.E.M. (EVA 65). A C.E.M. is a small, about 2", coiled glass tube coated internally with a thin layer of metallic lead or vanadium

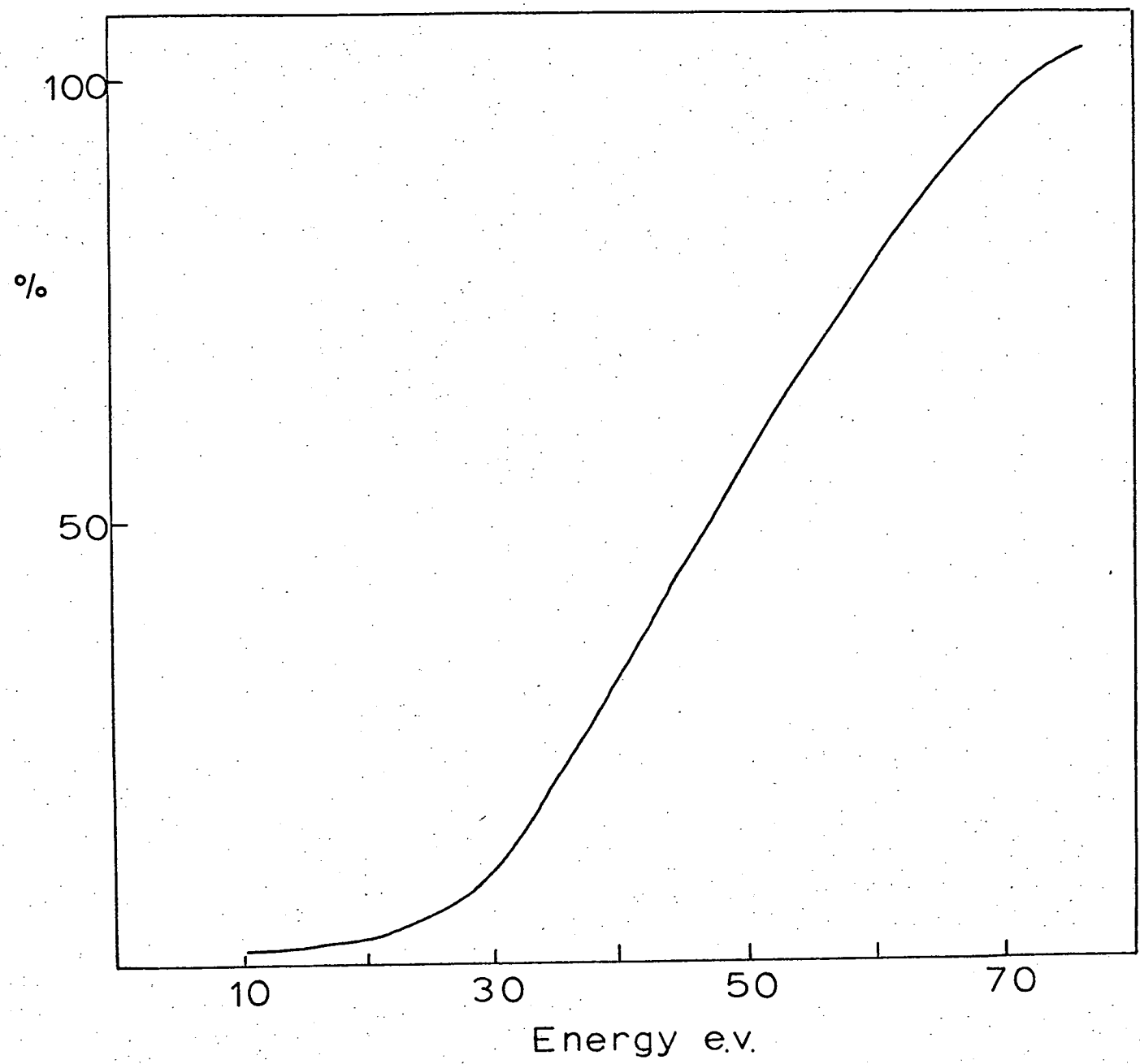

Fig. (3,16)

Ionisation efficiency versus energy.

phosphate glass. A high potential, 2.5 Kv in our case, is connected across the C.E.M., the internal coating then functions as a continuous dynode. Ions, from the quadrapole, are accelerated into the C.E.M., on striking the surface secondary electrons are produced, the efficiency is about 50%. Under the influence of the applied field they zig-zag up the tube producing a cascade of electrons. Electron gains of better than 10^8 are possible, however nature being what it is C.E.M's have their drawbacks. The maximum incident flux which can be measured is limited by the nature of the surface coating. In any multiplier the current which can be drawn must be less than about 1% of the current flowing in the dynode resistance chain. If too large a current flows, corresponding to an excess flux, then the effect is to reduce the size of the output pulse, if this falls below the detection threshold then the multiplier is said to be saturated. In a conventional multiplier the resistor chain current is in the region of a milliamp. hence there is no real restriction on the incident flux. A C.E.M. on the other hand has a resistance of about $5 \times 10^9 \Omega$ and hence draws about 0.5 μa. If we assume an amplifier input capacitance of around 40 pF and a minimum detectable output pulse of 100 mv then the equivalent threshold is 2.5×10^5 electrons. If we restrict the average pulse current to 2% of the wall current then the multiplier will saturate at an incident flux of about 2×10^5 ions/sec. In practice the C.E.M. was found to saturate at 9×10^4 ions/sec. The multiplier background noise at this equivalent threshold was about 2

pulses/sec. If required the maximum count rate for saturation could be increased by raising the E.H.T. up to a maximum of 3.5 Kv but this is accompanied by a disproportionate increase in background noise. The output from the C.E.M. is fed, via a protection circuit, to an amplifier. The amplifier used was a Hewlett-Packard 462A on 40 db gain, an attempt was made to place a 0 db Keithley 111 high impedance pulse amplifier between the C.E.M. and the 462A but this was unsuccessful due to R.F. pickup from the quadrapole. Pulses from the 462A were selected using a variable threshold discriminator (COW 68). The discriminator gave 4 volt pulses about 20 nanoseconds long, these were split in an impedance matching network and fed to the inputs of a Chronetics Nanocounter 100.

Performance of main-beam source.

It was not possible to make a direct calculation of the neutral beam flux as neither the ion-beam geometry nor the detector ionisation efficiency were known. At best only crude estimates of expected intensity could be made, a better idea of the source performance could be obtained by comparison with other similar sources.

The main beam flux, as measured at the electron multiplier, is shown versus beam energy in Fig. (3,17). In order to obtain the actual flux at the detector the following must be known; the detector ionisation efficiency, the quadrapole transmission and the multiplier efficiency, none of these quantities were accurately known.

At 100 e.v. the measured beam flux was 7.5×10^4 particles/sec, taking the detector and multiplier efficiencies as 50% and the quadrapole transmission of 8% then the flux at the detector was about 3.8×10^6 particles/sec. The angular area of the detector was 2.8×10^{-6} str which gives a flux of 1.4×10^{12} particles/str/sec. This compares with about 10^{13} particles/str/sec obtained by Pauly (PAU 66).

The measured ion-current at 100 e.v. was 8.8×10^{-10}A, if 60% neutralisation is assumed then a maximum neutral flux of 3.3×10^9 particles/sec is predicted. This implies that the beam divergence was about 1^o. At 60 e.v. the flux at the detector was 7.8×10^{11} particles/str/sec, this compares with Pauly's value of about 8×10^{12} particles/str/sec. The beam divergence was again about 1^o.

The figures are encouraging in that they show that improvements can still be made in the system. The two main points of attack are clear, to improve the overall detection efficiency and to decrease the beam divergence. The problem of the detector may easily be solved by removing the quadrapole, this should increase the measured signal by a factor of ten or more. Clearly such action will introduce a source of noise into the system, in the present arrangement this should not be a problem, any noise arising being second order of smallness. If differential cross-sections are to be measured at energies less than about 50 e.v. then the detector must be modified. The solution to the problem of beam divergence is not so clear; energy resolution may have to be sacrificed and the length of the charge exchange chamber decreased.

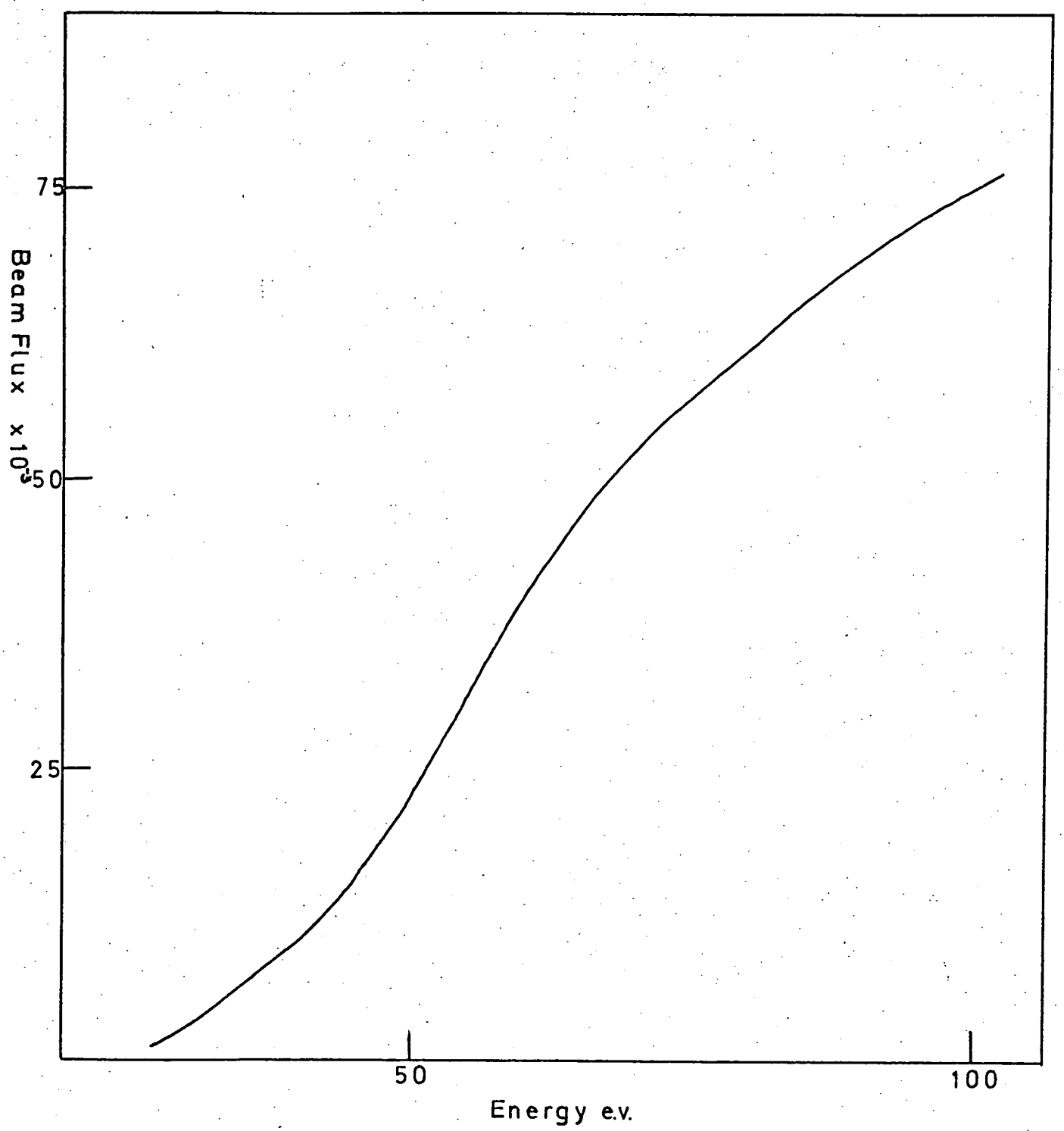

Fig. (3,17)

Beam Flux vs Energy.

Cross-Beam

Source

The cross-beam was directed vertically downwards in order that, after intersecting the main beam, it passed directly into the diffusion pump hence maximising pumping.

The cross-beam source is shown in Fig. (3,18), it consisted of two separately heated monel chambers. It was intended that the source be used initially for producing beams of iodine molecules or atoms, the iodine atoms to be formed by thermal dissociation. The thermal dissociation of iodine molecules is treated in detail in the Ph.D. Thesis "Theoretical and Experimental Studies of Atomic and Molecular Scattering" by D.S. Horne (Edinburgh, 69) and only the results will be quoted here. The percentage dissociation of iodine as a function of temperature, at various pressures, is shown in Fig. (3,19). It was intended to run the dissociation chamber at about 500°C to give around 95% dissociation, however overheating of the source prevented this and to date beams of iodine molecules only have been produced. It is hoped that the introduction of water cooling will overcome the problem. The source can, of course, be used for a variety of other substances provided source temperatures in excess of about 400°C are not required.

The choice of materials for the source slits was restricted by the problem of corrosion, iodine will attack even stainless steel. It is well known that a multi-channel array gives a higher intensity than a single slit of the same dimensions (AND 66), however such arrays, Zacharias foil

Fig. (3.18)

Cross-beam Source.

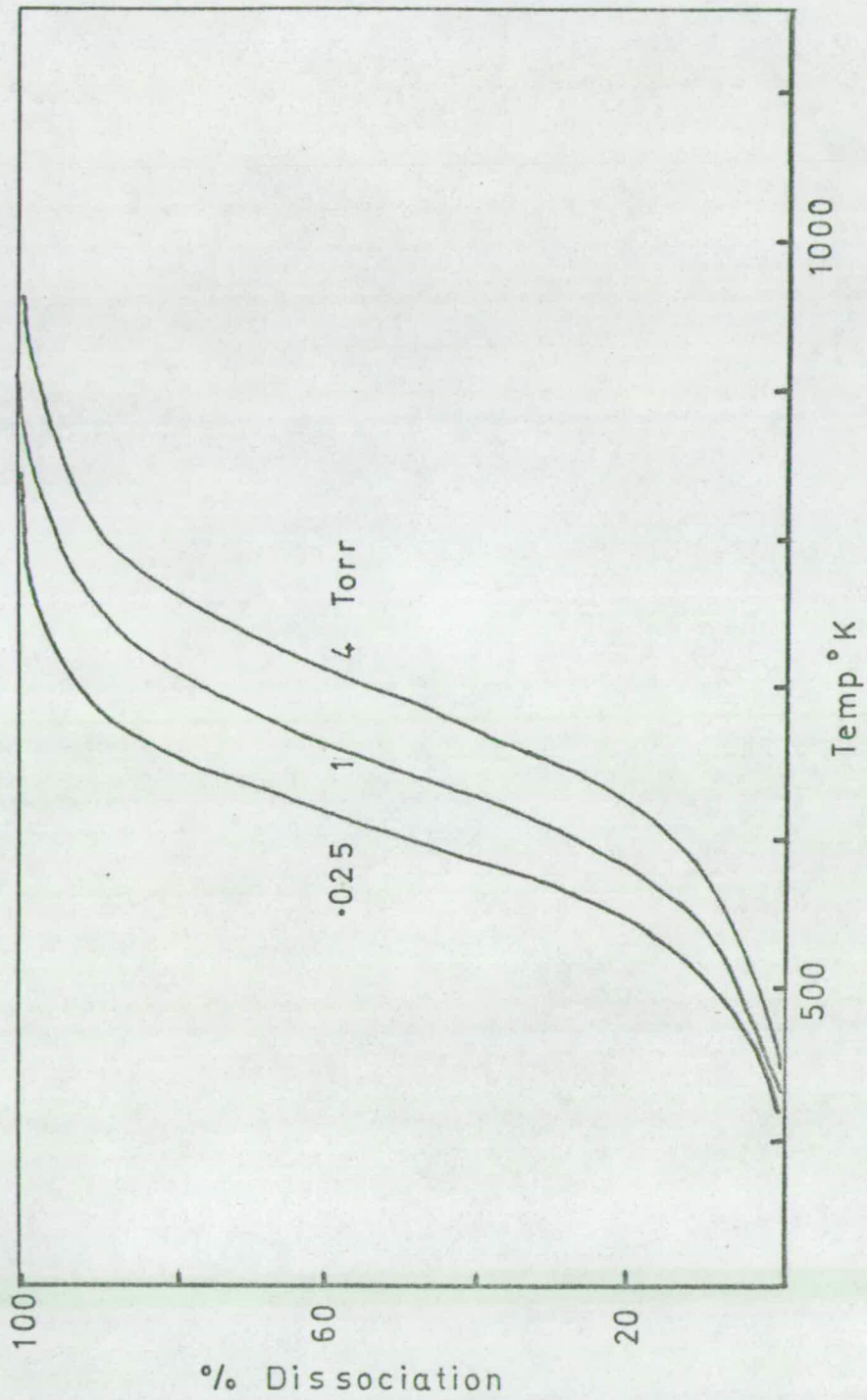

Fig. (3,19)

Percentage Iodine dissociation vs Temperature.

etc. are normally formed from nickel which is badly attacked by iodine.

The solution found to this problem was to use a glass capillary array. This material, "Permionics", was 0.25 cms thick, had pores 50 μ in diameter and was about 70% transparent. A section of the material 0.6 cms x 0.2 cms was "araldited" in a channel machined in the source, the beam was defined by means of gold slits 0.6 cms x 0.05 cms.

Mount

The cross-beam mount is shown in Fig. (3,20). The upper plate, which carried the source etc., was supported by four stainless steel pillars mounted on the base plate. The source was located on three rounded tungsten pins. The beam was modulated (see next section) by a sixteen slot disc driven by a Smiths MHS/3 Motor which was mounted on the upper plate. In order to prevent the main beam 'seeing" the chopper disc the disc was enclosed by a copper sheet. Also mounted on the upper plate were two 9 way electrical connectors and a light bulb which formed part of the modulation system. On the base plate was attached a photo-cell and main-beam collimating slits.

Performance

The intensity obtained from a long narrow channel has been studied by Giordmaine and Wang (GIO 60), following their results an intensity of 3.3×10^{14} atoms/str was calculated for an iodine vapour pressure of 5 torr. It

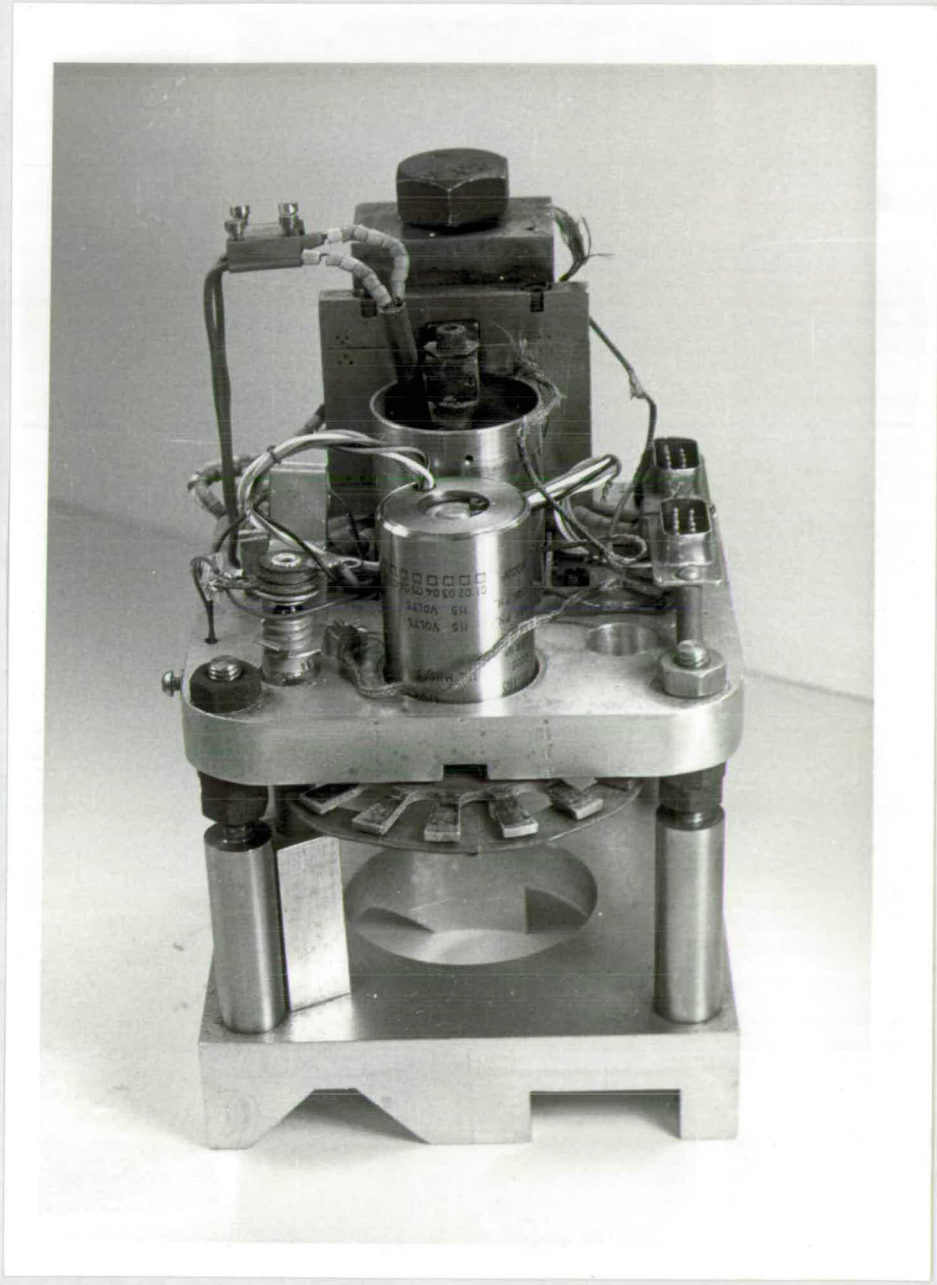

Fig. (3.20)

Cross-Beam Mount.

was not possible to measure the cross-beam flux directly, it could be inferred, however, from the attenuation of the main beam.

Assuming a total cross-section of 20 A^2 and a scattering region 0.4 cm long the main beam attenuation was calculated to be 2.9%, this compared with a measured value of around 2.5%. It would clearly be an advantage if the attenuation could be increased, this was not possible with the present source, in fact a nozzle source would be required.

Expected Scattered Flux

The scattered flux at an angle Θ is given by

$$I(\Theta) = \frac{N_m N_x V_s \, 6(\Theta) \, V_r W_o h_o}{V_m V_x l^2}$$

where

N_m = main-beam flux

N_x = cross-beam flux

V_s = scattering volume

V_m = main-beam velocity

V_x = cross-beam velocity

V_r = relative velocity

W_o = detector width

h_o = detector height

$6(\Theta)$ = differential cross-section

l = distance from detector to scattering centre

Now $V_m \sim V_r \gg V_x$

and $V_s \sim h_o^2 W_o$

$$\therefore \quad I(\Theta) \lesssim \frac{N_m N_x \, 6(\Theta) \, W_o h_o^3}{V_x \, l^2}$$

Taking

$N_x \sim 10^{17}$ atoms $cm^{-2} sec^{-1}$

$N_m \sim 2 \times 10^{7}$ atoms $cm^{-2} sec^{-1}$

$V_m \sim 2 \times 10^{6}$ cms sec^{-1}

$V_x \sim 1.7 \times 10^{4}$ cms sec^{-1}

$h_o = 0.5$ cms

$W_o = 0.05$ cms

$l = 58$ cm

$$I(\theta) \lesssim 10^{13} \times 6\ (\theta) \quad \text{particles/sec}$$

Using the calculated values of 6 (θ) a scattered flux of the order of 100-10 particles/sec was predicted which was in fair accord with experiment.

Power Supplies

The cross-beam source heater was supplied by a 20 v 5A D.C. power unit and the dissociation chamber heater by a 30 v 10A D.C. power unit. The A.C. power to each unit was controlled by an Ether type 991 temperature controller. Temperatures were measured using NiCr/NiAl thermocouples. The chopper motor was supplied by an 8 volts 2 phase 50 hz A.C. power unit, a starting voltage of 14 volts was also available.

Modulation.

The experiment in which the measured signal corresponds to the scattered flux alone is realised in experimentalists dreams only. In practice the signal, at any angle, is made up of a number of contributions. These

are -

1. Main-beam atoms scattered by the cross-beam
2. Main-beam atoms scattered by the background gas
3. At small angles the main beam "wings"
4. Noise from the ion-pump
5. Noise in the detection electronics I.E. multiplier dark current.

If the noise, I.E. contributions 2,3,4 and 5, was constant then the true scattered signal, contribution 1, could be easily found by switching the cross-beam off and on with a beam flag. However none of these quantities is constant with time, some are slowly varying some rapidly.

Consider first the contributions from the ion-pump and detector electronics, these are essentially random in nature and present no real problem. In fact it was normal when collecting data to turn the ion-pump off hence removing a major source of noise. More important is the contribution due to scattering from the background gas, this will fluctuate due to uneveness in the pumping of the diffusion pumps. The effect of these fluctuations may be reduced by modulating the cross-beam.

The theory behind the modulation technique has recently been reviewed (FON 66) and will not be gone into here. Suffice to say that the vacuum system may be treated in a manner analageous to an RC electrical filter handling voltage fluctuations. Associated with the vacuum system

there is a pressure time constant τ given by

$$\tau = V/S$$

Where V is the system volume and S the pumping speed. It can be shown that an improvement in the signal:noise ratio is obtained if

$$\tau > 1/\nu$$

where ν is the cross-beam modulation frequency. In our case the volume of the cross-beam chamber was eighteen litres while the pumping speed was 1000 L/S hence

$$\tau = 18 \text{ ms}$$

The time constants of the source and detector chambers are 30 ms and 100 ms respectively. The modulation frequency used was 266.7 Hz.

Experimental arrangement

The cross-beam was chopped by means of a rotating disc, this has been described in the section dealing with the cross-beam source. A reference signal was taken from the disc by means of a lamp and photocell, this was arranged so that the reference pulse and the pulse leaving the cross-beam were in phase. The photocell used was an M.S.P. 6 silicon photodiode, this was arranged in the input of a Schmitt trigger Fig. (3,21). The Schmitt was somewhat unusual in that both its trigger point and hysteresis were adjustable. The smallest possible value of hysteresis, a few millivolts, was used in order to reduce jitter in the pick off point. After the cross-beam is turned on

there is a delay of around 100μs, corresponding to flight times in the apparatus, before a signal appears at the detector. The duration of the signal is 2.2 ms there then follows a noise period of 1.6 ms when the cross-beam is shut off. The situation is summarised in Fig. (3,22). The two counters are arranged so that one counts during the signal on period only and the other during the signal off period.

The opening and closing of the counters is controlled by delay lines fed from the Schmitt, these are shown in Fig. (3.23). Each delay line consists of two Aim PWD 103 pulse width/delay units and an Aim PPA 104 pulse amplifier. The sequence of operation is best inferred from the diagram, in outline it is as follows. The output pulse from the Schmitt is connected to the input of the first PWD 103 of the signal line, I.E. the delay line which opens the counter during the signal on period. The pulse on emerging from the PPA 104 amplifier has an amplitude swinging from +1 to -1 volts set by the amplifier, a width W1 of 1 ms set by the second PWD 103 in the line and is delayed with respect to the input pulse by an amount D1 0.6 ms set by the first PWD 103. The output pulse is connected to the inhibit line of one of the counters. The counter is turned on by +1 volts and off by -1 volts. A similar sequence occurs in the other delay line except that for reasons of stability, it is fed not from the Schmitt but from the output of the first PWD 103 in the signal line. The delay D2 was 1.8 ms hence the total delay of the noise line was 2.4 ms, I.E. D1 + D2, the width W2 was 1 ms.

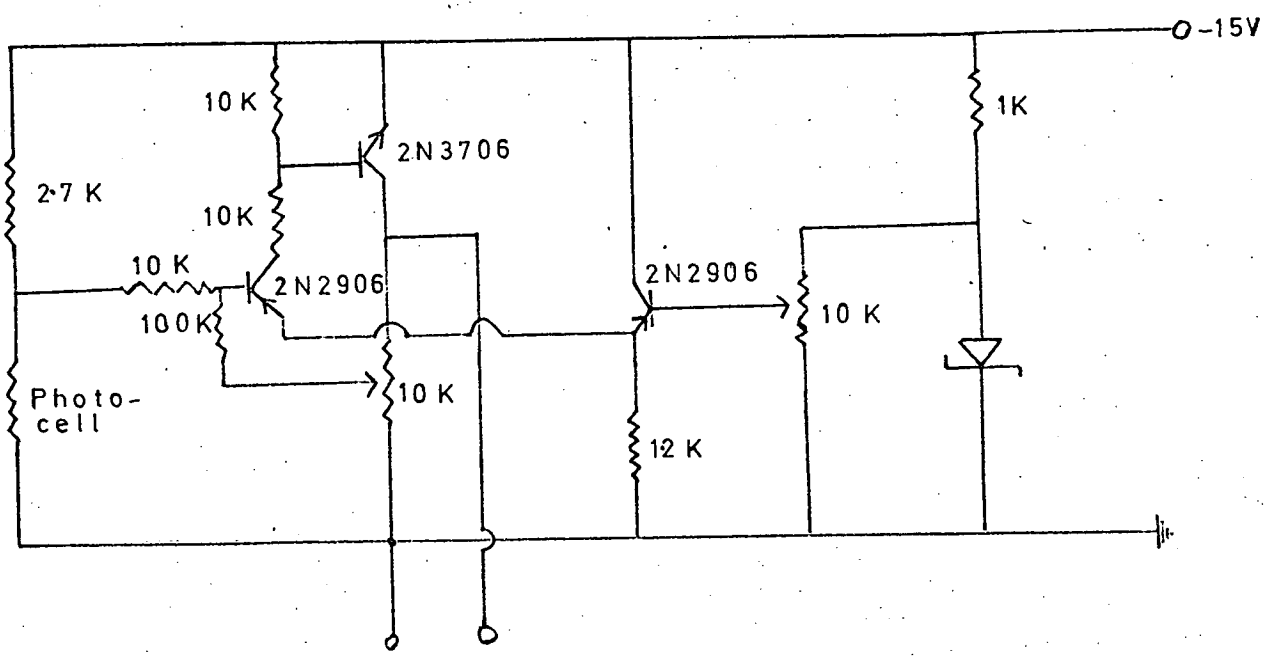

Fig. (3,21)

Schmitt Trigger.

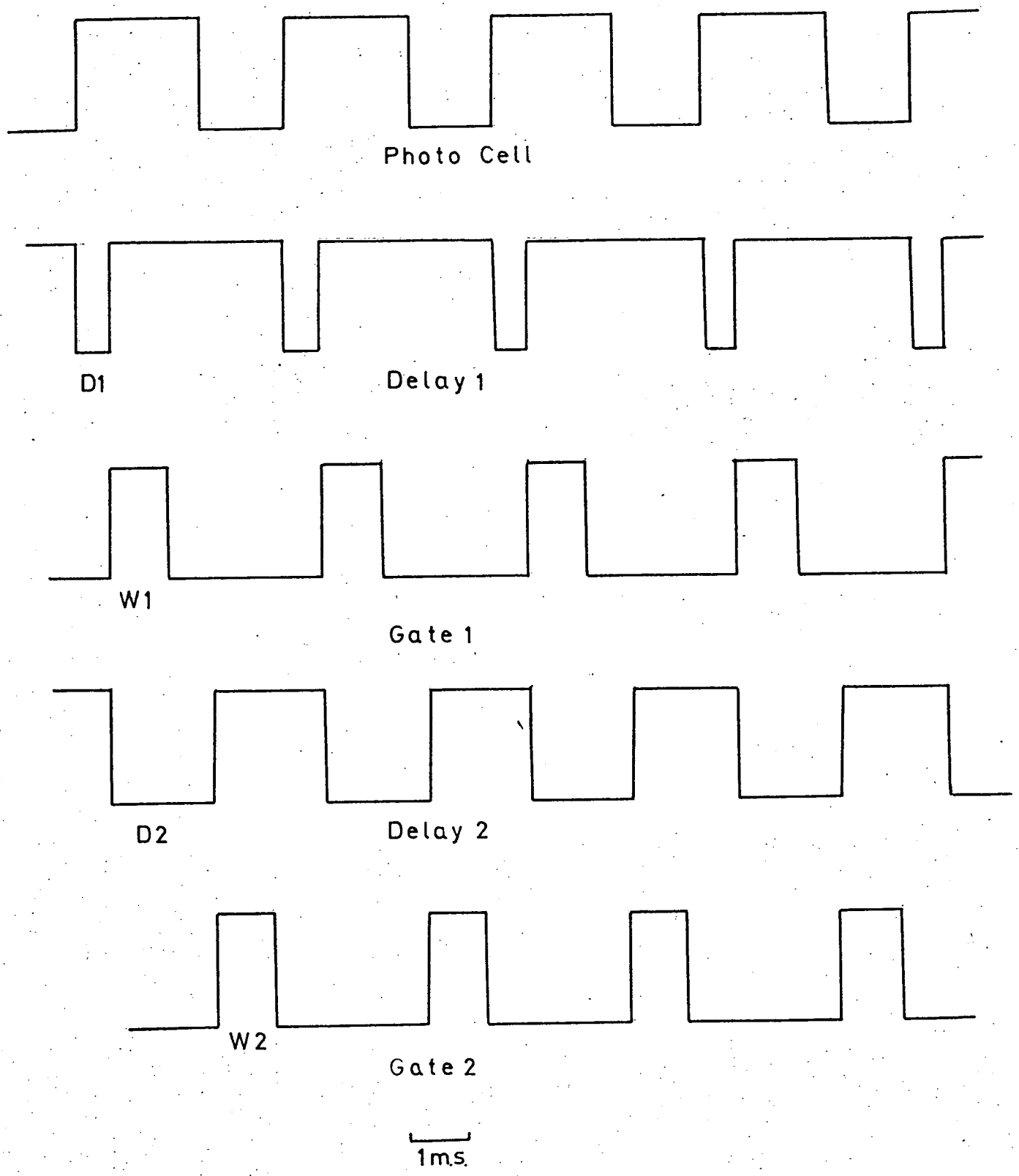

Fig. (3.22)

Modulation Sequence.

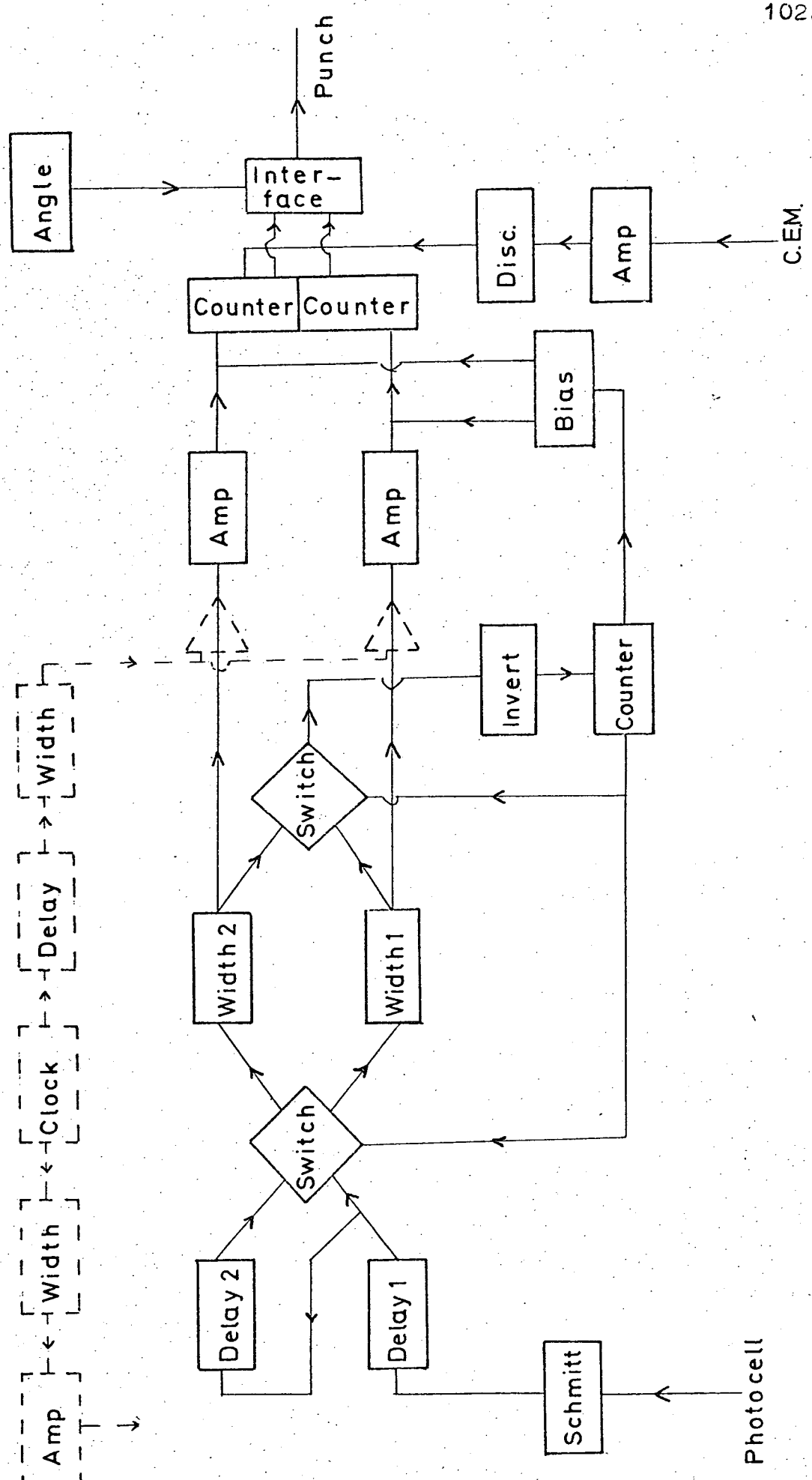

Fig. (3,23)

Modulation Circuit.

Having started this sequence off it is necessary to stop it when sufficient data has been collected, this was achieved using a Wateeta 500 series batching counter. The Wateeta counts the modulation pulses, at the output of the last PPA 103 in the noise line, when a preset number is reached the counters are closed by biasing the inhibit lines negative. No further data can be recorded until the Wateeta reaches another preset number at which it resets itself and opens the counters again. During the time in which the counters are closed the data accumulated is recorded either manually or on paper tape, the counters then being reset to zero.

If the signal is S Hz and the noise N Hz and the counters were open for n modulation periods, then the numbers recorded on the two counters will be nW1 (S+N) and nW2 N. In order, therefore, to obtain the scattered signal S it would be necessary to know W1 and W2, although they are nominally equal they may differ by several percent. In order to obtain the true signal S it is therefore necessary to switch the widths W1 and W2 between the two delay lines, it is of course necessary to switch the input to the batching counter at the same time. Switching occurred at the end of each batch of n modulation cycles. The numbers recorded on the counters in two successive batches will be

$$nW1(S+N) \qquad nW2\ N$$

$$nW1\ N \qquad nW2(S+N)$$

Hence one may easily obtain

$$n.(W1+W2).\ S$$

In order to check the counting system for any possible systematic error the background signal from the ion-pump was used as a source of random noise. About six hundred observations were taken and the mean of the difference between consecutive observations calculated, this should be zero. For a total of 636 observations each of 1000 modulation cycles the mean count per observation was 118.5 and the mean difference between consecutive observations was 0.98 with a standard deviation of 0.66. This may be interpreted by saying that at the 95% confidence level there is no systematic bias greater than about 0.8%.

Recording of data.

The amount of data obtained during a scattering experiment may be enormous. It is necessary to have a system capable of handling this data if the potential of the numerical output is to be realised in full. At any one angle the scattered signal and its variance is required. The order of ten observations at up to a hundred angles must therefore be made. This is clearly not practicable by hand.

The ideal solution to the problem of data handling would be an on line computer, this would provide immediate feed-back to the operator and hence the experimental conditions could be optimised. This ideal has not yet been realised.

In the data handling system used, numbers from the counters and the angle encoder were punched on paper

tape which was later analysed by computer. The hub of the system was the interface unit, this interrogated the counters and angle encoder and operated the tape punch. The operation of the system will be briefly described.

Numbers recorded by the counters appeared on 7 x 4 B.C.D. lines, in addition there were 4 identifier lines, the angle (or rather a linear measurement related to the angle) appeared on 4 x 4 B.C.D. lines. In addition there were three manual flag lines and a line indicating the state of the width switching unit. There were therefore a total of 84 B.C.D. lines, these were punched on eleven lines of eight hole tape. This system is therefore very efficient giving two decimal digits per line of paper tape. The punching sequence was as follows: At the end of a counting period the Watesta batching counter sent a pulse to the interface unit which then selected eight B.C.D. lines, punched them to tape and advanced the tape, another eight B.C.D. lines were then selected and punched, this occurred eleven times making a total of eighty-eight characters. The four extra characters were used as check digits by repeating previous characters. The punching rate, controlled by an internal oscillator, was 30 tape lines/sec. hence the total time taken to punch eightyeight characters was less than half a second. At the end of a punching sequence the interface reset.the counters to zero.

If required the frequency of the internal oscillator could be raised, this would allow a much higher sampling rate.

Apparatus Resolution

If the apparatus were ideal then the observed scattering pattern would have the form predicted above, see Fig. (3,25). In the case of a real apparatus what is observed is the "ideal" scattering pattern convoluted with the apparatus constants.

The following must be taken into account in a "real" apparatus:

(a) Finite main-beam size

(b) Finite cross-beam size

(c) Energy distribution in main beam

(d) Cross-beam energy distribution

(e) Finite detector size.

In this case the energy of the cross-beam, about 0.1 e.v., was unimportant hence contribution d could be neglected. The main-beam energy spread was about 0.25 e.v. and hence was unimportant. It has been shown (COW 68) that b is unimportant in the case of small angle scattering. It was decided therefore to average the "ideal" scattered signal over the detector and main beam only. Of special interest was the effect of finite detector height on the angular resolution at small angles, for $\phi \leq h/l$, where h is the detector height and l the distance from the scattering centre.

It was considered that this part of the work was particularly important as much of the early high energy beam work has been found to be invalid due to neglect of

apparatus averaging.

The observed scattered flux at an angle ϕ may be written as

$$I'(\phi) = \int_0^{h'} \int_{\phi-d\phi}^{\phi+d\phi} \int_0^{h} \int_{-\gamma/2}^{\gamma/2} F(\psi, \xi, Y, Z)\, d\psi\, d\xi\, dY\, dZ$$

Clearly the problem falls into two parts, averaging over the main-beam and averaging over the detector.

Averaging over main beam.

The coordinate system used is shown in Fig. (3,24). The scattered intensity at a height Z and angle ϕ is

$$I(\phi, Z) = \int_0^{h} \int_{-\gamma/2}^{\gamma/2} F(\psi, Y)\, d\psi\, dY$$

where h and γ are the heights and angular width of the main beam. From the figure

$$x^2 = \ell'^2 + \ell^2 - 2\ell\ell' \cos\alpha$$

but

$$x^2 = y^2 + 2\ell^2 - 2\ell^2 \cos\phi$$

and

$$\ell'^2 = y^2 + \ell^2$$

$$\therefore \quad \alpha = \cos^{-1}\left[\ell \cos\phi / (y^2+\ell^2)^{1/2}\right]$$

hence

$$F(\psi, Y) = I(\alpha)\, P(\psi)$$

where I (α) is the "ideal" intensity at an angle α and P (ψ) the main beam profile.

I(ϕ Z) was obtained from the previously calculated I(ϕ), the main beam profile being taken as trapezoidal. The values of Z chosen were the abscissae of a seven point Gauss quadrature.

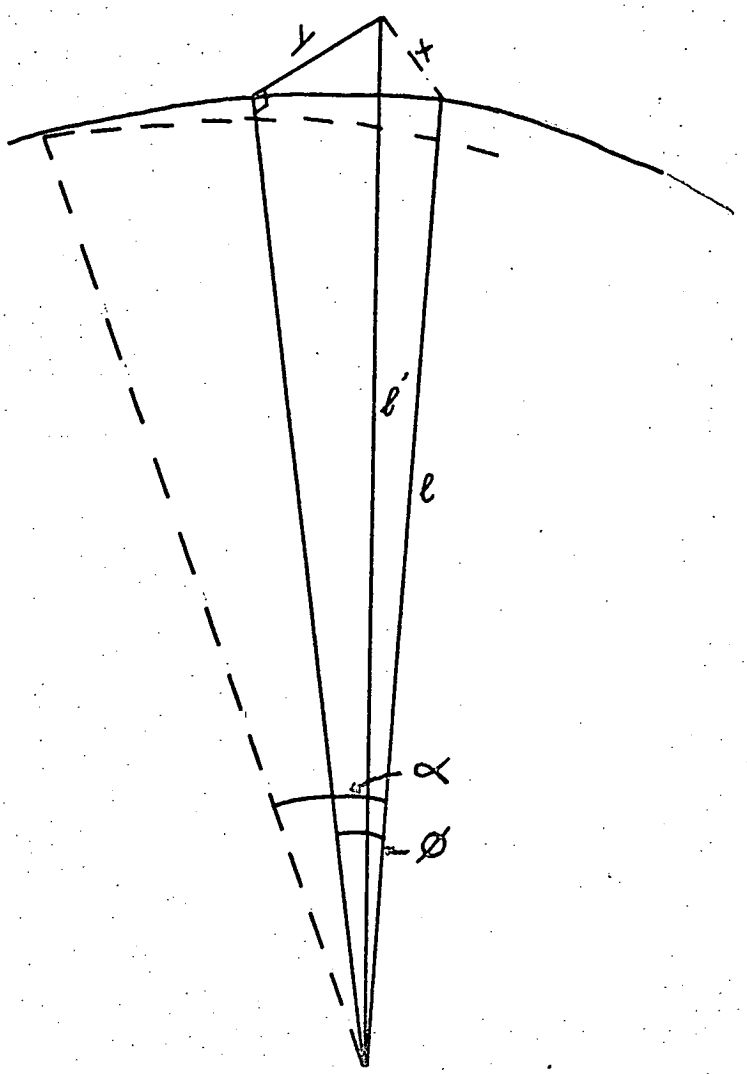

Fig. (3,24)

Apparatus Averaging Coordinates.

Averaging over detector.

The measured intensity at an angle ϕ may be written as

$$I'(\phi) = \int_0^{h'} \int_{\phi-d\phi}^{\phi+d\phi} I(\xi, Z)\, d\xi\, dZ$$

where h^1 is the detector height and $d\phi$ is the detector angular half-width, $d\phi = \tan^{-1}(W/21)$ where W is the detector width. The integral was evaluated using Simpsons rule over ξ and a seven point Gauss quadrature over Z. The values taken for the apparatus parameters were $h = h^1 = 0.31"$, $W = 0.020"$ $l = 22.7"$, $\gamma = 0.12^0$

General Predictions

In order to assess the importance of the various apparatus parameters the apparatus averaged scattering pattern was calculated using different values of the detector height. The potential used was the Lennard-Jones 12-6 with $\epsilon = 1.0$ p.erg and $r_m = 3.0\text{Å}$, the ideal scattered intensity is shown in Fig. (3,25). The rainbow angle is seen to be 0.65^0 with secondary bows at 0.35^0 and 0.15^0, superimposed on the bows are much faster oscillations having a separation of about 0.05^0. The apparatus averaged scattering pattern, calculated using the above values of the apparatus parameters, is shown in Fig. (3,26). It will be seen that although the primary and secondary bows are still visible the short wavelength oscillations have been smeared out. The apparatus resolution was therefore better than 0.2^0 for angles greater than about 0.1^0. It was considered that an apparatus resolution of this magnitude would be adequate as a knowledge

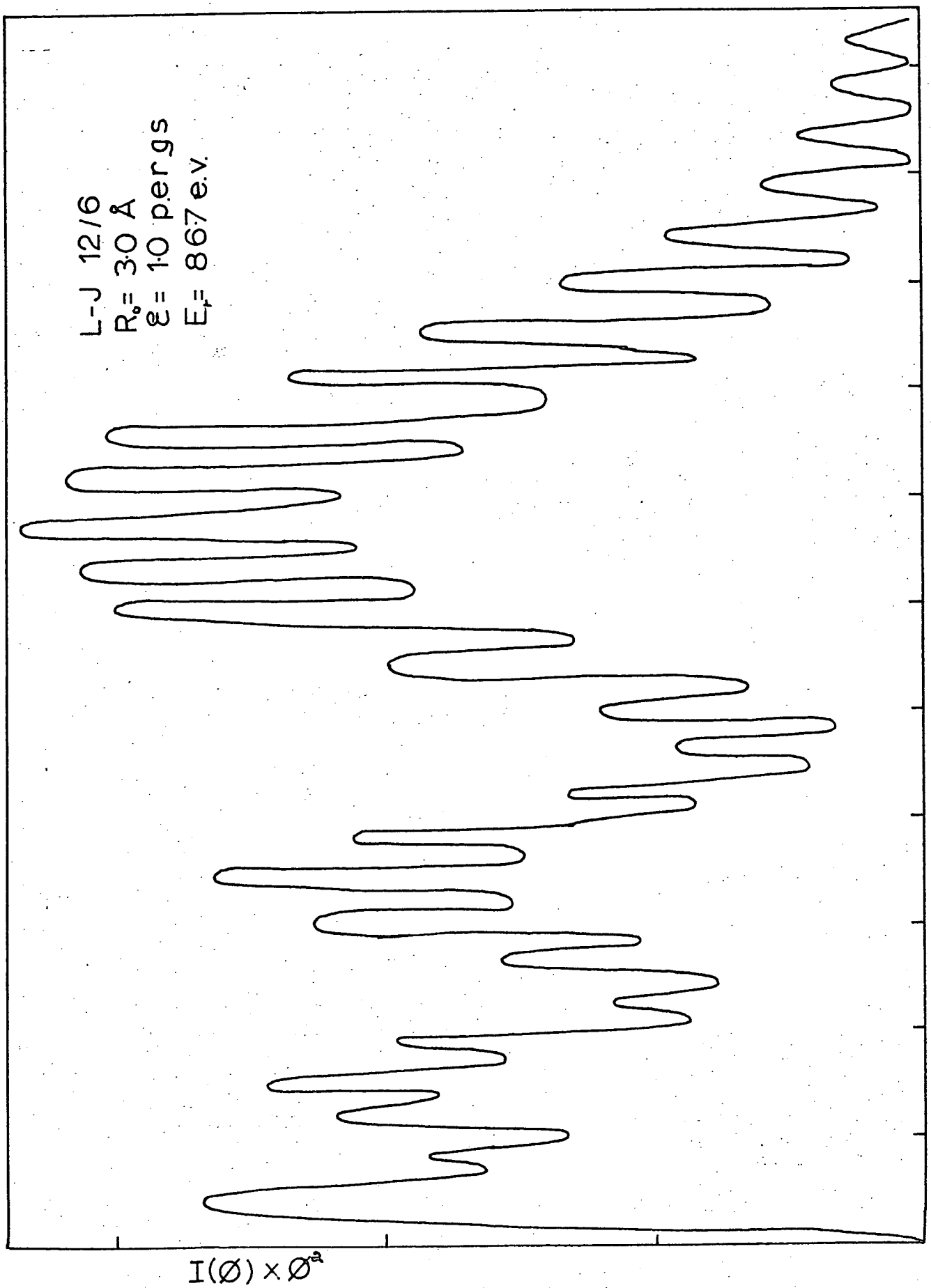

Fig. (3,25)

Ideal Scattered Intensity.

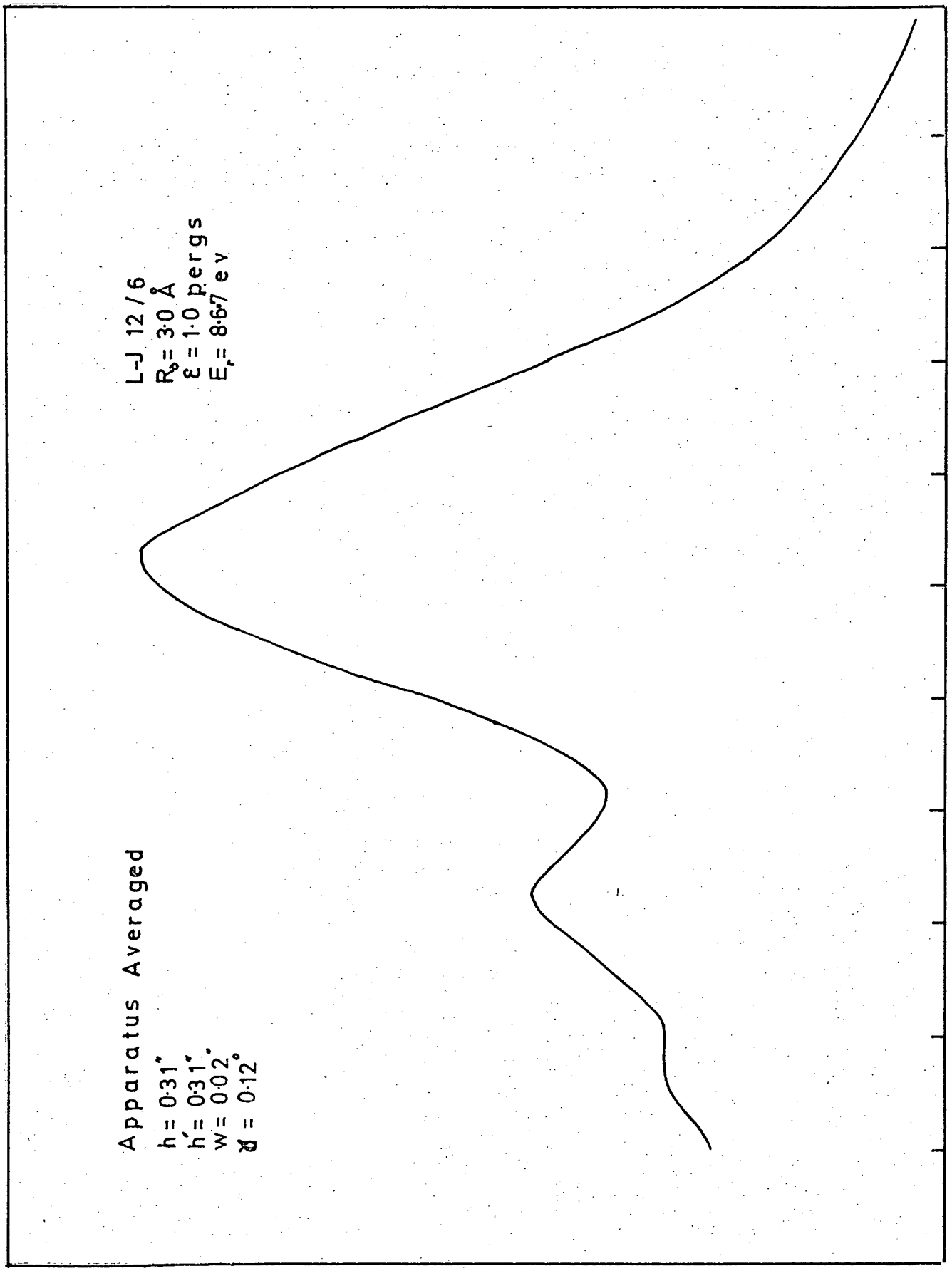

Fig. (3,26)

Apparatus Averaged Intensity.

of the rainbow structure is sufficient for most purposes, moreover an improvement in the resolution can only be gained at the expense of signal.

In order to separate the effects of the various apparatus parameters the averaged scattered intensity was calculated using the following values of apparatus parameters $h = 0.31"$, $h^1 = 0.31"$, $W = 0.001"$, $\gamma = 0.001^o$ and $h = 0.001"$, $h^1 = 0.001$, $W = 0.020"$, $\gamma = 0.12^o$. The results are shown in Fig. (3.27) and (Fig. 3.28). It will be seen that in neither case is there any real improvement in resolution, it is therefore clear that an increased resolution, if required, can be achieved only by reducing both the width and height of the detector and main-beam. The resulting decrease in signal does not recommend such action.

Experimental Procedure.

Alignment

It is of critical importance in any scattering experiment that the components are correctly aligned. The maintenance of alignment, once set, was facilitated by the optical bench arrangement; components, once aligned, could be removed from the system without the alignment being lost.

First the components of the main beam source were aligned, lenses, charge-exchange chamber etc., so that the main beam axis coincided with the centre of the detector. A section of base plate with a pin driven into it was used as an alignment jig Fig (3.3). The point of the pin lay on the beam axis and was used to align a telescope, permanently

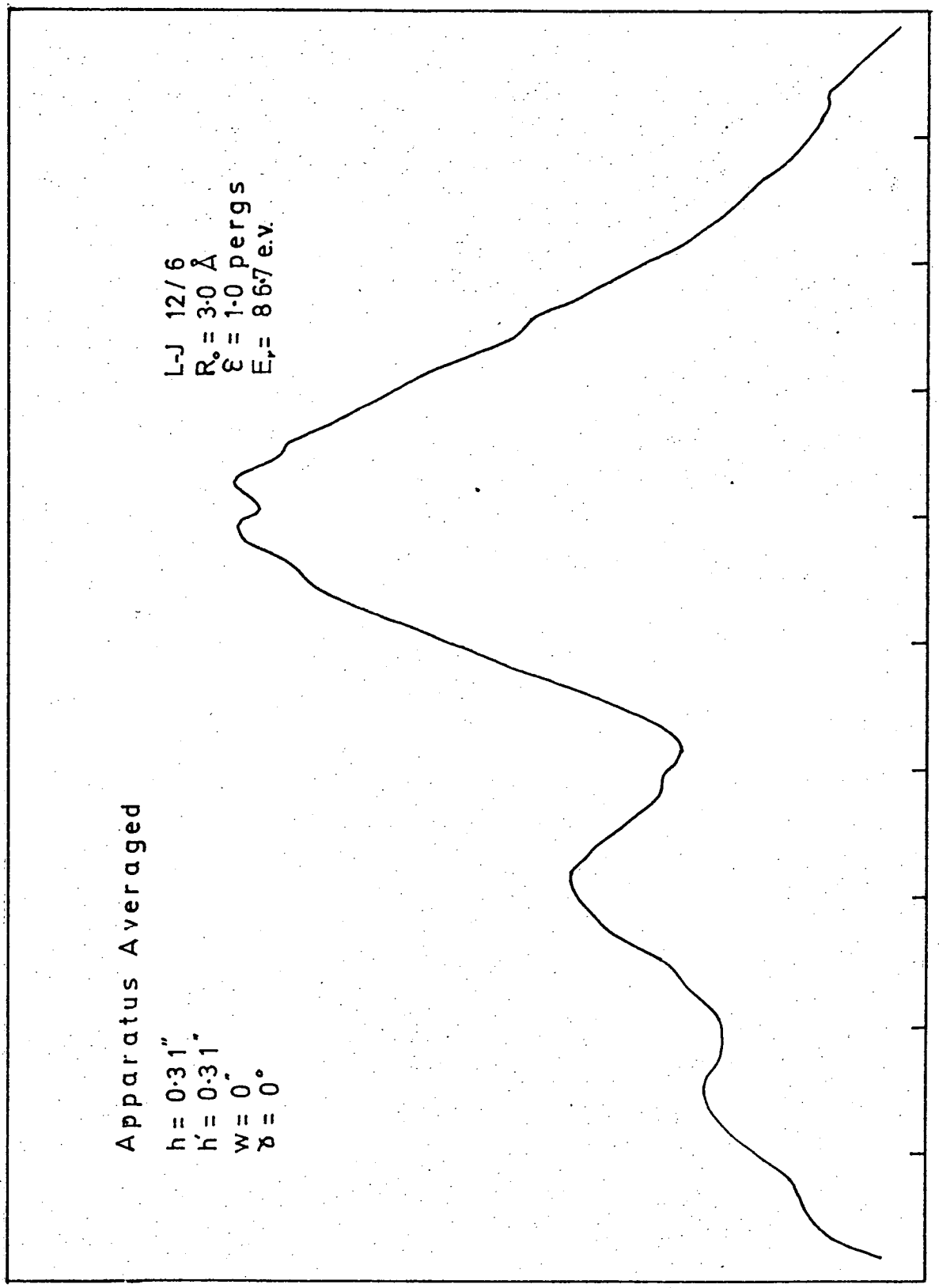

Fig. (3,27)

Apparatus Averaged Intensity.

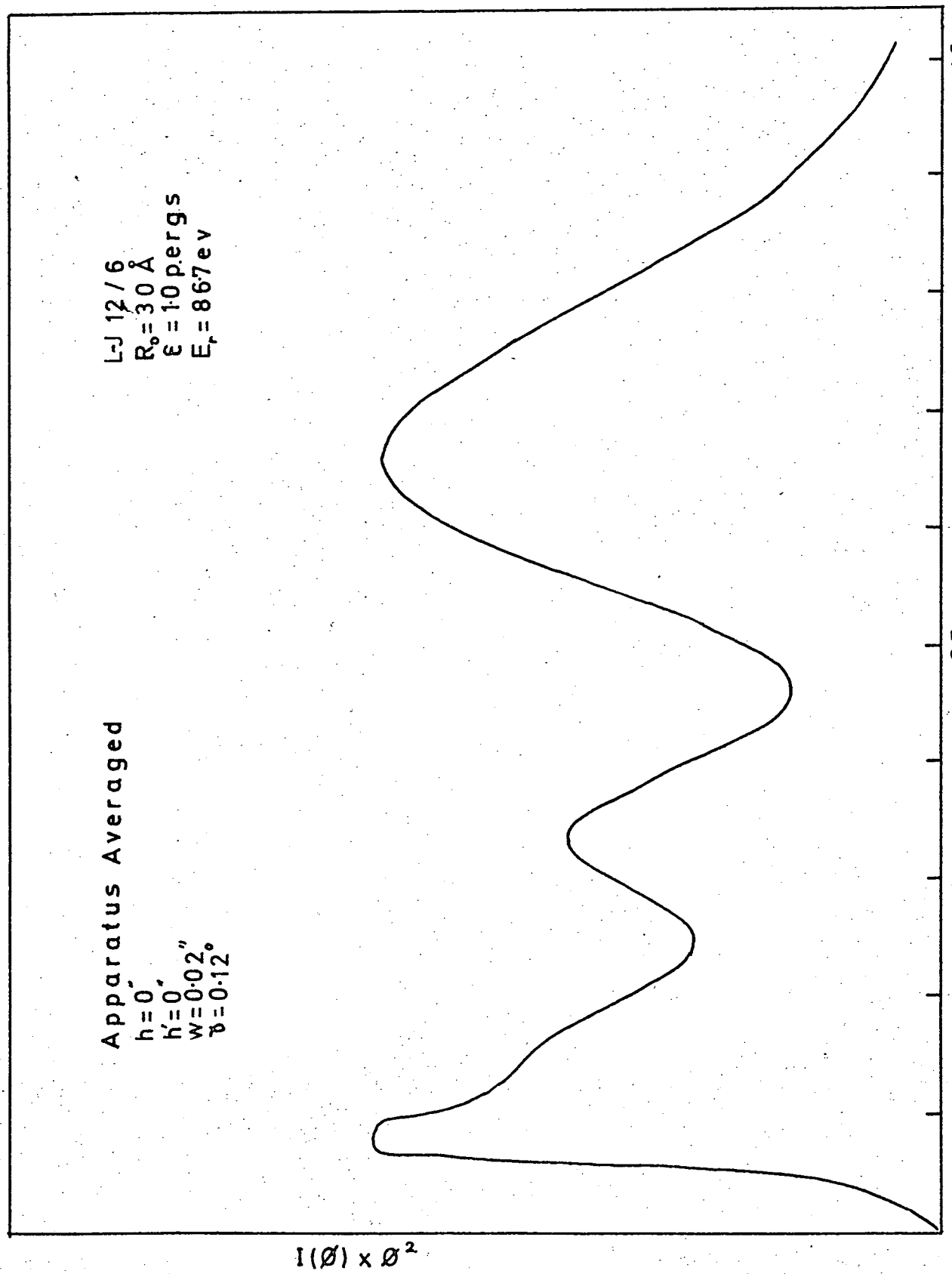

Fig. (3,28)

Apparatus Averaged Intensity.

mounted on one end of the apparatus, along the beam axis.

Alignment of the cross-beam was a more difficult problem, as it pointed downwards the slits could not be viewed directly. Alignment was carried out, therefore, on a flat table using an engineers height gauge.

Preliminary Procedures.

Having ensured the correct alignment of components the cross beam was loaded and placed in position, electrical connections were made and the system checked. The main beam supply oven and charge exchange chamber were loaded with glass phials of distilled potassium which were crushed on sealing the chambers. The source and charge exchange chamber were placed in position, electrical connections made and the system checked.

The system was roughed down to 0.2 torr, the backing line traps filled with liquid nitrogen and the diffusion pumps started. When the pumps were boiling the cryo-baffles were filled with liquid nitrogen, the levels being thereafter maintained automatically. The apparatus was then generally left to pump overnight. When the pressure had fallen to about 10^{-5} torr the ion-source cooling water was turned on and the cold traps filled with liquid nitrogen. The charge exchange chamber, source oven and ioniser heater were then slowly warmed, the source and ioniser being brought to operating temperature first. The ion beam was located and steered through the charge exchange chamber using the deflector plates, the ion current was then maximised by adjusting the grid and acceleration voltages. The charge exchange chamber was then brought to its operating

temperature and the main beam flux at the detector maximised by adjusting the deflector, grid and accelerator voltages. A preliminary angle scan was then made to determine the main-beam profile. The cross-beam was brought up to operating temperature and the apparatus allowed to stabilise.

Data Collection

At the start of a sweep the detector was positioned just to one side of the main-beam, a start of sweep code was set up on the interface manual flags and counting begun. After the first counting period the manual flag was changed to the normal run code. After about twenty counting periods the detector position was changed by about 0.04°. The detector was swung through the main beam and one to two degrees from it. As the detector was moved further from the main beam the time spent at each angle was increased. When it appeared that sufficient data had been collected the end of sweep code was punched and counting stopped. Each sweep took about 1½ hours and about a dozen sweeps were taken in any one run.

Preliminary data reduction.

Details such as collision partners, main beam energy etc. were added to each data tape and the tapes read to magnetic tape prior to analysis.

The analysis program first reconstructed the decimal data, the format of each sentence is shown in Fig. (3,29). The program searched the data until the start code was located, it then continued until the sentence end code was found, the sentence was then checked to see if it had the correct format, if not it was rejected. The sentence, if accepted, was stored

Tape Characters 1 - 4	Tape Characters 5 - 8
Start Code	Scaler "A" 10^0
Scaler "A" 10^1	Scaler "A" 10^2
Scaler "A" 10^3	Scaler "A" 10^4
Scaler "A" 10^5	Scaler "A" 10^6
Flags	Angle 10^{-3}
Angle 10^{-2}	Angle 10^{-1}
Angle 10^0	Scaler "B" 10^0
Scaler "B" 10^1	Scaler "B" 10^2
Scaler "B" 10^3	Scaler "B" 10^4
Scaler "B" 10^5	Scaler "B" 10^6
Check digits	End Code

Fig. (3,29)

Sentence Format.

and the next sentence located, this procedure continued until the angle was found to have changed, all the data taken at one angle were then processed. The mean and standard deviations of the scattered signal were calculated, any observations differing by more than two standard deviations from the mean were rejected and the mean and standard deviation recalculated. This procedure removed the effect of any burst noise. The procedure was continued until the end of sweep code was identified, a summary of the data was printed and also stored on disc for subsequent analysis.

Analysis of data

The method of analysis used was similar to that described by Cowley (COW 69b) and Horne (HOR 69) which was based on the method of Morrison (MOR 63), deconvolution using the main beam profile was not included however.

Data, previously reduced by the method outlined above, were read from magnetic tape and then filtered using Morrisons method. In this method a smoothing function f, in our case f was the main beam profile, is applied, I.E.

$$I_1(\theta) = I(\theta)_{obs} * f$$

$$I_i(\theta) = I_{i-1}(\theta) + \left(I(\theta)_{obs} - I_{i-1}(\theta) \right) * f$$

the iterated values being constrained to lie within four standard deviations of the observed intensity. This has the effect of removing attenuation, I.E., apparently negative

scattered intensity at small angles, and noise incompatable with the transform f.

Time of flight

The importance of energy transfer studies to reaction kinetics, gaseous transport properties etc. has already been mentioned. A method of finding the translational energy lost, or gained, by a particle during a collision is to measure its time of flight over a known distance. Although experiments of this kind were not done during the course of this work, the apparatus and experimental procedures have been developed to the point where such an experiment would be feasible. It is worthwhile, therefore, going into the possibilities and difficulties of such an experiment. The collision partners of immediate interest were K/I_2. Neglecting electron excitation there are two inelastic channels of interest.

$$K + I_2 \longrightarrow K + I_2^* \qquad (1)$$

$$K + I_2 \longrightarrow KI + I \qquad (2)$$

The arrival spectrum resulting from these processes was calculated. It was assumed that in process (1) the potassium lost a maximum of 1.5 e.v. (the iodine bond strength) to vibrational excitation, in process (2) it was assumed that about 75% of the reaction exothermicity went into vibrational excitation of KI. To make these calculations meaningful account must be taken of the initial energy distribution of the potassium, this was assumed to be Maxwellian with a

temperature corresponding to that of the ion emitter (this is discussed in the next section). The arrival spectrum for a range of initial energies is shown in Fig. (3,30). It will be seen that to detect process (1) a time resolution of 0.5 μs or better is required. This appears to be within the bounds of possibility but requires further study. A point of encouragement is that provided the arrival spectrum can be measured accurately it is possible to deconvolute it to remove the effect of the initial energy spread the form of which is known. The detection of any slower KI should present no problems.

Experimental Arrangement

In essence the technique is quite simple, the main beam is modulated to form short, ~ 1 μs. pulses. A short time later the detector is enabled for about 1 μs. and the signal noted. By varying the delay between the start of the main beam pulse and enabling the detector the arrival spectrum may be mapped. However the remarks made in the section dealing with cross-beam modulation still hold hence the time of flight procedure must be tied in with it. A block diagram of the cross-beam modulation and time of flight electronics is shown in Fig. (3,23). The relationship to the original system can be easily seen, the only additions are a clock generator and delay line, and two AND gates. An attempt will be made to describe the operation of the system. Modulation pulses are provided by an AIM C.G.U. 102 clock generator, these are fed to two lines, one to modulate the main beam and one to open the counters. The width of the beam

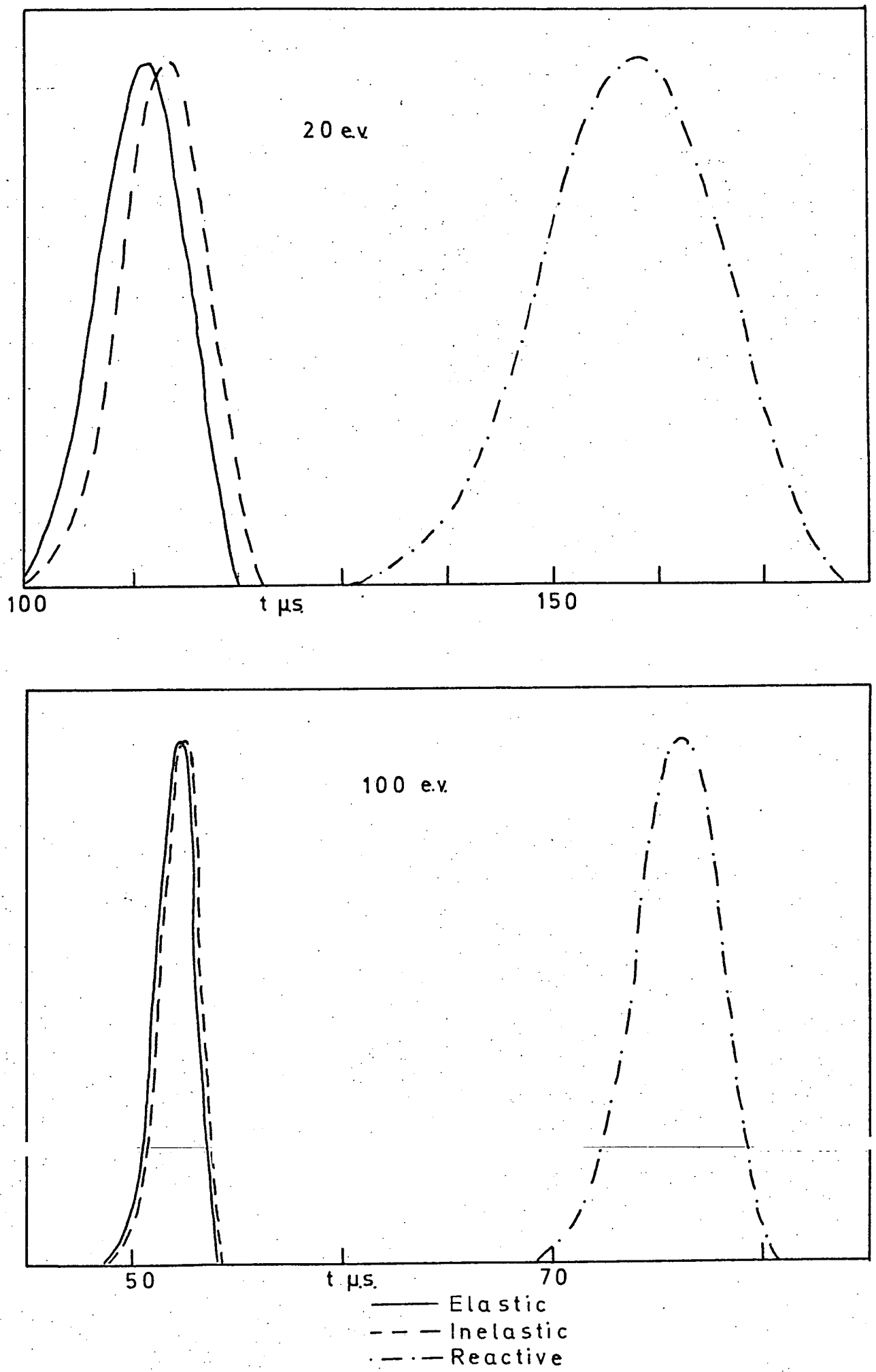

Fig. (3,30)

modulation pulse is set using an AIM PWD 103 and the levels using an AIM PPA 104, the pulse is then applied to the ion-beam deflector plates, the pulse levels set such that when the pulse is "On" the ion-beam is on. The counter control pulse is delayed by two PWD 103's and then paralleled to one input of each AND gate. The other inputs of the AND gates are connected to the outputs of the modulation lines final PWD 103's, and the AND gate outputs fed into the modulation line PPA 104's. The relationships between the various pulses is shown in Fig. (3,31). The remainder of the data handling system is unchanged.

In order to check the system the flight time of potassium, without a collision partner, was measured. The results are shown in Fig. (3,32). A large discrepancy was found between the measured and calculated flight times, about 14μs. This has, however, been accounted for in the flight time of ions in the quadrapole, this was found to be 14.9μs.

More data are required in order to calibrate the apparatus. This is necessary as the actual beam energy does not correspond exactly to the set voltage due to contact potentials. It is thought that this effect will give rise to an error of less than 1 e.v. and hence is unimportant in elastic scattering studies except at low energies. A restriction of the present system is the time taken to collect data. This could be improved upon by replacing the counters with a fast multi-channel analyser or an on-line computer. Such systems have not yet been tried.

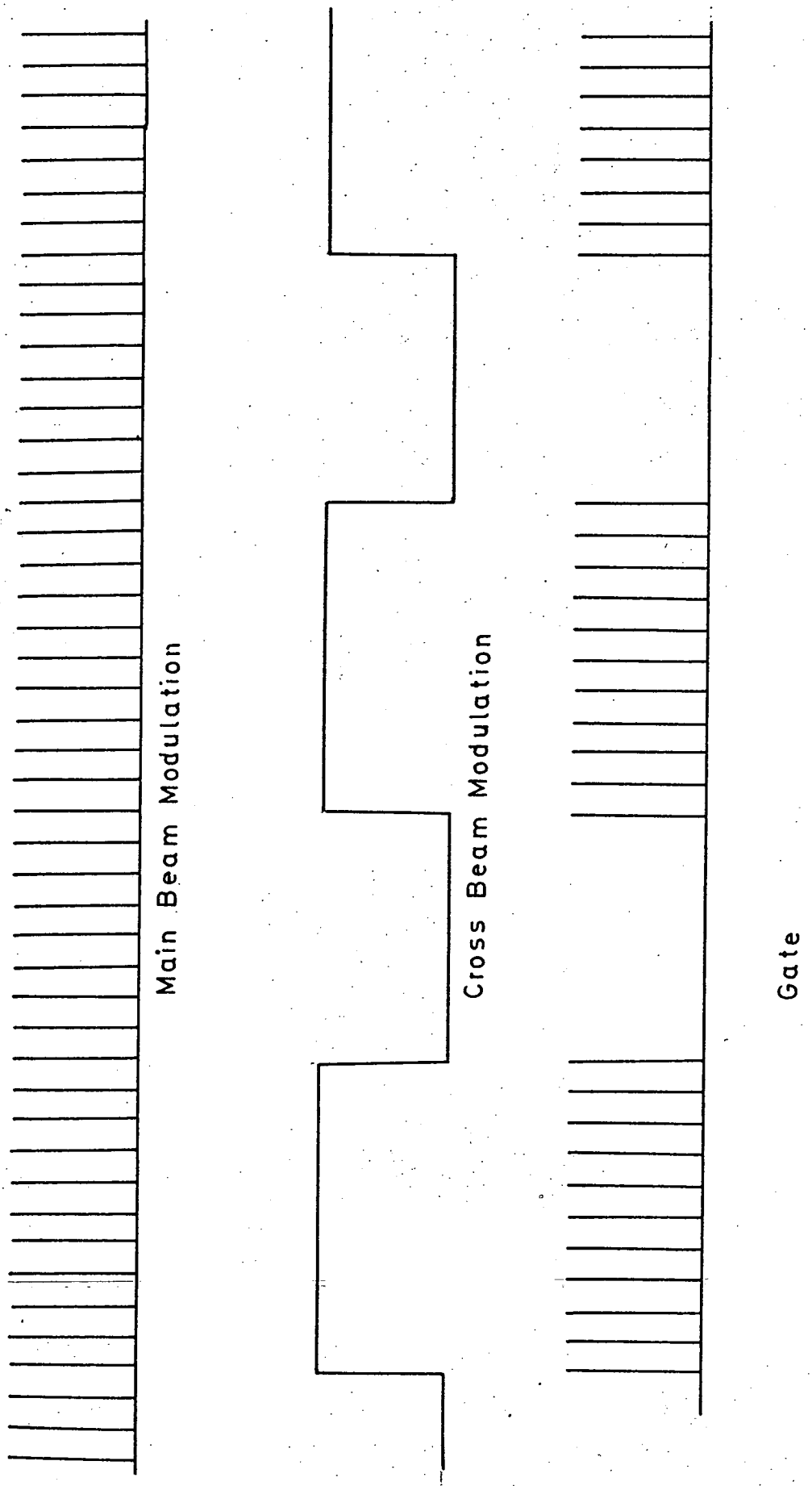

Fig. (3,31)

Time of flight modulation and gate pulses.

Main Beam Energy Spread.

It has been already mentioned that the expected energy spread would be Maxwellian with a temperature corresponding to that of the ion-emitter. Such behaviour has been observed in a similar type of ion-emitter. An attempt was made to measure the energy spread of the neutral beam by time of flight. This was partially successful.

The number of particles having a velocity in the range $v \rightarrow v + dv$ is

$$N(v) = \frac{4\ nv^2}{\pi^{\frac{1}{2}} \alpha^3} \exp(-v^2/\alpha^2)\ dv$$

where $\alpha = \sqrt{(2kT/m)}$, the most probable velocity. If this velocity distribution is superimposed on a velocity V then similarly

$$N(V + v) = \frac{4\ nv^2}{\pi^{\frac{1}{2}} \alpha^3} \exp(-v^2/\alpha^2)$$

If the distance from source to detector is d, then the flight time t is

$$t = d/V+v$$

and $dv = \frac{-d\ dt}{t^2}$

The number of particles arriving between times $t \rightarrow t + dt$ is therefore

$$N(t) = \frac{4n}{\pi^{\frac{1}{2}} \alpha^3} \frac{d(d-Vt)^2}{t^4} \exp(-(d-Vt)^2/t^2\alpha^2)\ dt$$

This is the distribution which would arise if the initial pulse was a δ function. In practice, however, it has a finite length, say the initial pulse is described by the

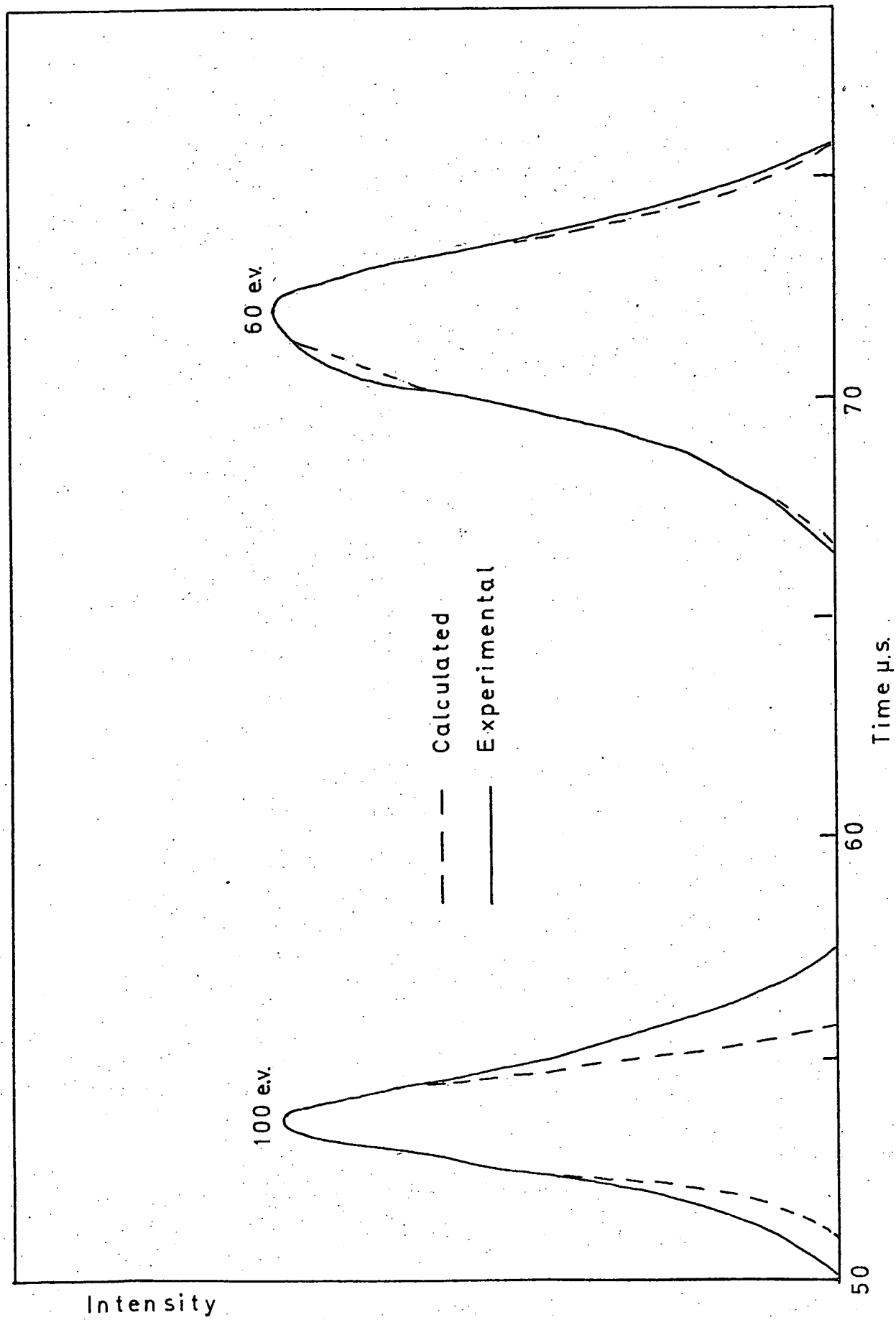

Fig. (3,32) Potassium
Arrival Spectrum.

function I(t), then the arrival spectrum is given by

$$A(t) = C \int_0^{\infty} I(t') \, d \frac{(d - v(t-t'))^2}{(t-t')^4} \exp\left(\frac{-(d - v(t-t'))^2}{(t-t')^2 \alpha^2} \right)$$

where C is a constant.

If the initial pulse is rectangular and of length t_0 then

$$A(t) = C \int_0^{t_0} \frac{d(d - vx)^2}{x^4} \exp\left(-(d - vx)^2 / x^2 \alpha^2\right) dx$$

where $X = t - t'$

It is also important to take into account the finite time "aperture" of the detector. If the detector is open for a time t_g then the measured arrival spectrum is given by

$$M(t) = \int_b^{t+t_g} A(t') dt'$$

Arrival spectra were calculated using the above expression, and compered with experimental results Fig. (3,32). It will be seen that a general agreement exists but firm conclusions can not be drawn because of the poor quality of the data.

In conclusion it may be said that although some development is still required, the possibility of studying inelastic processes by time of flight techniques exists.

CHAPTER IV

RESULTS AND DISCUSSION

Preliminary data were obtained for the systems K/Hg and K/I_2. Although the data must be regarded as exploratory only and the conclusions reached tentative the main features of the apparatus design and experimental procedures proved sound and gave encouragement to future work.

K/Hg

The system K/Hg has been the subject of many collision studies and the potential is now well known for part of its range at least. It was considered therefore that it would provide a good test of the apparatus and experimental procedures.

Reliable data were obtained for 100 e.v. only. Data obtained at 60 e.v. and 80 e.v. were unreliable because of main beam fluctuations occurring at these energies. In all five angular sweeps were taken at 100 e.v., a typical sweep is shown in Fig. (4,1), the intensity is multiplied by $\phi^{7/3}$ to remove the steep angular dependence. The average of the five smoothed sweeps is shown in Fig. (4,2). The main features are a maximum at about 0.08° the intensity there after increasing approximately linearly with angle. At angles greater than about 1.0° there is some evidence of oscillatory structure though the data can not be taken as reliable in this region. Any assumed model for the potential must account for these features and also should be compatible with previous work.

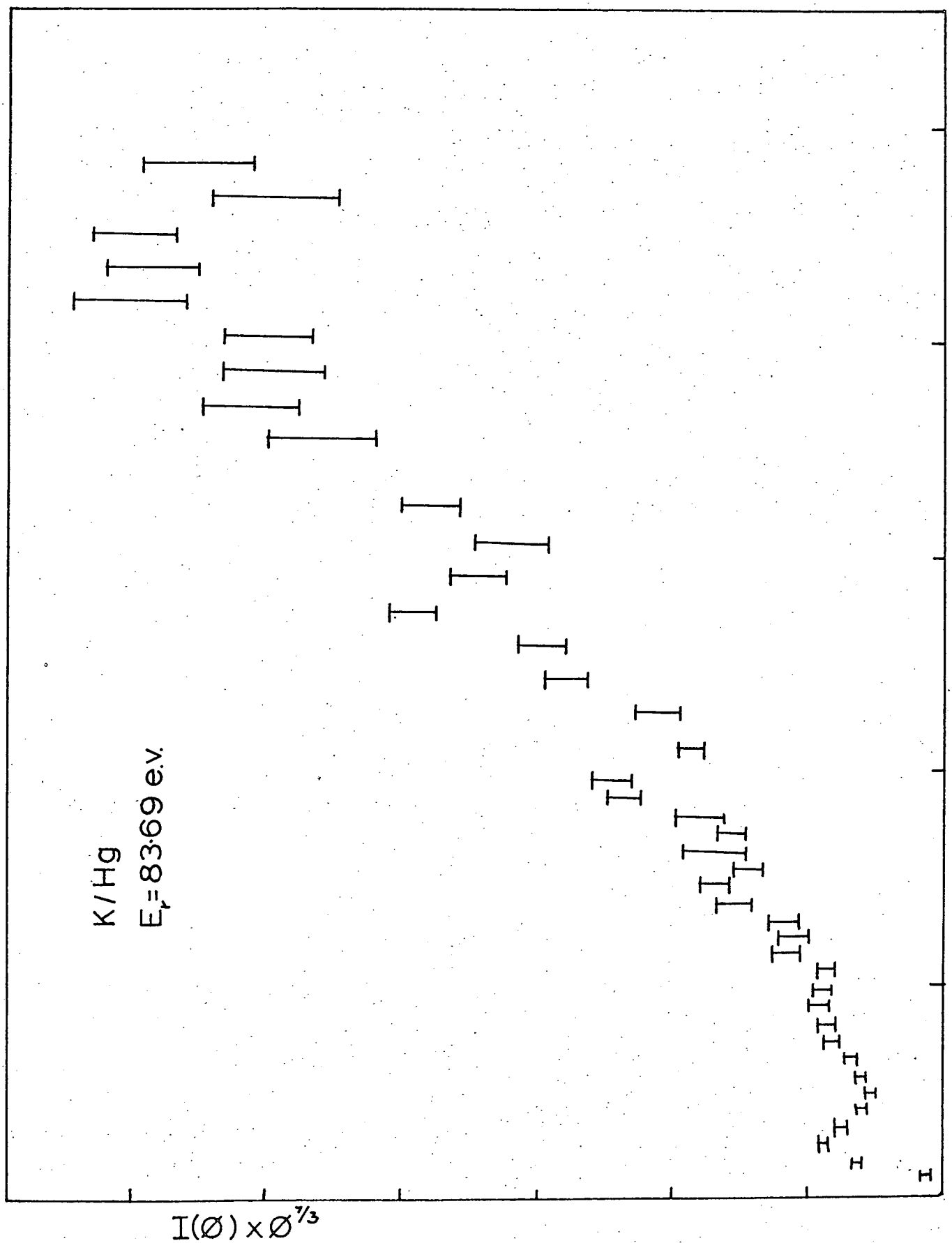

Fig. (4,1)

Typical sweep. K/Hg 100 e.v. LAB

Fig. (4.2)

Smoothed and averaged data K/Hg.

The K/Hg system has been previously studied at thermal energies, for a bibliography see the article by Bernstein and Muckerman (BER 67), and at superthermal energies (PAU 70). The presently accepted model for the K/Hg potential is a Lennard-Jones n-6 with r_m = 4.8 Å, ε = 0.087 pico-ergs and n about 8. Using the methods outlined in Chapter II the differential cross-sections were calculated and averaged over the apparatus parameters, Fig. (4,3) and Fig. (4,4). A maximum is predicted at 0.06° in fair confirmation of experiment, the slight discrepancy (about 0.02°) may be due to an error in the angular zero or in the assumed beam height. At angles greater than the maximum the curve does rise almost linearly in good agreement with experiment, no structure is however predicted.

The effects of varying n were investigated and the results for n = 18 are shown in Fig. (4,5) and Fig. (4,6), they will be seen to be little different from the 8/6 case. On the basis of the gradient at larger angles the "harder" 18/6 potential is favoured.

That exact agreement is not obtained at larger angles is not surprising when the region of the potential corresponding to those angles is considered. The region in question may be found as follows: the corresponding l value is obtained from the relationship

$$\eta_l' = \theta/2$$

the turning points for each l value being tabulated, the region of the potential mapped is known. For a lab

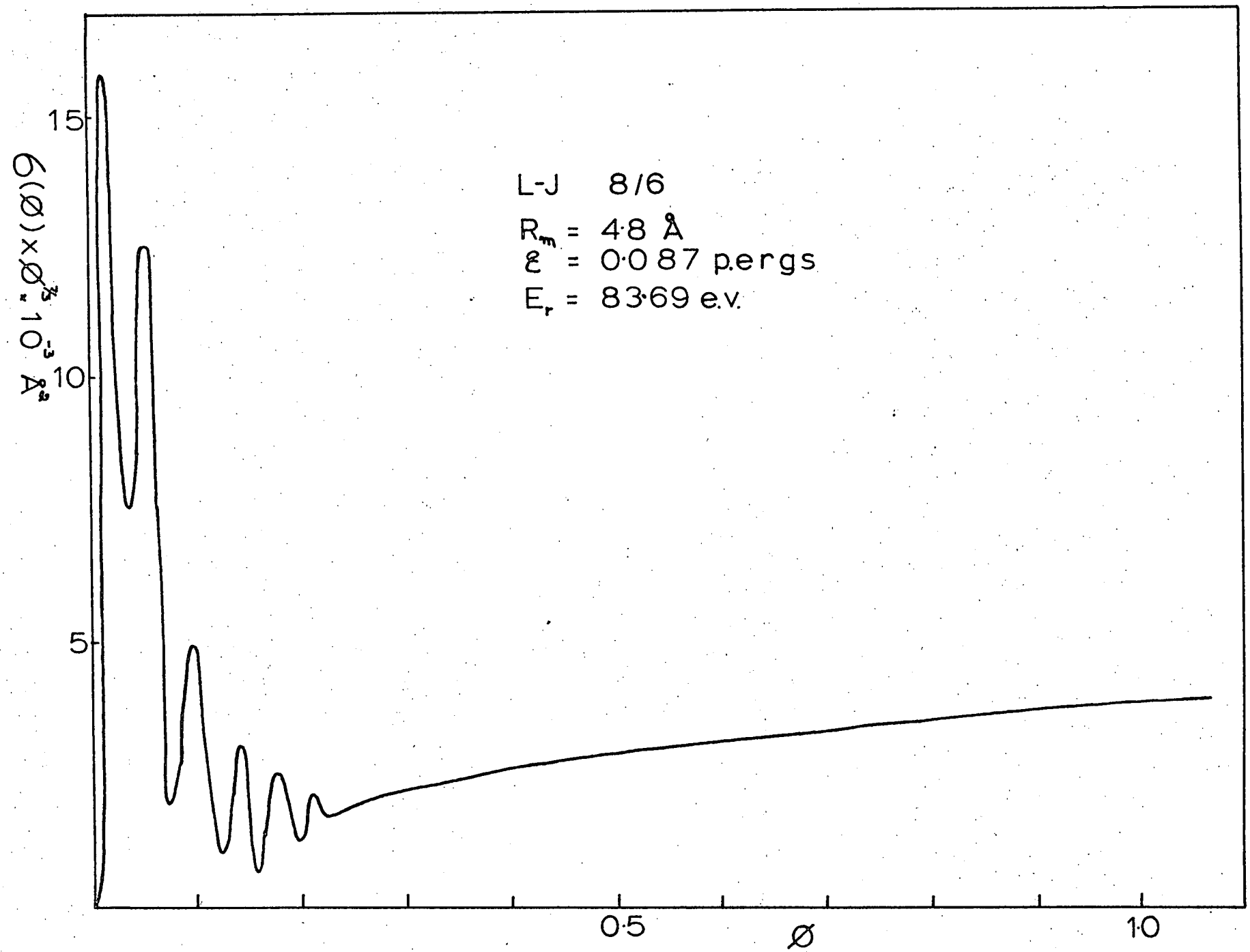
L-J 8/6
R_m = 4·8 Å
ε = 0·087 p.ergs
E_r = 83·69 e.v.
$\sigma(\phi) \times \phi^{\frac{3}{2}} \times 10^{-3}$ Å^2
15
10
5
0·5
ϕ
1·0

Fig. (4,3)

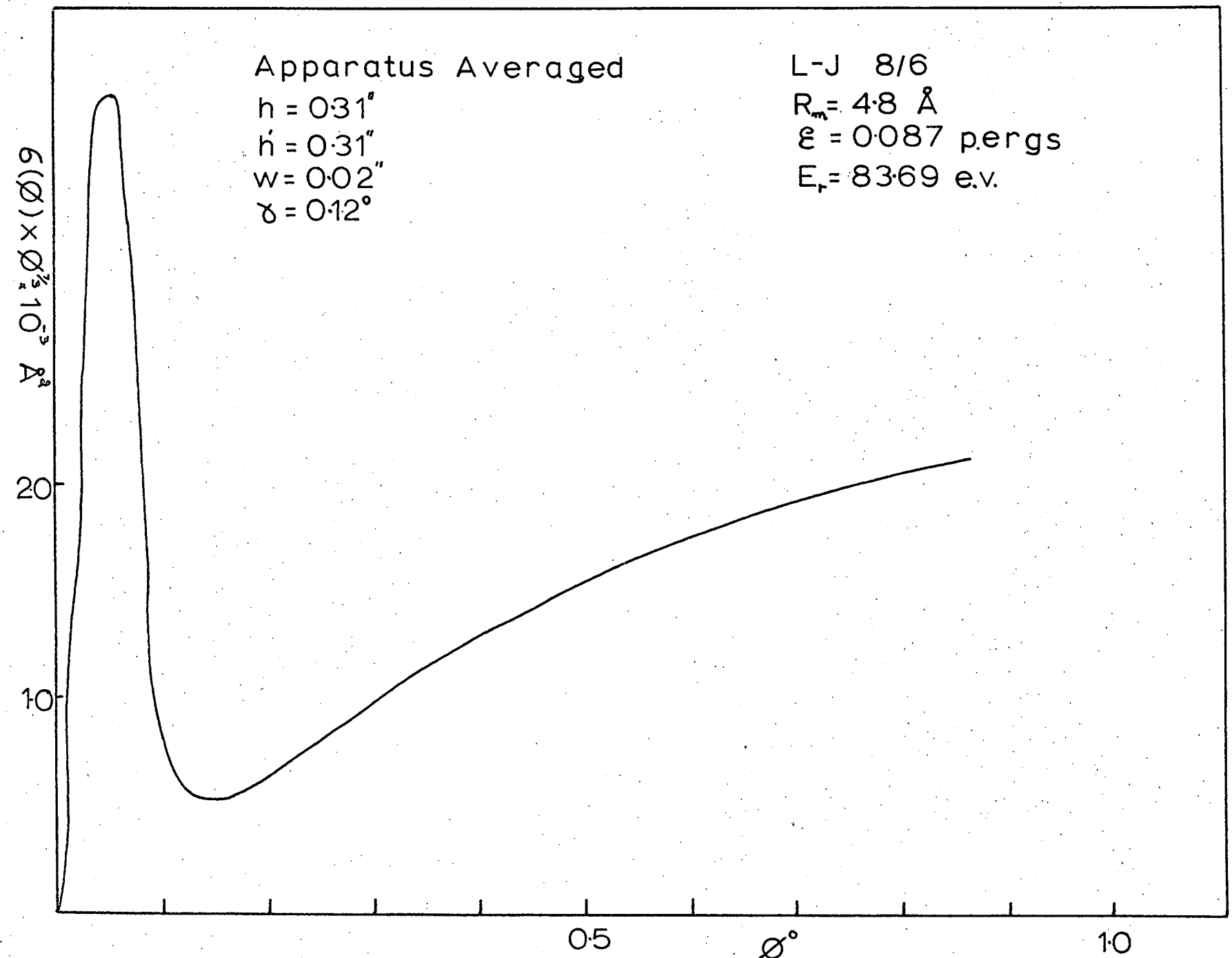
Apparatus Averaged
h = 0·31"
h' = 0·31"
w = 0·02"
γ = 0·12°
L-J 8/6
R_m = 4·8 Å
ε = 0·087 p.ergs
E_r = 83·69 e.v.
$\sigma(\phi) \times \phi^{2/3} \times 10^{-3}$ Å^2
20
10
0·5
ϕ°
1·0

Fig. (4,4)

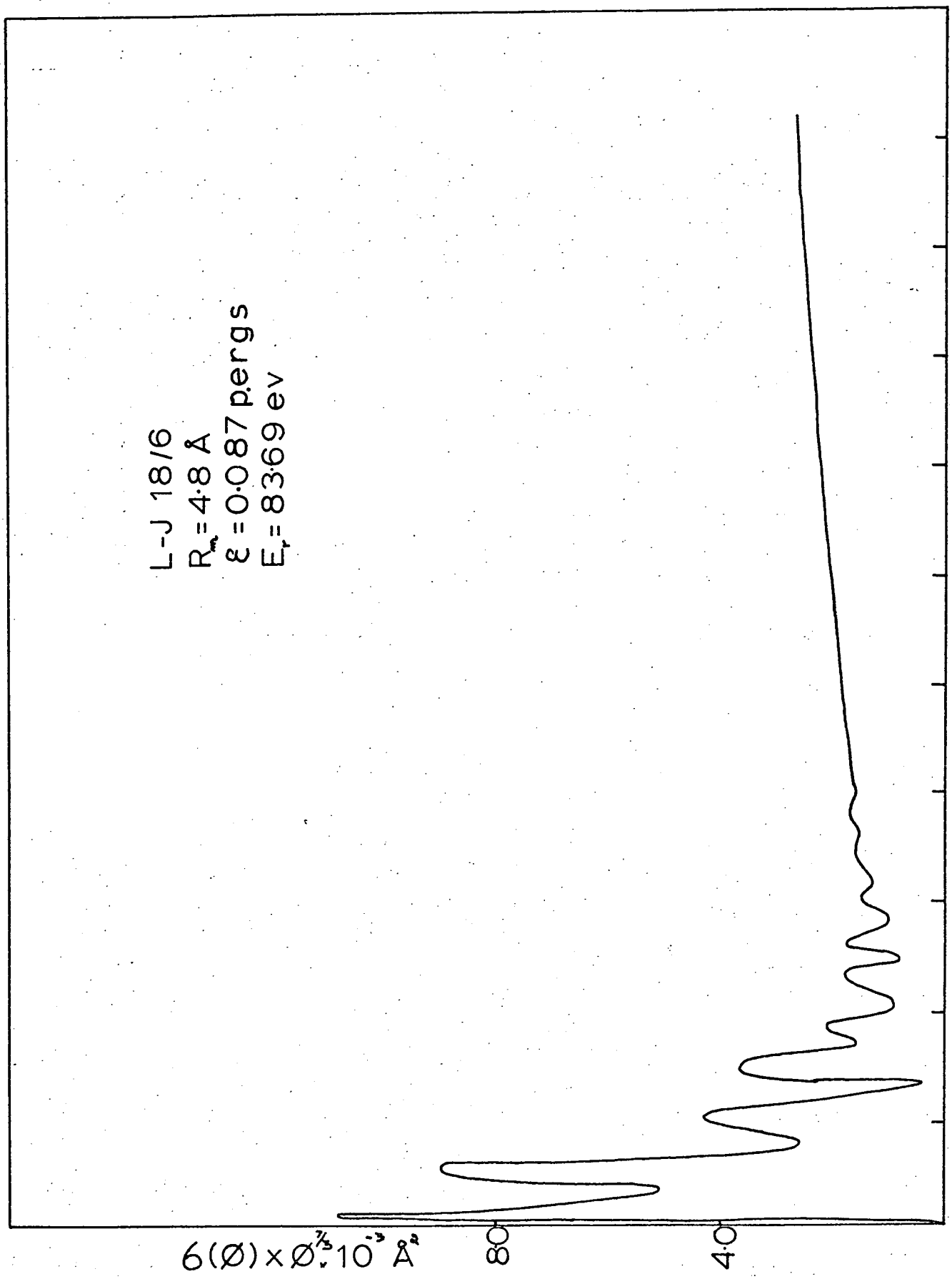

Fig. (4,5)

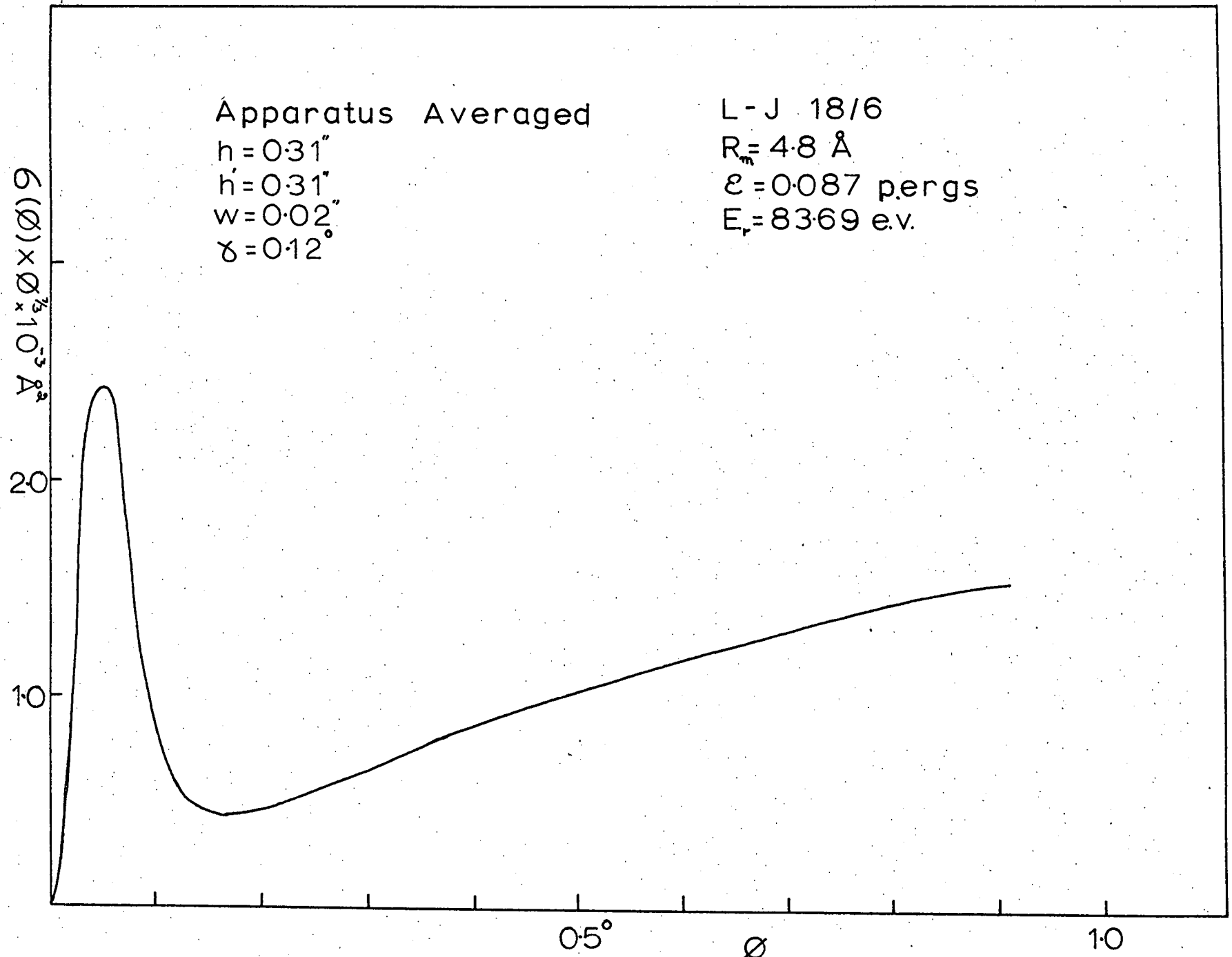
Apparatus Averaged
h = 0·31"
h' = 0·31"
w = 0·02"
γ = 0·12°
L-J 18/6
R_m = 4·8 Å
ε = 0·087 p.ergs
E_r = 83·69 e.v.
σ(Ø) × Ø^{7/3} × 10^{-3} Å²
2·0
1·0
0·5°
Ø
1·0

Fig. (4.6)

scattering angle of 1^{o} η_{l}' is 1.05×10^{-2} rad, this was found to correspond to a turning point of about $0.75\ r_m$. Previous work at thermal energies has mapped only that region of the potential corresponding to the rainbow angle I.E. values of r greater than r_m. These measurements are not therefore sensitive to the form of the short range forces. Similarly the work of Pauly (PAU 70) although at superthermal energies, is not sensitive to the short range forces being based on measurement of glory oscillations in the total cross-section.

The data presented here are therefore unique arising from a previously unmapped region of the potential.

Lack of time has precluded any real attempt to fit the larger angle scattering by varying the form of the short range potential. It is probable that if structure is present then it arises from an inelastic effect and hence will be more difficult to treat.

It is however evident that we have a useful tool for elucidating short and intermediate range molecular interactions.

K/I_2

Much information has been obtained about the potassium/halogen systems. The measurement of elastic differential cross-sections (HOR 69), (GRE 66), reactive differential cross-sections (TOE 68) and product energy distributions allow the testing of detailed models of the

systems. These have been corroborated by trajectory calculations (BLA 68) which make it possible to reproduce the collision dynamics, assuming a suitable potential. To date the vast majority of these experiments have been at thermal energies, however it was shown in Chapter II that performing these experiments at superthermal energies should yield new information. There have been two recent studies of the alkali metal/halogen systems. Los and Baede (LOS 70) have measured total ionisation cross-sections, Schlier et als (SCH 70) have measured differential elastic cross-sections for the halogens and halogen containing compounds.

As in the case of K/Hg reliable data were obtained at 100 e.v. only. A typical sweep, again multiplied by $\phi^{2/3}$ is shown in Fig. (4,7), the average of five smoothed sweeps is shown in Fig. (4,8).

The model used for the K/I_2 system has already been discussed and will be only outlined here. It is assumed that initially the particles approach along a covalent potential but at a certain separation r_c an electron is transferred from the K to the I_2.

It is further assumed that the I^-_2 ion behaves as I^- + I, the I atom having the role of a spectator only. The K^+ then picks up the I^-, by means of coulombic attraction, to form the excited product KI. When it is attempted to extend this model to higher energies two

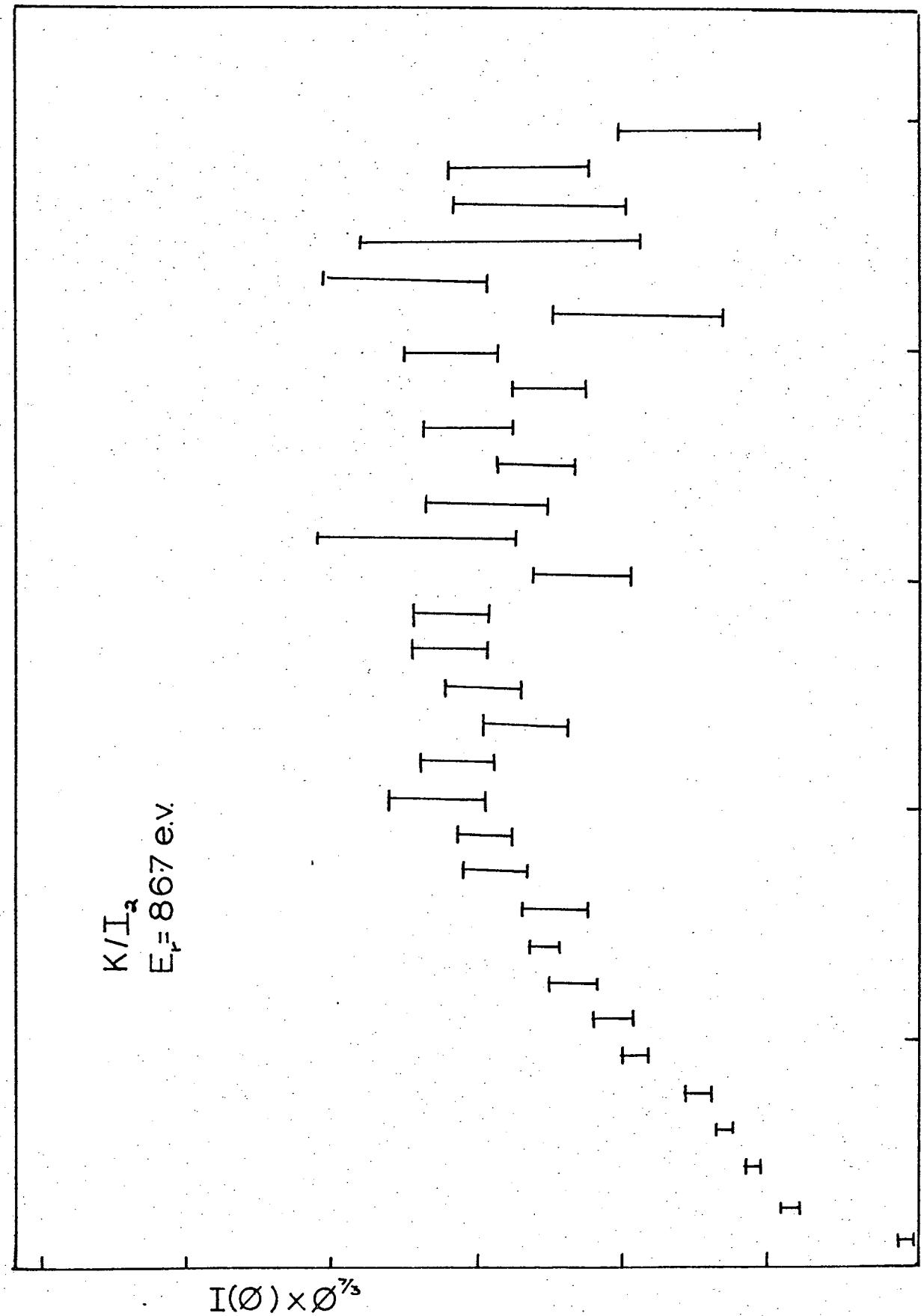

Fig. (4,7)

Typical sweep, K/I_2 100 e.v. LAB.

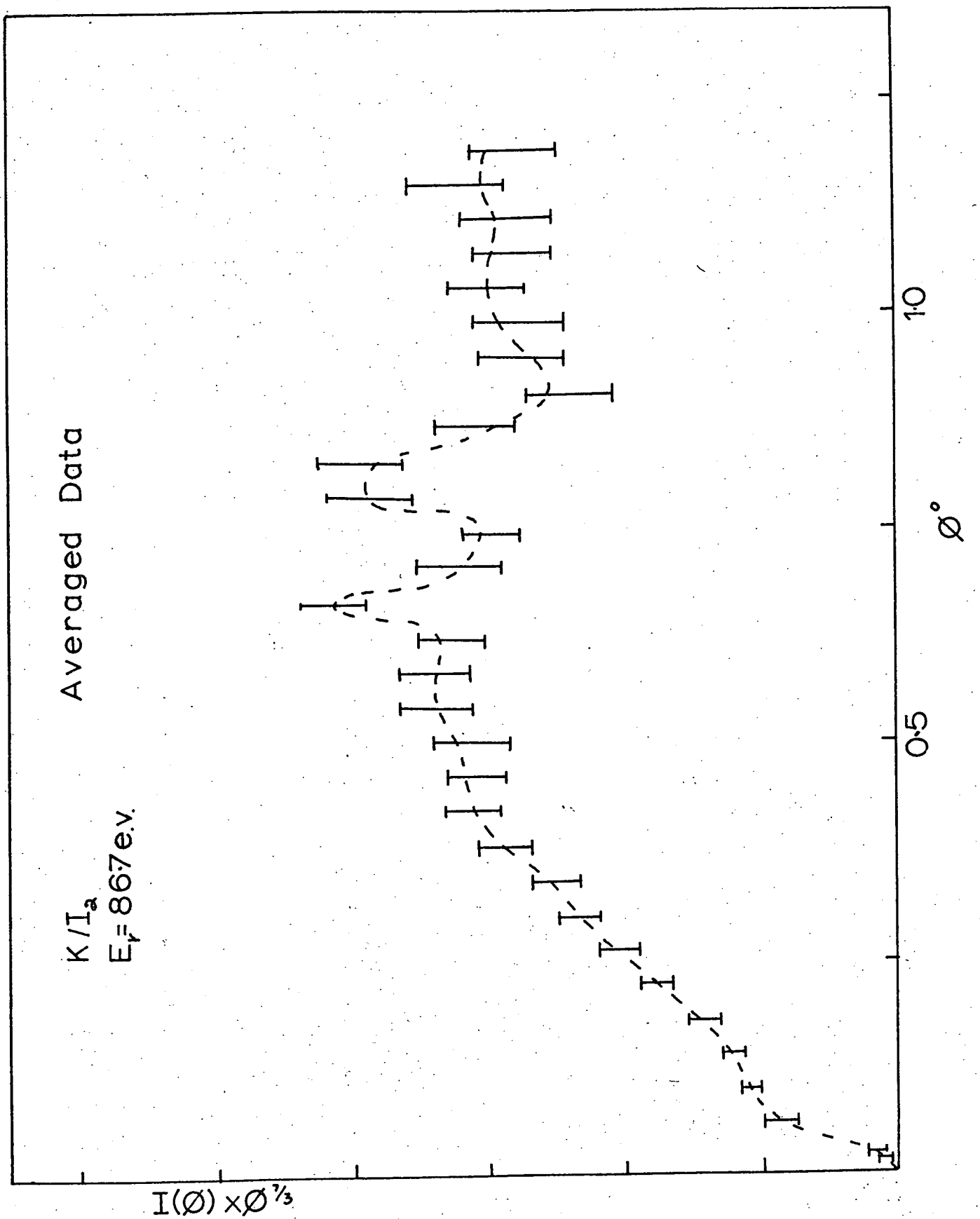

Fig. (4,8)

Smoothed and averaged data K/I_2.

points must be borne in mind; the system may no longer follow the adiabatic potential I.E. electron transfer may not occur. Also it may not be energetically possible to form the product K I. These possibilities were discussed more fully in a previous chapter.

As a first step the scattering pattern for the diabatic potential was calculated using a Lennard-Jones 12/6 potential with r_m = 4.5 A and ϵ = 0.024 pico-ergs (HOR 69). The calculated differential cross-sections are shown in Fig. (4,9) and Fig. (4,10). Comparison with the experimental data shows little agreement, at best only the general shape of the curve is given at small angles.

At the other extreme we may have purely adiabatic behaviour, in this case the system may be described up to the crossing point r_c in terms of the above diabatic potential and after the crossing point in terms of some form of coulombic potential. If the assumption as to the nature of I_2^- is followed then it is clear that the coulombic potential will be simply that for K I, which is well known. To test this possibility the procedure outlined by Horne (HOR 69) was used. In this the Lennard-Jones potential switches smoothly to a modified Varshni-Shukla potential (PAT 67). This potential contains essentially no adjustable parameters. The results are shown in Fig. (4,11) and Fig. (4,12).

It is clear that this potential also does not completely describe the data. Some similarity may however be found, e.g. there is rough agreement with the predicted

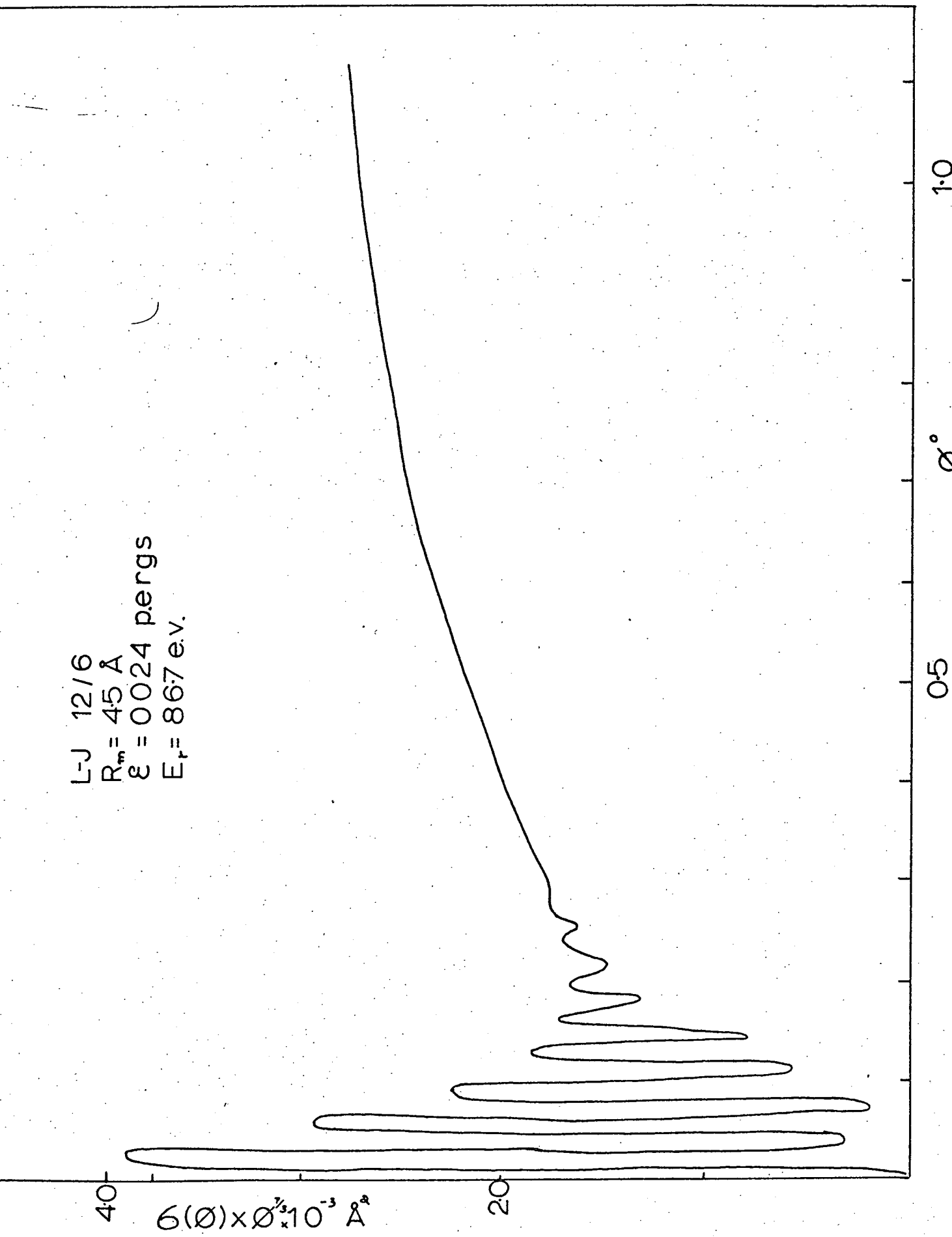

Fig. (4,9)

Ideal diabatic differential cross-sections.

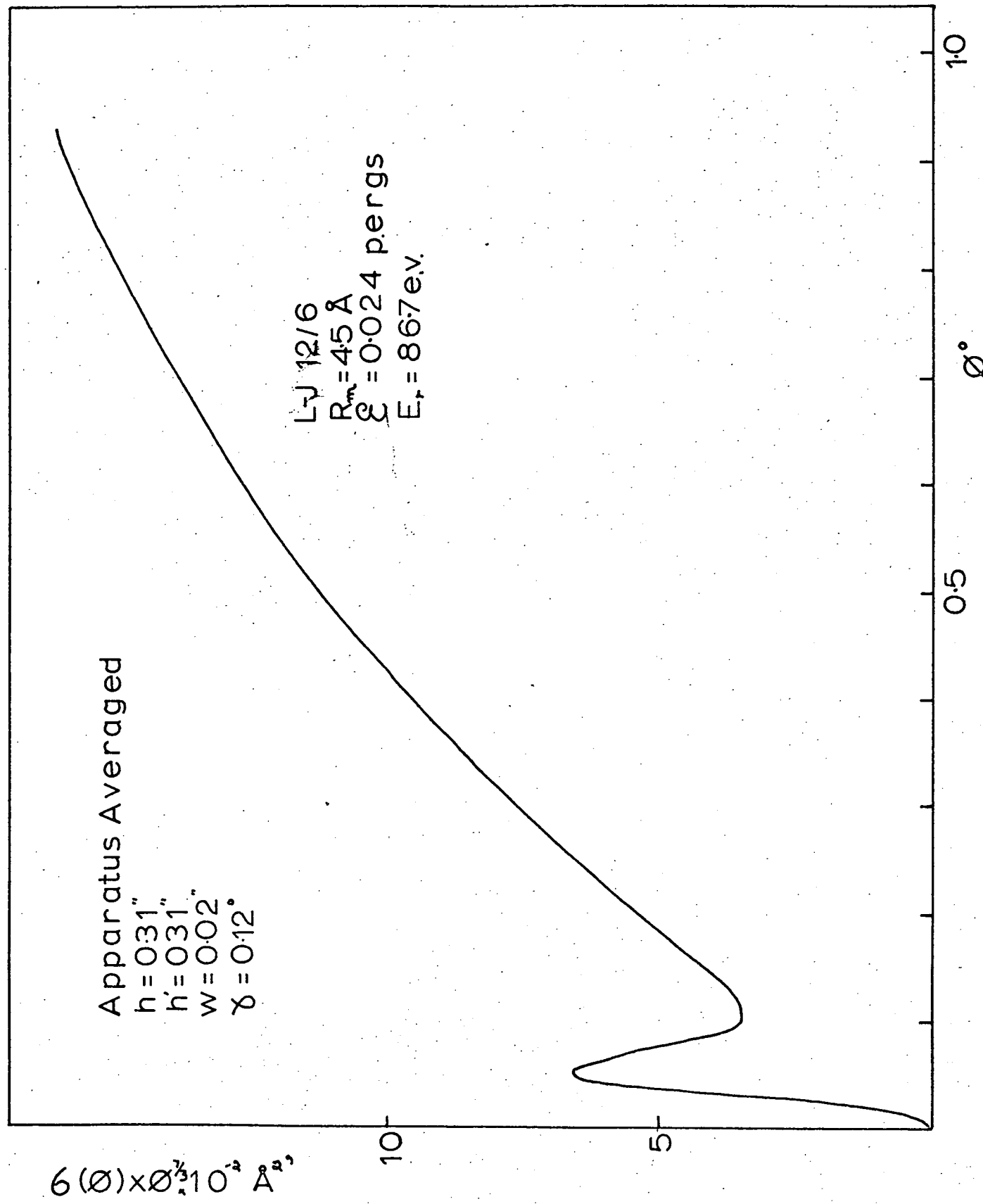

Fig. (4,10)

Apparatus averaged diabatic differential cross-sections.

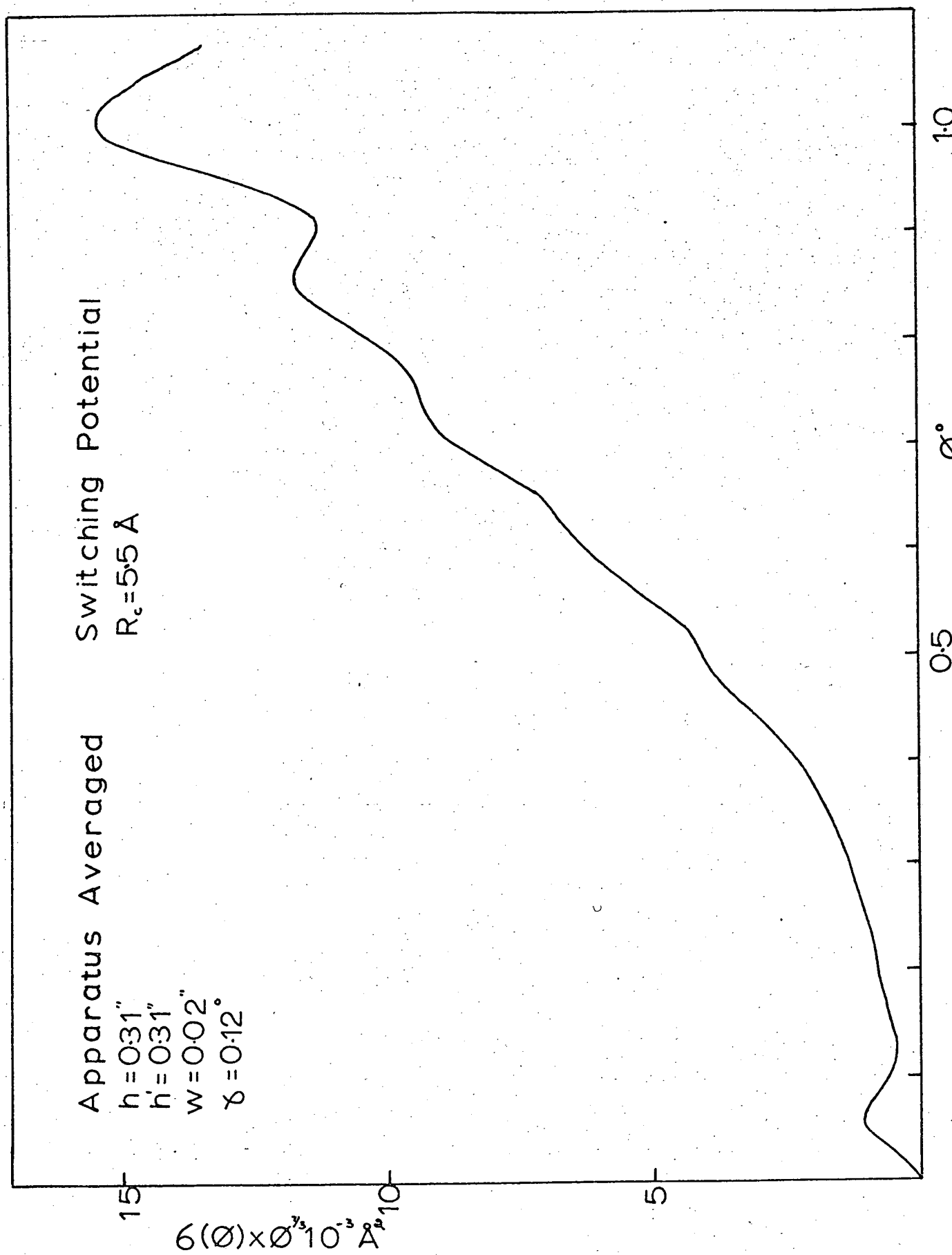

Fig. (4,12)

Apparatus averaged adiabatic differential

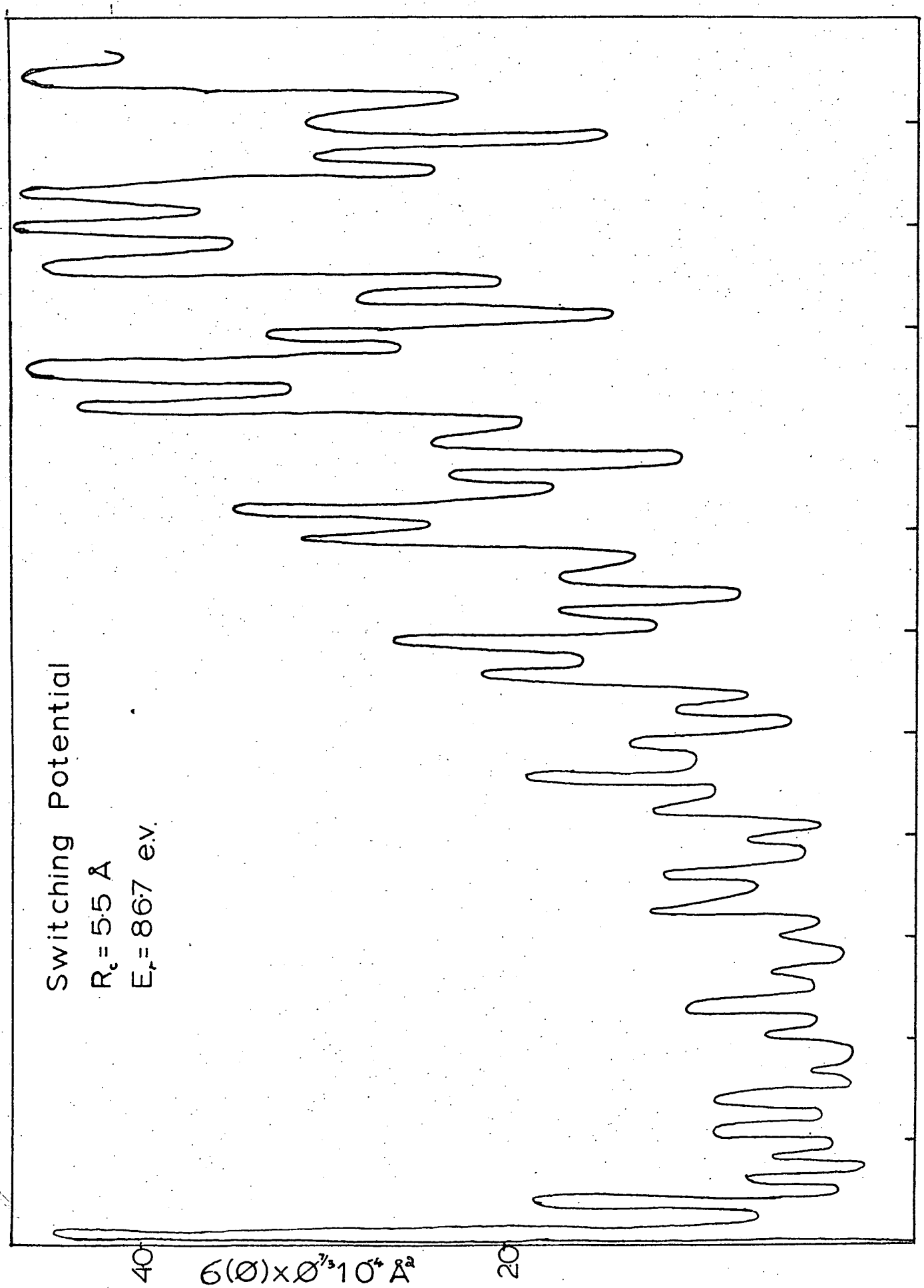

Fig. (4,11)

Ideal adiabatic differential cross-sections.

inflexions and maxima at 0.46°, 0.57°, 0.73° and 0.85°. At angles greater than about 0.5° it was found that the measured I (ϕ) x $\phi^{2/3}$ levelled off whereas the theoretical curve continued to rise out to about 1.5°. A further possibility is that both the above processes may contribute to a greater or lesser extent. On the basis of the results of Chapter II it would be expected that the probability of diabatic or adiabatic behaviour would be a function of impact parameter. In addition contributions from the two channels are coherent and hence interference effects are possible. It is clear that a very complex scattering pattern may result. If interference effects are neglected then this model may be used to give a partial description of the data. At small angles I.E. less than about 0.4° it has been noted that there is some similarity between the scattering from the diabatic potential and the experimental data. At angles greater than about 0.4° however there exists several inflexions and maxima which are more compatible with the adiabatic potential although the overall shape of the curve is not predicted.

On the basis of the above model it may be concluded that the small angle scattering is dominated by the diabatic potential, while at larger angles there is a contribution from the adiabatic potential. On the basis of the calculated differential cross-sections the adiabatic contribution was estimated to be very approximately 30%. Two possible explanations present themselves for the fall off at larger angles, either the contribution from the

adiabatic potential has diminished or inelastic processes have become important. The results of Chapter II would tend to favour the first possibility.

It may be argued that the process

$$K + I_2 \longrightarrow K^+ + I_2^-$$

is dominant and the scattering is not purely elastic. Although the above and similar processes have been studied (ROT 69) (LOS 70) it was considered to be of little importance in this case.

To check this the total ionisation cross-section was calculated by means of the Landau-Zener approximation. R_c was taken as 5.5 Å and H_{12} as 6.1×10^{-14} ergs (LOS 70), the total cross-section was found to be 3.0 $Å^2$ at 100 e.v., this is at least an order of magnitude less than the elastic total cross-section. It therefore appears unlikely that this process is of importance. The spectator stripping model for the reaction

$$K + I_2 \longrightarrow KI + I$$

predicts a product scattering angle ϕ given by

$$\phi = \tan^{-1} \frac{m_I V_{I_2}}{m_K V_K}$$

For $V_{I_2} = 10^4$ cms/sec, $V_K = 2.2 \times 10^6$ cms/sec this gives $\phi = 0.8^\circ$. It was shown in Chapter II however that reaction was unimportant at this energy.

Elastic differential cross-sections for K/Cl_2 and K/Br_2 and some halogen containing compounds have been measured in the energy range 0.5-12 e.v. by Schlier (SCH 70).

He found, in the alkali metal/halogen case, enhanced scattering at large angles. This was interpreted in terms of a contribution from the diabatic potential. However as Schlier appears to take no account of the possibility of the adiabatic potential not leading to reaction it is considered that his conclusions are suspect.

It is clear that no firm conclusions may be drawn at this stage, more extensive data, including time of flight analysis, being required. That the problem also merits further theoretical effort is obvious, it is suggested that the optical model may provide a useful insight.

CONCLUSIONS

Differential cross-sections have been measured for collisions between potassium and mercury atoms at 100 e.v. At small angles the results are consistent with the known elastic potential, at large angles a more complex treatment appears to be called for.

Measurements were also made for the system potassium and moleculor iodine. No clear conclusions could be drawn in this case. It appeared that the data could be best described as arising from a mixture of diabatic and adiabatic behaviour.

REFERENCES

AMD 66 I. Amdur, J.E. Jordan. Adv.Chem.Phys.10, 29 (1966)

AND 66 J.B. Anderson, R.P.Andres, J.B.Fenn, Adv. Chem.Phys. 10, 275 (1966)

BAN 69 A.D. Bandrauk. Mol Phys. 5, 523 (1969)

BAT 65 D.G. Bate, U.K.A.E.A. report CLM-R 53

BAT 54 D.R. Bates B.L. Moiseiwitsch, Proc.Phys.Soc. 67, 805, (1954)

BAT 58 D.R. Bates, R.McCarroll. Proc.Roy.Soc. A245, 175, (1958)

BAT 59 D.R. Bates, N. Lynn, Proc.Roy Soc. A253, 141,(1959)

BAT 60 D.R. Bates, Proc.Roy Soc. A257, 22, (1960)

BAT 64 D.R. Bates, H.C. Johnston, I.Stewart, Proc.Phys. Soc. 84, 517 (1964)

BER 57 R.S. Berry, J.Chem. Phys. 27, 1288 (1957)

BER 60 R.B. Bernstein, H.U. Hostettler, Phys. Rev.Letters 5, 318, (1960)

BER 64 R.B. Bernstein, Science 144, 141, (1964)

BER 66 R.B. Bernstein, Adv.Chem.Phys. 10, 75, (1966)

BER 67 R.B. Bernstein, J.T. Muckermann, Adv. Chem.Phys. 12, 389, (1967)

BLA 68 N.C. Blais, J.Chem. Phys. 49, 9 (1968)

BUL 54 T.H. Bull, P.B.Moon, Disc.Farad.Soc. 17,54 (1954)

CHI 69 M.S. Child, Mol Phys. 16, 313 (1969)

COU 52 C.A. Coulson "Valence" Oxford University Press 1952.

COU 62 C.A. Coulson, K. Zalewski, Proc.Roy.Soc. A268, 437, (1962)

COW 68 L.T. Cowley, Ph.D. Thesis Edinburgh, 1968.

COW 69A L.T. Cowley, M.A.D. Fluendy, K.P.Lawley, Trans. Farad.Soc.65, 2027 (1969)

COW 69B L.T. Cowley, M.A.D. Fluendy, D.S. Horne, K.P. Lawley, J.Sci.Inst.2, 1021 (1969)

CRO 70 R.J. Cross, C.J. Malerich, J.Chem.Phys. 52, 386,(1970)

DAL 56 A.Dalgarno, N. Lynn, Proc.Phys.Soc. 69, 821 (1956)

DAT 68 S. Datz, P.F. Dittner, J.Chem.Phys. 49, 1969, (1968)

DAV 31 C.J. Davisson, C.Colbick, Phys.Rev. 38, 585, (1931)

DYK 63 A.M. Dykhne, A.V. Chaplik, Soviet Phys. J.E.T.P. 16, 631, (1963)

EVA 65 D.S. Evans, Rev.Sci.Inst. 36, 375, (1965)

FEN 68 J.B. Fenn, Project Squid Technical Report PR-115-P

FLU 70 M.A.D. Fluendy, D.S. Horne, K.P. Lawley, A.W. Morris, Mol.Phys. 19, 659 (1970)

FON 66 S.N. Foner, Adv.At & Mol.Phys. 2, 385, (1966)

GAY 68 A.G. Gaydon, "Dissociation Energies and Spectra of Diatomic Molecules" Chapman and Hall, 1968.

GIO 60 J.A. Giodmaine, T.C. Wang, J.Appl.Phys. 31, 463,(1960)

GOL 50 H.Goldstein, "Classical Mechanics" Addison Wesley, 1950.

GRE 66 E.F. Greene, A.L. Moursund, J.Ross, Adv.Chem.Phys., 10, 135, (1966)

HAS 66 H.B. Haskell, O.Heinz, Rev.Sci.Inst. 37, 607, (1966)

HAS 62 J.B. Hasted, "Atomic and Molecular Processes." Ed. D.R. Bates, Academic Press 1962.

HAS 63 J.B. Hasted "Physics of Atomic Collisions" Butterworth 1963.

HEI 68 O. Heinz, R.T. Reaves. Rev.Sci.Inst. 39, 1229, (1968).

HER 63 F. Hermann, S. Skilman, "Atomic Structure Calculations" Prentice-Hall Inc. New Jersey, 1963.

HER 65 D.R. Hersbach, Appl.Optics. Suppl.2, 128,(1965)

HER 66 D.R. Hersbach, Adv.Chem.Phys. 10, 319 (1966)

HIR 54 J.D. Hirschfelder, C.F. Curtis, R.B. Bird, "Molecular Theory of Gases and Liquids" Wiley 1954.

HOR 69 D.S. Horne, Ph.D. Thesis Edinburgh, 1969.

HUL 67 E. Hulpke, C.Schlier, Z.Physik 207, 294 (1967)

HUS 63 O.K.Husman "Progress in Astronautics and Aeronautics" 9, 195, (1963)

KLE 53 O. Klemperer "Electron Optics" Oxford University Press (1953)

KUS 65 G. Kuskevics, M.Lachance, B.Thompson, A.I.A.A.Journal, 3, 1498, (1965)

LOS 68 J. Los, J. Politiek, P.K.Rol,P.G. Ikelarr, Rev.Sci. Inst. 39, 1147 (1968)

LOS 69A J. Los, A.P.M. Baede, A.M.C. Moutinho, Proc. 6th Inter. Conf.Phys.Electron Atom Collisions. M.I.T. Cambridge Mass 1969, p.492.

LOS 69B J. Los, J. Politiek, Rev.Sci.Inst. 40, 1576 (1969)

LOS 70 J. Los, A.P.M. Baede, F.O.M. Institut Voor Atoom en Moleculafysica Report No. 807.

MAH 68 B.H. Mahan, W.R. Gentry, Y.Lee, J. Chem.Phys. 49, 1758 (1968)

MAR 69 H.Margenau, N.R. Kestner, "Theory of Intermolecular Forces" Pergammon Press, 1969.

MAS 55 E.A. Mason, M.M. Kreevay, J.Amer.Chem.Soc. 77, 5808, (1955.)

MAS 62 E.A. Mason, J.T. Vanderlice, "Atomic and Molecular Processes". Ed. D.R. Bates, Academic Press 1962.

MAS 67 E.A. Mason, L.Monchik, Adv.Chem.Phys., 12, 329 (1967)

MON 57 L. Monchik, K. Eunabashi, J.L. Magee J.Chem.Phys. 27 734, (1957)

MOR 62 F.A. Morse, R.B. Bernstein, J.Chem.Phys. 37, 2019 (1962)

MOR 63 J.D. Morrison, J.Chem.Phys. 39, 200, (1963)

MOT 65 N.F. Mott, H.S.W. Massey. "The Theory of Atomic Collisions" Oxford University Press, 1965.

MOU 71 A.M.C. Moutinho Private Communication

NAR 69 P.T. Narasimhan Private Communication

PAT 67 M. M. Patel, V. B. Gohel, M.D. Trivedi, Ind.J.Phys. 41, 235, (1967)

PAU 65 H. Pauly, J.P. Toennies, Adv. in Atomic Molecular Physics, 1, 201 (1965)

PAU 66 H. Pauly, M. Hollstein, Z. Physik 196, 353 (1966)

PAU 68 H. Pauly, J.P. Toennies, Methods of Experimental Physics, 7A, 227, (1968)

PAU 70 H. Pauly, W. Neumann, J.Chem.Phys. 52, 2548, (1970)

PER 63 W. B. Person, J.Chem.Phys. 38, 109 (1963)

RIT 51 E.S. Rittner, J.Chem.Phys. 19, 1030, (1951)

ROS 67 J. Ross. H.Y. Sun. J.Chem.Phys. 46, 3306,(1967)

ROT 68 E.W. Rothe, R.K.B. Helbing, Rev.Sci.Inst.39, 1948 (1968)

ROT 69 E.W. Rothe, R.K.B. Helbing, J.Chem.Phys. 51, 1607 (1969)

SCH 68 J. Schottler, J.P. Toennies, Z.Physik 214, 472 (1968)

SCH 70 C.Schlier, V.Kemptor, T.Kneser, J.Chem.Phys. 52, 5851 (1970)

SIM 63A J.A. Simpson, C.E. Kuyatt, J.Res.Natl.Bur.Std. (U.S.) 67C, 279, (1963)

SIM 63B J.A. Simpson, C.E. Kuyatt, Rev.Sci.Inst. 34, 265 (1963)

SKI 61 G.T. Skinner, Physics of Fluids 4, 1172 (1961)

SOA 59 E.A. Soa, Jenaur Jahrbuck, 1, 115, (1959)

SPA 43 K.R. Spangenberg, L.M. Field, Elec.Comm.21, 194 (1943)

TOE 68 J.P. Toennies, Ber Bunsenges physik Chem. 72, 927 (1968)

UTT 63 N.B. Utterback, Phys.Rev. 129, 219 (1963)

WAT 27 E.C. Watson, Phil. Mag. 3, 849, (1927)

WOL 69 R. Wolfgang, Z. Hormann, J.D. Kerstetter, Rev.Sci. Inst. 40, 538, (1969)

WU 68 T. Wu T. Ohmura, Quantum Theory of Scattering Prentice-Hall, 1962.

YOU 69 W. Young, University of California, School of Engineering and Applied Science, Report No.69-39.

ZEN 32 C. Zener, Proc.Roy. Soc. A137, 696, (1932).